Analysis of Free Piston Composite Cycle Engine Performance

Efe Kulaksizoglu

Delft University of Technology

TU Delft

Analysis of Free Piston Composite Cycle Engine Performance

by

Efe Kulaksizoglu

to obtain the degree of Master of Science
at the Delft University of Technology,
to be defended publicly on May 17, 2024 at 2:00 PM.

Student number:	4650409	
Project duration:	June 15, 2023 – May 17, 2024	
Thesis committee:	Prof. dr. ir. A.G. Rao,	TU Delft, supervisor
	Dr. F. Yin,	TU Delft
	Ir. J.A. Melkert,	TU Delft

This thesis is confidential and cannot be made public until May 17, 2026

TU Delft

Abstract

Civil aviation has been going through continuous development since the invention of jet engines. Still, with the continuing increasing demands, there are still challenges to be faced in order to meet the emission goals. Even with operational improvements, novel combustion technologies with hydrogen and drop-in fuels and increased component efficiencies, there is still need for more efficient engines. Previously, the increase in engine efficiency was achieved through increasing Overall Pressure Ratio (OPR), Bypass Ratio (BPR) and Turbine Inlet Temperature (TIT). This method is approaching its limit for the conventional Joule-Brayton cycle. The current high BPR engines reach a BPR of 12 which results in a 85% propulsive efficiency where 93% is the theoretical limit. So, already the propulsive efficiency of conventional state-of-the-art turbofan engines are already quite high. On the other hand, the thermal efficiencies of conventional turbofan engines are only around 45-50%. The OPR of the state-of-the-art turbofan engines reach around 60. Further increase from an OPR of 50 to 70 in the conventional Joule-Brayton cycle will only result in a 3% efficiency improvement. So, increasing OPR further in the conventional Joule-Brayton cycle is not a viable option. Due to higher OPR, the TIT will also be higher. Especially reaching 1800K, NOx production increases significantly. To summarize, there is much more room for improvement in the thermal efficiency of turbofan engines and new technologies to tackle this are needed to meet the ACARE 2050 goals.

There has been efforts made to define the main loss sources in the conventional turbofan. The main loss sources are found to be: combustor loss, core exhaust loss and bypass flow loss. The most prominent loss, combustor loss, is caused by the irreversibilities caused by heat addition through internal combustion. It is argued that this loss can be mitigated by the use of a composite cycle that uses a constant volume process along with the conventional turbofan cycle. With this method, OPR on the order of 150 could be reached through isochoric combustion than shaft work. The free piston composite cycle engine concept (FP-CCE) is a novel concept that aims to increase the core efficiency of the future aircraft engines. In the FP-CCE concept, a free piston engine is placed between the HPC and the combustor. The free pistons energize the flow using constant volume combustion. Therefore, the increase in pressure does not depend only on shaft work. Furthermore, due to the stationary operation of the pistons, the high temperatures reached during the combustion process are only present for a very short amount of time. Therefore, the mechanical loads are also lower compared to the case where the same temperature levels are reached using the conventional Brayton cycle. The free piston engine sare modelled using 0-D chemical kinetics approach, implemented using Cantera. The free piston engines will be burning hydrogen in HCCI mode. The species are tracked using a reactor network in order to analyze the thermodynamic properties and emissions. The previous analysis done on the free piston concepts have not been made considering aircraft applications. So, the free piston designs are also scaled-up to meet the performance requirements of the LEAP-1A26 engine, a state-of-the-art high bypass turbofan engine. Then, the scaled-up free piston design is implemented into the aircraft engine simulation environment.

In this study, three different concepts are made that could be used in the future FP-CCE concepts: multi-fuel concept (C1) where hydrogen is burned in the pistons and Jet-A1 in the combustor, H2 concept (C2) where hydrogen is burned in both the piston and the combustor and finally, the only piston concept (C3) where only the pistons are burning hydrogen and there is no combsutor. Each design is put into an optimization problem to come up with a feasible design. In this study, the cascading mass effects are not considered, therefore, the designs are set such that each achieve the same thrust. The different concepts are compared and it was determined that the H2 concept (C2) provides the best performance between the three concepts. With C2, the core efficiency of the engine cycle increased from 46% to 66%. Furthermore, since this concept only burns hydrogen, there is no carbon emissions. As a downside, the NOX emissions of this concept was found to be 3 times higher than the baseline LEAP-1A26 aircraft engine.

Acknowledgements

I would like to express my sincere gratitude to my thesis supervisor, Prof. Arvind Rao, for their unwavering support and guidance throughout the entire process of researching and writing this thesis. Their expertise, patience, and constructive feedback have been invaluable in shaping this work. I would also like to thank my daily supervisor Turhan Eker for his valuable feedback and encouragement throughout this project.

I would also like to acknowledge the TU Delft Faculty of Aerospace Engineering for providing the necessary resources and facilities for conducting this study.

My heartfelt appreciation goes to my family and friends for their great support, understanding, and encouragement throughout this journey.

Contents

List of Figures

Nomenclature

Abbrevations

ACARE	Advisory Council for Aeronautics Research in Europe
FP-CCE	Free Piston Composite Cycle Engine
ERF	Effective Radiative Forcing
UHC	Unburned Hydrocarbons
CORSIA	Carbon Offsetting and Reduction Scheme for International Aviation
SRIA	The Strategic Research and Innovation Agenda
TDC	Top Dead Center
BDC	Bottom Dead Center
LPT	Low Pressure Turbine
HPT	High Pressure Turbine
LPC	Low Pressure Compressor
HPC	High Pressure Compressor
OPR	Overall Pressure Ratio
BPR	Bypass Ratio
FPR	Fan Pressure Ratio
TIT	Turbine Inlet Temperature [K]
TSFC	Thrust Specific Fuel Consumption [N.s/kg]
SFC	Specific Fuel Consumption
ITB	Interstage Turbine Burner
SI	Spark Ignition
CI	Compression Ignition
IC	Internal Combustion
EGR	Exhaust Gas Re-circulation
CI	Compression Ignition
SI	Spark ignition
HCCI	Homogeneous Charge Compression Ignition
VTOL	Vertical Take-off and Landing
LNG	Liquid Natural Gas
HVO	Hydrotreated Vegetable Oil
FPE	Free Piston Engine
OFPE	Opposed Free Piston Engine
CPE	Conventional Reciprocating Piston Engine
EVC	Exhaust Valve Close
EVO	Exhaust Valve OPEN
IVC	Intake Valve Close
IVO	Intake Valve Open
CCE	Composite Cycle Engine
GTF	Geared Turbofan
IRA	Intercooled Recuperated Aero Engine
ULTIMATE	Ultra Low emission Technology Innovations for Mid-century Aircraft Turbine century Aircraft Turbine Eng
MDO	Multidisciplinary Design and Optimization

Greek Symbols

Δ	variation
η	efficiency
λ	ratio of specific heats

Symbols

P	Pressure [Pa] [bar]
V	Volume [m^3]
S	Entropy [J/kg.K]
T	Temperature [K]
u	Specific internal energy [J/kg]
q	specific heat transfer [J/kg]
h	specific enthalpy [J/kg]
h	specific enthalpy [J/kg]
c_p	specific heat capacity at isobaric conditions [J/kg.K]
c_v	specific heat capacity at isochoric conditions [J/kg.K]
r	Compression ratio [-]
M	Mach Number [-]
W	Work [J]
P	Power [W]
$\dot{m}$	mass flow rate [kg/s]
V	velocity [kg/s]
FN	Net Thrust [N]
R	Specific gas constant [J/kg.K]
D	Characteristic Diameter [m]
N	Rotational speed [rad/s]
T	Torque [N.m]
z	number of cylinders
λ_a	air expenditure
ρ	Density [kg/m^3]
s	Piston path [m]

Subscripts

suppl.	supplied
remov.	removed
th	thermal
prop	propulsive
tot	total
c	compressor
t	turbine
j	jet
0	free stream

1

Introduction

Climate change is an urgent global issue that requires our immediate attention. With the rapid growth of technology, it has become necessary to limit emissions in order to prevent a further rise in temperatures.With the growing demand to fly, the emissions from the aircraft industry has also been a problem. The average reduction of fuel consumption per passanger-km has decreased 1.3% per year since the 1960's, and is expected to continue at a similar rate until 2037 [1][2]. On the other hand, the demand for flying has also been increasing over the years. According to the predictions of Airbus, the aviation sector will undergo 4.4% annual growth in revenue passenger-km for the next two decades. Meanwhile, Boeing expects in its Commercial Market Outlook an annual growth of 4.6% [3]. Therefore, the speed at which the fuel consumption is decreasing can not keep up with the increasing demand to fly.

Aviation contributes to climate change by releasing combustion products to the atmosphere. As a result of combustion, carbon dioxide (CO_2), water vapour (H_2O), nitrogen oxides (NO_x), sulphate aerosols, compounds from incomplete combustion such as unburnt hydrocarbons (UHC) and non-volatile particulate matter (nvPM) such as soot are emitted to the atmosphere. The emitted species can lead to a wide range of atmospheric processes including the formation of contrail-cirrus and ozone and the depletion of methane.

In order to decrease emissions and fight climate change, global and local agreements in the aviation sector are made. According to the CORSIA agreement, the growth in the sector must be offset such that to reach net zero[4]. Furthermore, The Advisory Council for Aviation Research and Innovation in Europe (ACARE) has set targets to reduce emissions[5]. This agenda targets further significant improvements on engine level: CO2 emissions per passenger kilometer should decrease by 30% by 2035 compared to the year 2000 technology standard. Furthermore, it is stated that a reduction of 75% of CO2 and 90% of NOx emission per passenger-km by 2050 has to be achieved [5]. On the other hand the growth of the aviation sector is still too large to offset the emissionsIn order to meet the atmospheric temperature and CO2 emission targets, a significant improvement in technology has to be made. For the aviation sector to meet these targets, efficient and low emissions technologies have to be developed. This combination has the greatest potential to allow for the aviation sector to meet the emission demands.

The state-of-the-art engine scan reach propulsive efficiencies around 80-85%. Meanwhile the thermal efficiencies are still around 40-45%. There is a clear room for improvement in the thermal efficiencies in the modern aero engines. Therefore, studies on novel concepts are conducted that aim to increase the core efficiency of the next-gen aero engines[6]. Studies indicate that the use of constant volume combustion along with the constant pressure combustion in aero engines can have significant improvement on the thermal efficiencies. Constant volume combustion concepts are expected to increase the thermal efficiency by reaching hecto-pressure reatios of the order 100. The free piston composite cycle engine (FP-CCE) concept that has been investigated in this report is one of the concepts that aim to increase the core efficiencies of future turbofan aircraft. The free piston composite cycle engine (FP-CCE) concept is a concept that utilizes constant volume combustion to increase the core efficiency of the engine. The FP-CCE concept utilizes free piston engines to energize the flow with constant volume combustion within the aero engine cycle. This report will be investigating the whether the use of the FP-CCE engine will provide improvements in performance and emission characteristics.

In this report, an opposed free piston engine using HCCI combustion will be applied to a short-medium range aircraft engine. The effects on performance and emissions of this novel configuration will be analyzed.

Following the literature study on the free piston composite cycle engine, certain gaps in the field have been identified. The FP-CCE concept is a very new concept that is still under development and is analyzed for the year 2050. Previous investigations on this concept showed that there is no current piston design available to accommodate the power requirements of an aircraft engine. So, firstly, the conventional free opposed piston design will be scaled up. The performance of the the opposed free piston concept using hydrogen HCCI combustion has not been analyzed yet for various parameters. The SFC and NOx emissions emissions for this concept would be very valuable to analyze. Therefore, it is important to see whether the proposed free opposed piston concept can achieve higher thermal efficiency and low emissions with the upscaled design. As a result, the research question for this study is formulated as: **Can the opposed FP-CCE concept exhibit better performance and emissions characteristics compared to the state-of-the-art high bypass turbofan engines?**

To answer this question, certain sub questions or milestones were identified. These sub-questions relate to the gaps in literature about this new concept. To summarize, the milestones are:

- **RQ1**: When scaled-up, is the opposed free piston engine still feasible to be used in the aircraft in terms of performance
- **RQ2**: Does the FP-CCE engine concept achieve higher thermal efficiency with the designed free piston compared to the state-of-the-art turbofan engines?
- **RQ3**: Does the FP-CCE engine concept have better emission characteristics than the state-of-the-art turbofan engines?

This study will aim to answer the research questions provided. First the baseline free piston engine will be modelled. Then, the free opposed piston engine will be scaled-up to the performance requirements of LEAP-1A26. Then, the free opposed piston model will be implemented into the aircraft engine cycle model to analyze the performance and emissions.

2

Literature Review

2.1. Development of Aero Engines

In this section, the development of aero engine technology will be discussed. Various engine types, important performance characteristics and operation of aero engines were researched and summarized here. Until the end of World War II, the piston engine technology was widely used in aircraft. At that point, various piston engine configuration were already investigated but getting more power out of the piston engines became very difficult due to increased cooling requirements and shock losses. The materials being developed at the time were not able to perform at the required level. Sophisticated cooling techniques combined with the development of high-temperature materials allowed gas turbines to operate at higher turbine inlet temperatures. Furthermore, the development of new gas turbine configurations, such as turbofan aircraft engines and combined-cycle concepts for stationary applications, have significantly improved their performance and efficiency. As a result, gas turbine engines have become the primary choice for many applications. [7] [8]

2.1.1. Aero Engine Performance

The conventional turbojet engine is basically a gas generator that produces thrust by expanding the hot and pressurized gas. In this configuration, the compressor, combustor and turbine can be referred as the gas generator module of the jet engine. The hot gases at the exit of the gas generator could theoretically be expanded to ambient pressure in an isentropic expansion and work can be extracted from the flow. The work extracted from the gas generator is W_{gg} and this over time gives the gas generator power, referred as P_{gg}. While calculating the P_{gg} in case of turbo-fan engine, the work contribution of fan going towards core flow should also be considered as core consumption. Therefore, it is subtracted removed from total work output to obtain P_{gg}. The rest of the fan work going to bypass is a component of P_{gg} itself.[9]

Now, having defined P_{gg}, the jet power and power losses can be defined. In the equations below the propulsive jet power, thrust power and the power loss are shown respectively.

$$\begin{aligned} \dot{W}_{\text{prop. jet}} &= 0.5\dot{m}\left(v_j^2 - v_o^2\right) \\ \dot{W}_{\text{thrust}} &= \dot{m}\left(v_j - v_o\right)v_o \\ P_{\text{loss}} &= 0.5\dot{m}\left(v_j - v_o\right)^2 \end{aligned} \tag{2.1}$$

where v_j is the jet velocity, v_o is the flight velocity.

There are three primary sets of parameters commonly utilized to assess advancements in engine technologies. The initial set encompasses engine design parameters, namely BPR (Bypass Ratio), OPR (Overall Pressure Ratio), and TIT (Turbine Inlet Temperature). The boundaries defined by these parameters establish the design space for an engine. The second category comprises cycle dependent parameters, such as thermal efficiency, propulsive efficiency, and overall efficiency. These parameters represent the effectiveness of a specific cycle. Additionally, there exist constraints that delineate the operating conditions of an engine. These constraints are associated with thermal limits, mechanical limits, and emission limits[10]. Also, the ideal Brayton cycle is constructed using various assumptions.

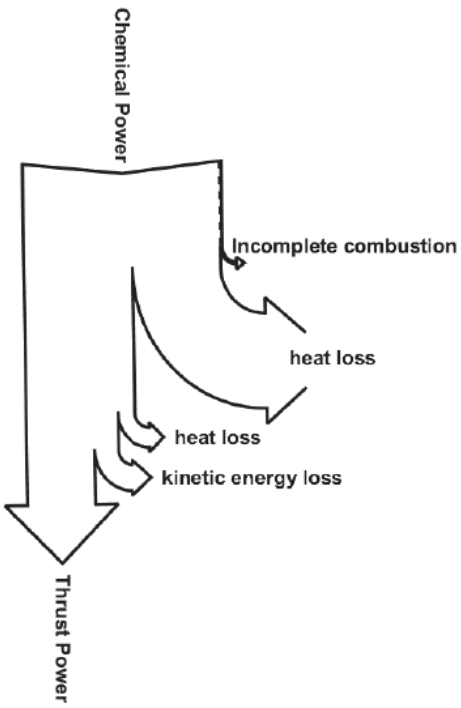

Figure 2.1: Sankey Diagram of losses in the aero engine [12]

In a real gas turbine engine, there are various losses that occur in different processes which leads to different efficiency definitions. These are visualized in the Sankey Diagram shown in Figure 2.1. The main goal for the gas turbine cycle in an aircraft is to convert the chemical power to thrust power efficiently. The engine fuel consumption is associated to three criteria, the thermal efficiency, the propulsive efficiency, and their product ,the total efficiency [11] [10][12]. Considering the losses in real life, only a minor portion of the total chemical power (approximately 40% in a modern civil aircraft engine) is converted into the mechanical power. [13]

Thermal Efficiency

The thermal efficiency η_{th} of a gas turbine shows how much of the chemical power is converted to mechanical power. In a gas turbine cycle, the chemical energy is extracted from the injected fuel. Meanwhile, the mechanical power output is represented by the difference between the power produced by the turbine and the power required to drive the compressor.The thermal efficiency can also be expressed as the multiplication of the combustion and thermodynamic efficiency. The combustion efficiency represents the losses due to the incomplete combustion processes. The thermodynamic efficiency is the amount of power generated at the exit of the turbine following an isentropic expansion through the nozzle divided by the energy of the fuel. This efficiency represents the heat losses occuring in the core which diminishes the useful power extracted from the gas generator portion of the engine. Lastly, the jet generator efficiency is the kinetic energy available at the nozzle divided by the gas power available at the exit of the of the nozzle following an isentropic expansion. This efficiency represents the heat losses that occur due to the expansion in the nozzle.[11] The thermal efficiency can be written as:

$$\eta_{th} = \frac{\text{Kinetic energy}}{\text{Thermal energy input}} = \frac{W_{t-}W_c}{\dot{m}_f \times LHV_f} = \frac{\Sigma\left\{1/2 \cdot \dot{m}_a \cdot \left(V_j^2 - V_0^2\right)\right\}}{\dot{m}_f \times LHV_f} \tag{2.2}$$

where W_t and W_c are the turbine work output and compressor work requirement respectively; $\dot{m}_f$ and $\dot{m}_a$ are the fuel flow rate and the air mass flow rate; LHV is the Lower Heating Value of a given fuel; V_j and V_0 are the jet velocity and the free stream velocity.The thermal efficiency of a modern turbofan engine is about 50%. It is expected the new generation engines will be able to reach a thermal efficiency of 55% with the increase in TIT and OPR[10]. On the other hand, the increase in TIT and

OPR are reaching a limit due component efficiencies, material cooling requirements, component scaling behaviour and real gas effects. Therefore, the further significant improvement of the thermodynamic efficiency of pure Joule-/Brayton-cycle based engines has become increasingly challenging[14].

Propulsive Efficiency
With the thermal efficiency, the efficiency in which the chemical energy is turned into mechanical energy is determined. Now, the mechanical energy has to be converted to thrust energy. The efficiency at which the mechanical energy is converted to thrust is represented by the propulsive efficiency, η_{prop}. The propulsive efficiency is determined by dividing the actual thrust power by the total useful kinetic energy. So, the propulsive efficiency represents the lost kinetic energy when converting the useful kinetic energy to thrust.

$$\eta_{\text{prop}} = \frac{\text{Thrust power}}{\text{Kinetic energy}} = \frac{FN \cdot V_0}{\Sigma\left\{1/2 \cdot \dot{m} \cdot \left(V_j^2 - V_0^2\right)\right\}} = \frac{\sum\{\dot{m} \cdot (V_j - V_0)\} \cdot V_0}{\sum\left\{1/2 \cdot \dot{m} \cdot \left(V_j^2 - V_0^2\right)\right\}} \tag{2.3}$$

where the FN is the net thrust. The notation of sum is valid when the objective is an unmixed turbofan with an unchoked nozzle[11].

Equation 2.3 shows that the maximum propulsive efficiency is reached if the jet velocity is equal to the free stream velocity. However, if this happens, there would be no thrust generated. So, the residual kinetic energy in the jet wake is inevitable. In reality, in order to increase the propulsive efficiency, the residual kinetic energy has to be decreased as much as possible. This can be achieved by increasing both FPR and BPR as they directly affect the residual kinetic energy[10]. The theoretical limit for propulsive efficiency is around 93% and the current high BPR engines reach 85% [12].

Overall Efficiency
The overall efficiency , η_{tot}, is defined as the product of the thermal and propulsive efficiency. It is deemed to be a more useful parameter to quantify the performance of the whole engine. The overall efficiency can be expressed as:

$$\eta_{\text{tot}} = \eta_{th} \times \eta_{\text{prop}} = \frac{FN \times V_0}{\dot{m}_f \times LHV_f} \tag{2.4}$$

With this expression, it can be seen that the overall efficiency shows the thrust power divided by the total used thermal power. TSFC is also a useful parameter to measure the performance of a gas turbine cycle. Then defining the thrust specific fuel consumption as $TSFC = \frac{\dot{m}}{FN}$, overall efficiency can be re-written as:

$$\eta_{\text{tot}} = \frac{V_0}{TSFC \times LHV_f} \tag{2.5}$$

From this expression, it can be seen that for a given flight speed and fuel, the total efficiency is inversely proportional to the thrust specific fuel consumption. So, decreasing the thrust specific fuel consumption is beneficial in increasing the overall efficiency of the engine.

Cycle Parameters
In this section, the important cycle parameters that define the design space for the engine to be optimized will be discussed. For a commercial turbofan aircraft engine, the main cycle parameters to be discussed are the BPR, OPR and TIT.

Bypass Ratio
The bypass ratio is a measure used in turbofan engines to indicate the amount of air that bypasses the engine core compared to the amount of air that passes through the engine core. It is defined as the ratio of the mass of air that passes through the bypass duct to the mass of air that passes through the engine core. The bypass ratio is an important parameter for turbofan engines because it affects their performance and efficiency. A higher bypass ratio means that more air is bypassing the engine core and therefore less fuel is being burned to produce the same amount of thrust. This results in a more fuel-efficient engine with lower emissions.The aim of such engine configurations is to improve the propulsive efficiency hence reducing the TSFC. Moreover, the jet noise decreases substantially because of the

lower jet velocity. Increasing the BPR also has certain drawbacks. When BPR is increased, the engine size also increases. This results in an increased engine drag. Another important point arises due to the fact that usually the low speed spool is connected to the fan. As BPR is increased, the fan rotational speed has to be decreased. Consequently, the rotational speed of the LPC and LPT will also be lower. As a result, more LPT stages are needed to extract the same amount of work. So, the engine weight will increase. In order to overcome this issue, the the geared turbofan concept can be used with high BPR turbofans to decouple the LPC from the fan.[15] [12]

In Figure 2.2, the change in BPR over the years with developing aero engine technology is given. From the figure, the increasing BPR trend can be seen clearly. For modern commercial turbofan aircraft engines, the BPR ranges from 5 to 10. Moreover, with the very recent Geared Turbofan by Pratt & Whitney, the BPR can even reach 12. [16]

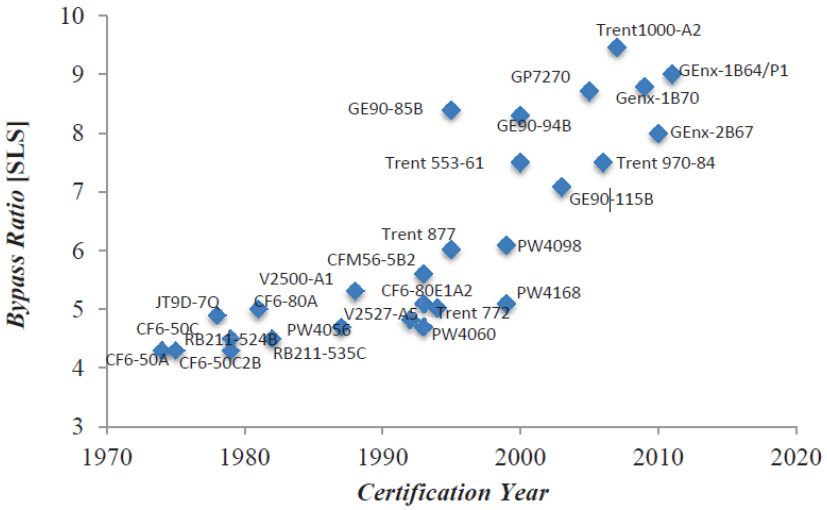

Figure 2.2: Bypass Ratio over the years [12]

Overall Pressure Ratio

The overall pressure ratio is the ratio of the maximum pressure at the compressor exit to the pressure at the inlet of the engine. The OPR is important for aircraft engines because it is a measure of the engine's ability to compress the incoming air, which affects the engine's overall performance, efficiency, and thrust output. A higher OPR generally results in a more efficient engine with higher thrust output. With a higher OPR, the inlet pressure and temperature going into the combustor increases. Theretofore, the required fuel to reach the desired turbine inlet temperature decreases. In addition, in order to achieve high OPR values, advanced compressor design and materials are required or more compressor stages have to be added. In either case, more complexity is added which leads to a higher engine mass. Therefore, the trade-off between high OPR and low mass and complexity have to be made.[14][10]

From Figure 2.3, the trend of increasing OPR over the years considering various engines are shown. Over the last few years, the overall pressure ratio has increased to be around 50. The latest Gen-x engine from GE reaches and OPR of 60[17].

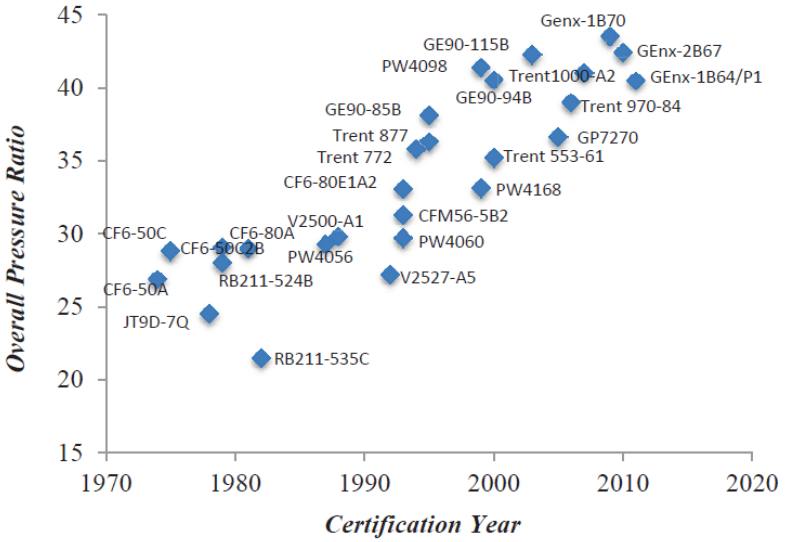

Figure 2.3: Overall Pressure Ratio over the years [12]

Turbine Inlet Temperature

Turbine inlet temperature (TIT) is the temperature of the air and fuel mixture before it enters the turbine section.Turbine inlet temperature is important because it has a significant effect on the performance and efficiency of the engine.

A higher TIT generally results in higher engine efficiency and better fuel consumption. When the temperature at the exit of the combustor is higher, than it means that the engine has been able to extract more energy from the products of the combustion process. Therefore, more power can be extracted to drive the compressor and produce thrust. On the other hand, the TIT can only be increased to a certain level. The achievable TIT depends on the material properties. When TIT is higher, the engine components will degrade faster as they are subjected to higher temperatures. Therefore, the reliability and the durability of the engine will decrease. Additionally, having a high TIT will cause problems in terms of NOx emissions. As the temperature gets higher, more NOx will be produced. Especially past 1800 K, NOx emissions show a significant increase. [12][10]

To summarize, BPR, TIT and OPR have been defined. The factors in which limit how these parameters were also presented. The parameters, BPR, TIT and OPR define the design space in which the gas turbine cycle can be optimized. They have a big influence on the thermal and propulsive efficiency. Therefore, these parameters have to be evaluated to asses the gas turbine performance accurately.

2.1.2. Current Turbofan Engine Technology

Firstly, the current turbofan engine technology was researched. In aero engine design, the goal is to keep reducing the TSFC by increasing the efficiencies. In Figure 2.4, the trend of specific fuel consumption as a function of year of certification for various are engine designs are given. From this figure, it can be seen that there is a clear trend of decreasing SFC over the years. Even though this decreasing trend seems to continue, the rate of decrease in SFC is also decreasing with the years as limits in component performances. Furthermore, with the addition of the emission requirements that became more apparent in the last few years, the design optimization problem became much more sensitive.

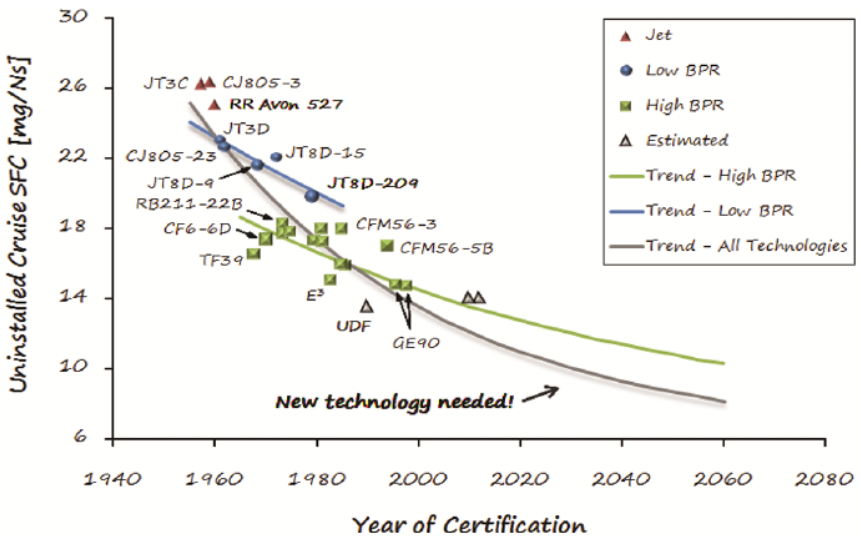

Figure 2.4: Trends of jet engine technology development quantifed in terms of uninstalled cruise SFC as a function of year of certifcation [18]

For commercial aviation, efforts are being made to reach higher an BPR and OPR. In Figure 2.5a and Figure 2.5b, the GE9X and Rolls-Royce Trent7000 engines are shown. The GE9X is a high BPR turbofan with a BPR of 9.9:1 and and OPR higher than 60:1[17]. The Trent7000 is also a high bypass turbofan engine with and OPR of 50:1 and BPR of 10:1[19]. In the engines coming into operation in the coming years, such as the new generation GEx90, the BPR is the highest so far.

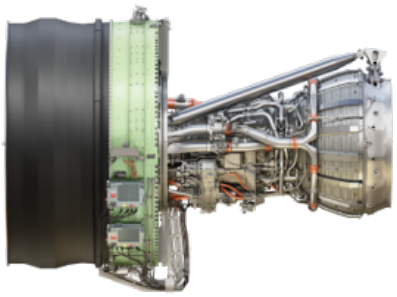

(a) GE9X High bypass turbofan[17]

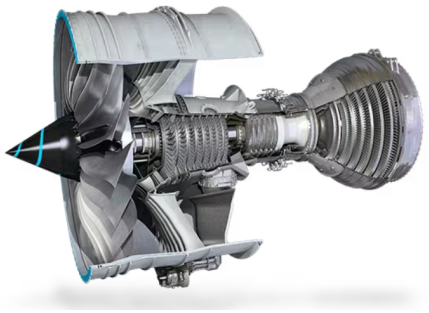

(b) Rolls-Royce Trent7000 High bypass turbofan[19]

Achieving high propulsive and thermal efficiency is favoured. Additionally, the propulsive efficiency and thermal efficiency are coupled. The design of the aircraft consists of compromises to optimize the thermal and propulsive efficiency.The propulsive efficiency can be improved through increasing the BPR, which in turn makes the engine bigger and heavier, aggravating installation penalties. Hence, it is not practical to constantly enlarge the engine BPR.Therefore, the engine propulsive efficiency is limited.[12] Especially, with the introduction of the geared turbofan engine, the propulsive efficiency can be kept on increasing towards the theoretical limit around 93%. For today's best turbofans propulsive efficiencies are now higher than 80% whereas thermal efficiencies only reach values around 50% and the rate of improvement is dropping. This is because the remaining losses in the turbofan architecture are becoming increasingly difficult to mitigate[6].

In the past, efforts to enhance thermal efficiency primarily focused on improving component efficiencies. However, a significant amount of the fuel's chemical energy continued to be wasted in the environment. Meanwhile, advancements in aero engine components and configurations only resulted in marginal performance gains, as the main turbomachinery component efficiencies have nearly reached their maximum potential. As a result, further improvements in this area cannot effectively drive future advancements.[13].

Increasing the thermal efficiency of the pure Joule-/Brayton-cycle based engines has become increasingly challenging over time. The increase in overall pressure ratio from 50 to 70 will only yield a 3% unit improvement.[6] Meanwhile complex cycles incorporating intercooling, reheat and regeneration can achieve thermal efficiencies of nearly 60%[20]. In order to meet the efficiency improvement goals, there is a need for a 40% reduction in losses of turbo components and an increase in OPR to 60 in order to reach the targets set for 2035. To achieve the targets set for 2050 using the Joule-/Brayton-cycle, turbo components would require 100% component efficiency and an OPR of 120. These figures are based on the assumption that the engine mass and relative turbine cooling air remain constant without any increase[21].To summarize, the propulsive efficiency for the state-of-the art turbofan engines are already high and is getting closer to the theoretical limit. On the other hand, there are much more room for improvement for the thermal efficiency for the new generation of aero engines.

The major loss sources for state-of-the-art turbofan engines for long-range applications that are relevant for the aero engines designs that will be released to the market in 2050 are identified[6]. Furthermore, various radical novel designs are elaborated that can potentially mitigate these losses. The breakdown of these losses are visualized in Figure 2.6. The three major loss sources are defined as the combustor irreversibilities, core exhaust losses and bypass flow losses.

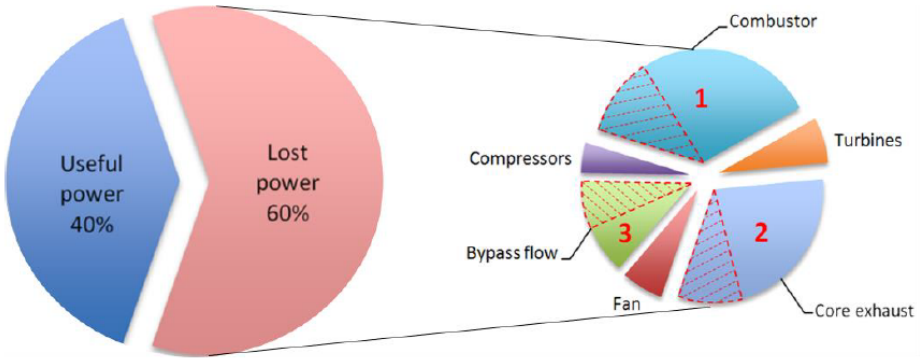

Figure 2.6: Breakdown of losses in a state-of-the-art turbofan for long-range applications[6]

The first loss source to be discussed is the combustor losses. Losses in the combustor occurs because of heat addition through internal combustion as it generates a considerable amount of entropy. By implementing a combustion process that involves a rise in pressure instead of maintaining constant pressure, significant advancements can be made in reducing combustor irreversibility. The composite cycle is a thermodynamic cycle that uses both the constant volume and the constant pressure combustion to increase efficiency which will be explained later in this part.

Three concepts that tackle this type of loss is the piston engine based composite cycle engine, nutating-disc engine and pulse detonation engine. The composite cycle piston engine will be detailed in the next section while the other two will be briefly explained here.

The second loss is the core exhaust loss, mainly caused by heat loss to the surroundings but excess kinetic energy and pressure losses due to fluid friction also contributes to this loss. To mitigate these losses, concepts such as bottoming cycle, recuperation and intercooling can be used.

The third loss source is the bypass flow loss. This loss is mainly associated to lost kinetic energy in the bypass flow. Friction losses in the fan, bypass duct and bypass nozzle also contribute to thus loss source. Tackling the bypass flow loss source is more straightforward then tackling the other two loss sources. By increasing the mass flow and reducing the exhaust jet velocities, the losses causes by excess kinetic energy in the bypass flow can be reduced substantially. Furthermore, it is expected that, by the year 2050, matured geared turbofan and open rotor technologies will be able to bring the bypass flow losses significantly. In conclusion, new and radically more efficient cores would have to make substantial reductions of combustor irreversibility and core exhaust loss, piece 1 and 2 in Figure 2.6, simply because other losses have become so small it is now difficult to make large cuts in these.

2.2. Aviation Fuels

In this section, various fuels that are used for aviation applications will be discussed. Firstly, important characteristics of aviation fuels will be presented, then different aviation fuels that are used will be explained.

From Figure 2.7, various energy carriers are compared. Having low weight is one of the most important criteria for flying. Therefore, fuels with high mass energy density and high volumetric density is crucial. Looking at Figure 2.7, it can be seen that kerosene has a high volumetric density and mass energy density. This makes kerosene quite favourable for aviation. Meanwhile, looking at hydrogen, it can be seen that it has a much higher mass energy density than kerosene but has a very low volumetric energy density. This makes hydrogen really difficult to store as very large tanks will be required to the required amount of fuel. Although storing hydrogen cryogenically increases the volumetric energy density, it causes other problems due to increased complexity of keeping the fuel in cryogenic temperatures. Therefore, storability and operability of the fuels are vital in design considerations. [22]

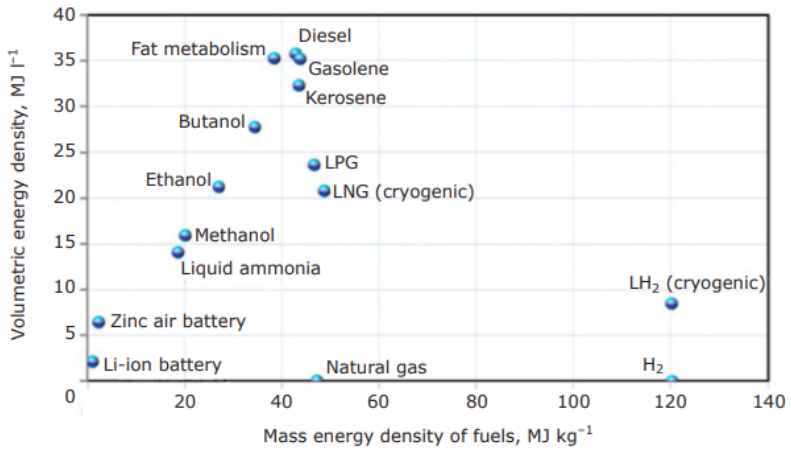

Figure 2.7: Comparison of various energy sources for aviation [23]

For reciprocating engines, there is two other fuel properties that is commonly used: the cetane and octane numbers[24]. Cetane number, or cetane rating, is a measure of the ignition value of a diesel fuel that represents the percentage by volume of cetane in a mixture of liquid methylnaphthalene that gives the same ignition lag as the oil being tested. Cetane number is important because it is an inverse function of the fuels ignition delay. Ignition delay is the time it takes between the start of ignition and the first measurable pressure increase during combustion. Lower cetane number fuels will have a higher ignition delay.

An octane rating, or octane number, is a standard measure of a fuel's ability to withstand compression in an internal combustion engine without detonating. The higher the octane number, the more compression the fuel can withstand before detonating. Octane rating does not relate directly to the power output or the energy content of the fuel per unit mass or volume, but simply indicates gasoline's capability against compression.

In contrast, fuels with lower octane but higher cetane numbers are ideal for diesel engines because diesel engines ,also called compression-ignition engines, do not compress the fuel, but rather compress only air and then inject fuel into the air that was heated by compression. Gasoline engines rely on ignition of air and fuel compressed together as a mixture, which is ignited near the end of the compression stroke by electric spark plugs. Therefore, high compressibility of the fuel matters mainly for gasoline engines. Using gasoline with lower octane may cause engine knocking or pre-ignition. The octane rating alone does not only determine the performance of the gasoline, but also the versatility of the fuel in handling a range of lean to rich operating conditions

In a typical Otto cycle spark-ignition engine, the air-fuel mixture is heated as a result of being compressed and is then ignited by the spark plug. This burning normally takes place via rapid propagation of a flame front through the mixture, but if the unburnt portion of the fuel in the combustion chamber is heated or compressed)too much, pockets of unburnt fuel may self-ignite before the main flame front

reaches them. Shockwaves produced by detonation can cause much higher pressures than engine components are designed for, and can cause a ”knocking” or ”pinging” sound. Knocking can cause major engine damage if severe.[25]

Octane ratings are directly linked to activation energies, which represent the energy needed to initiate combustion. Fuels with higher octane ratings require greater amounts of applied energy to initiate combustion. As a result, the likelihood of uncontrolled ignition, such as autoignition, self-ignition, pre-ignition, detonation, or knocking, is reduced when higher octane fuels are used during compression. [25]

2.2.1. Conventional Aircraft Fuel

The aviation sector uses petroleum based kerosene which is also called jet fuel. Kerosene based jet fuel is the most commonly used fuel in aviation. Such fuels are called jet fuel for gas turbines and aviation gasoline for piston-based engines such as United States (US) Jet A (European Jet A-1), Jet Propellant JP-4 (European F-40), JP-5 (European F-44), JP-7 (US only), JP-8 (F-34), JP-TS (US only), and JP-8 I 100 (US only)[26][27]. Kerosene based fuels are Jet A, Jet A-1, JP 5 and JP 8 with 8–18 carbons. Naphtha type fuels are Jet B and JP-4 with 5–15 carbons. These fuels are also used as blends of kerosene-naphtha and kerosene-gasoline (JP-4)[28].

Jet A: Jet A is a kerosene-based fuel that is widely used in commercial aviation. It has a high energy density, meaning it provides a lot of energy per unit of volume. Jet A is also relatively inexpensive and widely available. However, it produces emissions of carbon dioxide, nitrogen oxides, and sulfur oxides, which contribute to air pollution and climate change.

Jet B: Jet B is another kerosene-based fuel that is similar to Jet A but has a lower freezing point. It is often used in cold climates where the freezing point of Jet A may be too high. However, it is less energy-dense than Jet A and is therefore less efficient.

Avgas: Avgas, or aviation gasoline, is a high-octane fuel that is used in piston-engine aircraft. It has a higher energy density than Jet A but is also more expensive and less widely available. Additionally, it contains lead, which can be harmful to the environment and to human health.

2.2.2. Alternative Aviation Fuels

In order to reach the emission goals, alternative energy carriers for aviation has been gaining more attention[29]. In Figure 2.8, the alternative fuel routes for the future of aviation is presented. From this figure, it can be seen that various energy carriers are available for aviation applications. For jet engines, drop-in fuels produced from biofuels, which are more sustainable than kerosene, are being investigated. On the other hand, electric aviation is also considered to be an option especially for smaller aircraft. In that case, batteries can be used to run the electric motor of an aircraft. Hydrogen can both be used as a fuel for jet engines when stored cyrogenically or it can be used as a fuel cell to power an electric motor. For this report, fuels that are most relevant for jet engines for long range applications are of interest.[30] [31]

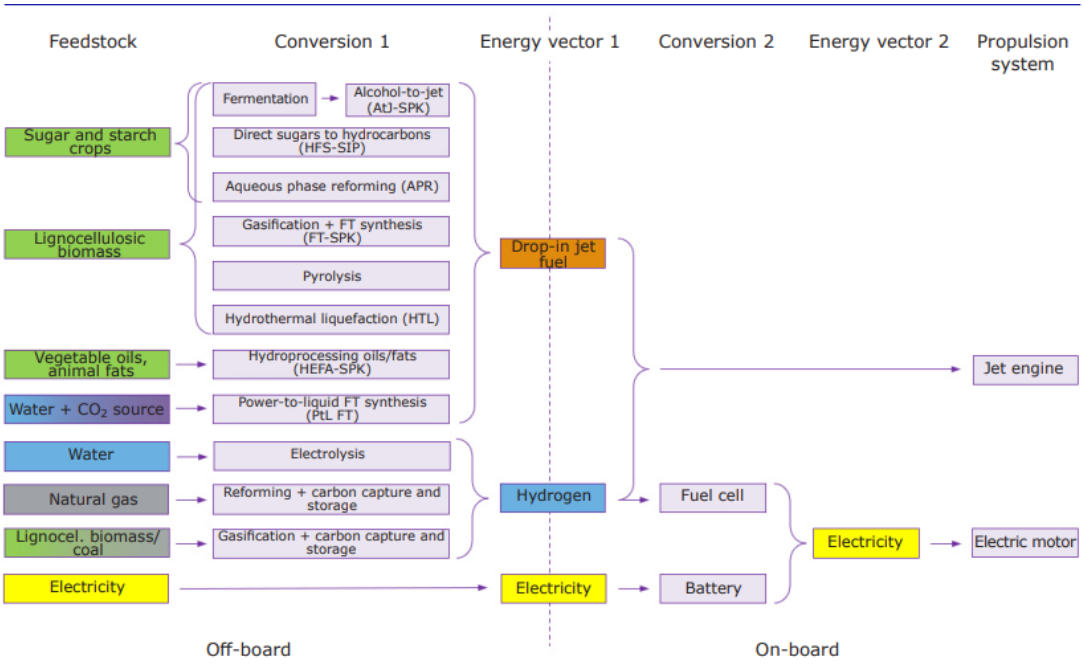

Figure 2.8: Overview of alternative fuel routes for aviation[31]

Hydrogen

Hydrogen can be used as a fuel for aircraft propulsion, either in fuel cells or in combustion engines. It is considered to be one of the main options to use as fuel to reach the emission goals as it offers great benefits to decrease emissions. The characteristic of hydrogen as a fuel and Jet-A are compared [32]. Hydrogen as a fuel is advantageous because it produces no carbon dioxide emissions. Besides the CO2, there are also no secondary emissions such as soot, CO, UHC and volatile organic compounds. Furthermore, H2 has a LHV that is almost three times the LHV of Jet A. Hydrogen can also be produced from renewable sources which is valuable for energy grid integration. On the other hand, hydrogen has certain disadvantages. Firstly, gaseous hydrogen has a low volumetric density. Therefore it has to be stored in cryogenic or in highly pressurized tanks. Also, these tanks can not be stored in the wings, only fuselage or in underwing pods. The liquid hydrogen requires pressurized tanks to be stored in extremely low boiling points. Adding the very diffusive nature of hydrogen into the equation, the storage tanks require high complexity. Lastly, compared to kerosene, there is much less infrastructure to support hydrogen aviation and hydrogen more expensive than kerosene. [22]

Hydrogen engines have the advantage of wide flammability limits, enabling their operation with significant dilution, either through excess air or exhaust gas recirculation (EGR). The laminar burning velocity and flame stability can exhibit considerable variation, making them crucial parameters to consider. The flame stretch rate is likely to have a significant impact on both the burning velocity and flame stability. [33]

The findings suggest that by progressively substituting conventional jet fuel (Jet A) with a fleet of aircraft powered by liquid hydrogen fuel, the cumulative CO2 emissions could reach a stabilized level and subsequently decrease below the specified target. This positive outcome can be achieved even with the continuous growth of air transportation demand. Specifically, the implementation of a cryogenic aircraft fleet, even at a conservative growth rate of 1,000% per year, could play a significant role in stabilizing, halting the increase, and subsequently reducing cumulative CO2 emissions. Alternatively, a more rapid introduction rate of 5% would have an immediate impact, effectively halting the emissions and leading to a continuous and substantial reduction by the end of the observed period (2060/65), surpassing the target of reducing emissions to 50% of the 2006/10 levels. [32]

Pratt & Whitney wants to associate its geared turbofan architecture with its Hydrogen Steam Injected, InterCooled Turbine Engine (HySIITE) project, to avoid carbon dioxide emissions, reduce NOx emissions by 80%, and reduce fuel consumption by 35% compared with the current jet-fuel PW1100G, for a service entry by 2035 with a compatible airframe.[34] The Airbus ZEROe project, unveiled in late

2020, aims to develop three concept aircraft: a turbofan, a turboprop, and a blended wing-body design. These aircraft are designed to be zero-emission and are scheduled to be operational by 2035. All three ZEROe concepts follow a hybrid-hydrogen approach, utilizing modified gas turbine engines that employ hydrogen combustion. Liquid hydrogen is used as fuel for combustion with oxygen.[35]

Electric

Although not classified as a traditional fuel source, electric power is gaining significant traction as a propulsion method for aircraft, particularly smaller ones like drones and electric planes. Electric aircraft are regarded as a promising solution to mitigate the environmental impact of aviation by offering zero emissions and reduced noise levels, while potentially attaining remarkable efficiencies. battery-electric motors have a higher efficiency (90%) than most jet engines (50%), which can be further exploited through emerging battery chemistries.Nonetheless, the range and speed of electric aircraft are currently constrained by battery capacity limitations[36]. Batteries serve as the predominant energy storage component for electric aircraft, owing to their comparatively high storage capacity. However, as of 2018, the specific energy of electricity storage remained a mere 2% of that offered by aviation fuel[37]. The 1:50 ratio renders electric propulsion unfeasible for long-range aircraft. To illustrate, a 930 km journey for a 12-passenger, all-electric aircraft would necessitate a six-fold enhancement in battery power density.[38].

Energy density is widely recognized to be the bottleneck for zero-emission electric powertrain.Hybridisation leads to better energy management with the benefits of reducing fuel consumption by up to 5% compared to a standard flight. The electrical sources could come from batteries or fuel cells which convert hydrogen into electricity. Electric aviation is mostly considered for Urban Mobility solutions. Electric VTOL aircraft or personal air vehicles are being considered for Urban Air Mobility. EVTOL's such as Lilium are getting attention[39]. Furthermore, in November 2022, Airbus unveiled its fuel cell-powered engine[40].

Liquefied methane - LNG

The studies and experimental tests have shown that LNG is a viable option as an alternative aviation fuel[28][30][31]; however, it is not used in normal service and operations. The main energy carrier in LNG is methane, which can also be produced from biomass pathways (e.g., liquefied biogas) and electrofuels pathways. However, several challenges remain in operating LCH4 aircraft, where design and construction of the LCH4 storage tanks and supply chain infrastructure are the biggest challenges. Cryogenic fuel tanks are required to operate LCH4 in an aircraft; these are larger and heavier than other fuel tanks. Compressed natural gas (CNG) and liquified natural gas (LNG) are fuel feedstocks that aircraft may use in the future[29] . Studies have been done on the feasibility of using natural gas[11] and include the "SUGAR Freeze" aircraft under NASA's N+4 Advanced Concept Development program (made by Boeing's Subsonic Ultra Green Aircraft Research (SUGAR) team). The Tupolev Tu-155 was an alternative fuel testbed which was fuelled on LNG.[27]

Biofuels

Biofuels are fuels made from renewable sources such as vegetable oils or animal fats. They can be used in aviation as a substitute for fossil fuels, and they produce fewer emissions than conventional fuels. However, they are currently more expensive than conventional fuels and can require modifications to aircraft engines[41].

Such fuels are also called "drop-in" fuels because these fuels can be implemented directly to the existing airplanes. These fuels are less restricted by crude oil resources. Moreover, the production process of these fuels is sustainable.[42]

Today, there are two biofuel types certified for aviation, both in maximum 50 % blends with conventional Jet A/A-1. One of these is hydrotreated vegetable oil (HVO) derived from oil seed plants. This type of biofuel is commercially available and in small quantities is already in use. The other type, Fischer-Tropsch (F-T) kerosene derived from lignocellulosic materials is to be expected on the market within 5-10 years. The life-cycle benefits of a HVO fuel are very sensitive to biomass feedstock as it needs oil seed crops. However, the fuel itself is cheaper than the other alternatives, and is expected to be competitive with aviation kerosene when subsidized. The F-T fuel is more expensive, but its feedstock is cheaper and it has a better environmental profile[43].

2.3. Aero Engine Solutions for the Future

The ambitious goals considering the emission requirements will need novel technologies with high performance to bring the to life. Especially solutions to increase the thermal efficiency of the engine will be of high importance. In this section, the aero engine design solutions that are considered for the future will be explained. The solutions that are discussed here mostly entails the design of the aircraft engine. Firstly, the current state of the aero engine technology will be put forth with details from state-of-the-art engines. Then, various novel technologies that will potentially be used for future aviation will be explained.

2.3.1. Concepts for Future

Following the identification of the main loss sources to be considered for future aero engine design, novel concepts for the future that tackle these losses were researched. In this subsection, the future applications for aero engines will be presented.

Open rotor

The use of high-speed advanced turboprops, also known as ”propfans,” on transonic transport aircraft gained considerable interest in the 1970s and 1980s when fuel efficiency was a primary concern in aeronautical research. However, with the significant decrease in fuel prices, the motivation to further develop this technology diminished. However, recent interest in unducted, open rotor propulsion systems has started investigations again[44].

This design is aims increase the propulsive efficiency by tackling the bypass flow loss. The open rotor concept is visualized in Figure 2.9a. As can be seen from this figure, this concept utilizes the advantages of the turboprop configuration where the intake fan is unshrouded.

At lower flight speeds, the turboprop configuration leads to a higher efficiency. On the other hand, with increasing Mach number, there is a sharp increase in the shock losses, which results in lower efficiency. Furthermore, the noise levels also increase substantially as flight speed increases. More recently, propellers incorporating sweep back have been developed, which can maintain their propulsive efficiency at higher flight Mach numbers. The ongoing research on the open rotor has demonstrated positive achievements regarding the increase in flight speed and noise reduction. With various developments of aero-acoustics and materials, the new generation open rotor designs achieve a considerable decrease in noise levels. Furthermore, such turbo-propeller turbines have been developed and demonstrated. They show that a 20% reduction in fuel consumption is possible[20].

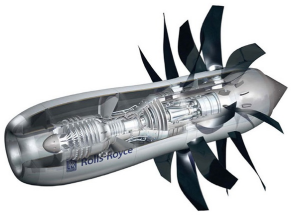

(a) Open Rotor Concept by Rolls-Royce[45]

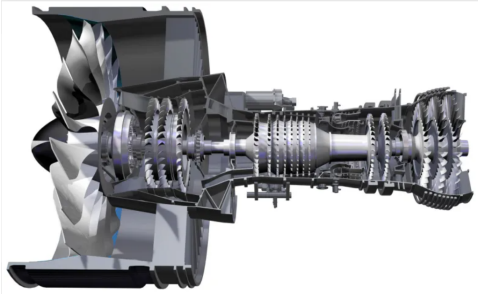

(b) The Pratt and Whitney PW1100G Geared Turbofan Engine[46]

Geared Turbofan

Another design aimed to increase the propulsive efficiency is the geared turbofan configuration. This system, similar to open rotor, is to decrease the bypass flow loss. In the geared turbofan configuration, the fan is decoupled from the LP shaft to enable for each component to rotate at their optimum speed. An example of the geared turbofan configuration can be seen in Figure 2.9b.

As the BPR increases, the SFC decreases, although at decreasing rate. However, with improved core performance, the high BPR engines can go upto a value of 12 for the BPR[17].The increasing BPR of the engine allows for higher propulsive efficiency. At such high BPRs, the LP turbine speed decreases. This is because, the LP shaft also drives the fan and the fan-tip speed is often the limiting factor for the LP turbine rotational speed. Therefore, the LP turbine will require more stages and increase the weight of the engine. With light-weight gearbox the LP turbine speed would increased,

reducing the number of LP turbine stages and hence the weight of the LP turbine. If the reduction in LP turbine weight were greater than the weight of the gearbox system, then the fuel burn would decrease[20].

To summarize, the de-coupling of the fan from the LP shaft with GTF configuration, increases efficiency, decreases noise and leads to a lighter system.

IRA - Intercooled Recuperated Aero Engine

The IRA concept is mainly designed to minimize heat losses in the engine and increase the thermal efficiency. This concept tackles one of the main sources of loss in the engine, the core exhaust loss. IRA concept was researched by MTU[13]. In Figure 2.10, the IRA concept developed by MTU is visualized.

To enhance the performance of the aero engine, a crucial factor is reducing the losses of waste heat energy. This can be effectively accomplished by integrating a recuperation system into the exhaust nozzle of the engine. In this approach, a series of heat exchangers are positioned within the exhaust nozzle, downstream of the low-pressure turbine exit. This arrangement enables the utilization of a portion of the high-temperature gas's thermal energy to heat the air discharged from the compressor before it enters the combustion chamber. As a result, this integration promotes fuel efficiency and contributes to lower levels of pollutant emissions.

Adding an intercooler and a recuperator adds considerable complexity and mass to the engine. Due to the significant weight increase, this engine has not been able enter the market. Although, due its ability to decrease the core exhaust losses, this concept has still potential to be used in the future.

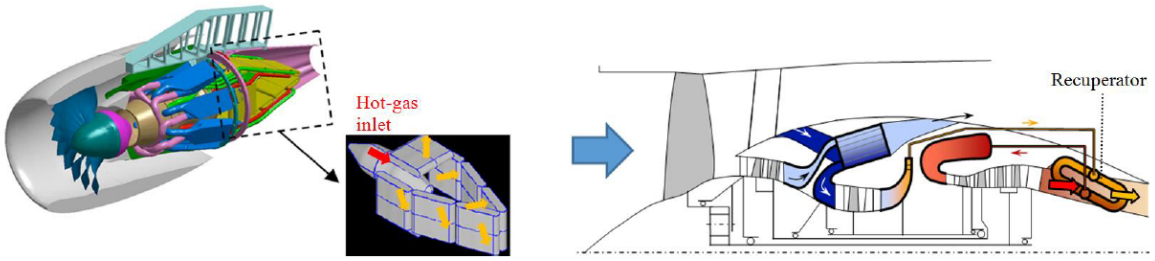

Figure 2.10: The IRA - Intercooled Recuperative Aero-engine Concept (red: hot gas inlet, orange: flow through recuperator banks) fromMTU[13]

ITB Burner concept

The interstage turbine burner (ITB) is also a concept to reach higher thermal efficiencies. It is an afterburner located in the duct between the HPT and LPT. In theory, with ITB burner, the specific thrust increases while efficiency decreases like an afterburner. Compared to the conventional afterburner, the ITB has a higher thermal efficiency. This is because, for the ITB, the secondary combustion occurs at a higher pressure than the conventional afterburner since the afterburner is located downstream of the LPT whereas ITB is located between HPT and LPT [12]. The ITB configuration increases complexity and mass of the engine, but can be beneficial in decreasing emissions. Especially with low NOx combustion methods, ITB offers promising solution. The ITB has been applied in industrial gas turbines due to its operating flexibility and potentials to reduce emissions but not applied to commercial aircraft due to lower efficiency and added mass.

Nutating Disc

One of the ways to increase thermal efficiency is by using constant volume combustion along with the constant pressure combustion as an intermittent cycle. There are various concept described in [47] that utilizes both constant volume and constant pressure combustion. Even though constant volume combustion through piston engines have been around for quite some time, its implementation to new generation aero engines is quite a recent innovation.

One of the concepts that utilize this is the nutating disc engine. Shown in Figure 2.11b, the Nutating Engine features an internal disk nutating (wobbling) on a Z-shaped power shaft. Similar to the combined pistone ngine concept, the nutating engine also uses the composite cycle. The nutating engine offers a notable benefit, wherein each side of the disk is utilized once during each revolution of the engine. This characteristic ensures a lightweight and consistent volume-based combustion solution[6].

Consequently, the engine is very compact, and several times more power dense than any conventional (reciprocating or rotary) IC engine.

After undergoing development and testing for a UAV engine, the nutating engine concept holds the potential to deliver a solution that is compact, highly efficient, and exhibits low vibration[47]. Besides addressing architectural considerations, there are significant technological hurdles to overcome. These challenges encompass the aero thermodynamic interaction between the piston and turbo components, optimizing engine rating and part power, and ensuring the maintenance of efficient combustion processes with ultra-low emissions[6][47].

Pulse Detonation

Unlike the two reciprocating concepts, the proposed implementation of the pulse detonation core concept eliminates the need for an additional conventional combustor to achieve the high temperatures characteristic of a gas turbine[47][6]. The pulse detonation concept is shown in Figure 2.11a.

The operation of the tubes follows a cyclic pattern consisting of four stages. In the initial stage, purge air is introduced into the tube to cool it down and remove any residual combustion products from previous detonations. Moving to the second stage of the cycle, the tubes are filled with a mixture of fuel and air. Alternatively, fuel injectors can be employed instead of pre-mixing the fuel and air. This approach helps mitigate the risk of autoignition. The subsequent stage involves closing the inlet valve and initiating combustion by creating a localized spark near the tube inlet. This ignition event causes a transition from deflagration to detonation combustion, with the detonation wave rapidly propagating through the tube. Following this swift step, the final stage is to allow the tube to discharge the hot, pressurized gases. The concept holds the potential to not only recover a portion of the dynamic energy produced during detonation waves but also surpass the performance of the two alternative constant volume combustor concepts[47].

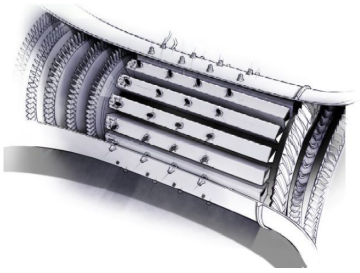

(a) Pulse Detonation[47]

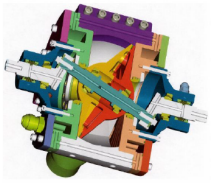

(b) Nutating disc[47]

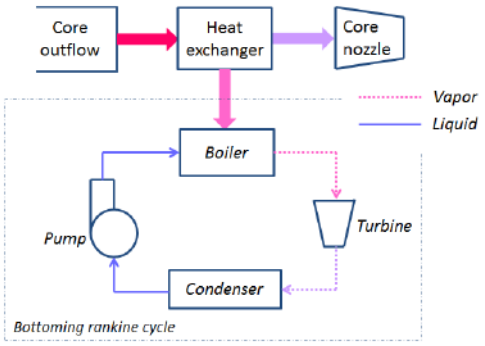

(c) Rankine Bottoming Cycle[47]

Rankine Bottoming

By extracting heat from the core flow, the Rankine bottoming cycle technology effectively lowers the temperature at the core nozzle exit. This heat is then employed to warm a fluid in a secondary fluid system, enabling the generation of additional power. The working principle of the Rankine bottoming cycle can be observed in Figure 2.11c. Combining this cycle with a topping gas turbine has proven to be a highly effective method in achieving exceptional efficiency for stationary power generation[47].

The utilization of Rankine bottoming for aero engine application has gained significant attention in recent times. This concept has prompted key research objectives, including the development and optimization of the secondary system regarding the design and integration of bottoming cycle components. Additionally, evaluating part load performance and investigating various secondary fluids are crucial research tasks. Notably, exploring synergies with intercooling and composite topping technology holds the potential to deliver fuel efficiency benefits[47].

Composite Cycle

Another important method that allows for an increased thermal efficiency is the composite cycle concept. A composite cycle is defined as an integrated assembly of at least two heat engine cycles featuring independent compression, heat source, and expansion operating on the same working fluid[48].

The primary advantage of the Composite Cycle is the higher peak pressure and temperature. The second major benefit is the (partially) isochoric combustion, which results in a pressure increase achieved through heat addition rather than relying on shaft power like in a turbo compressor[47]. The piston cycle added to the conventional turbofan cycle leads to higher peak pressures. Furthermore, utilizing constant volume combustion along with the conventional turbofan cycle can result in a significant decrease in the combustor losses[6][49]. In Figure 2.12, a qualitative comparison of the temperature-over-entropy diagram for a conventional turbofan and the composite cycle is presented.In this figure, the straight lines represent the conventional Joule-Brayton cycle and the dotted lines represent the composite cycle. It improves the thermodynamic cycle by putting a topping cycle upon the Joule-/Brayton-cycle[21]. The thermodynamic benefit of the composite cycle is due to the unsteady operating principle of the piston engine[49]. The unsteady cycle starts with a mixture of fresh air coming in at station 3' and the residual gas from the previous piston cycle. Compression at high pressure in the pistons leads to a higher efficiency than compression in the turbocomponents. One of the reasons for this is that at small reduced mass flows, clearance losses dominate. Furthermore, due to very small amount of heat losses occuring, the piston compression can be assumed to be isentropic. Then, when the combustion takes place at isochoric conditions, there is also a large pressure rise. In the subsequent stages of combustion, expansion occurs simultaneously with piston movement. This expansion involves an isobaric heat addition. Furthermore, the expansion process remains close to isentropic due to heat losses. The air is subsequently expelled at station 35'.

The unsteady nature of the operation permits significantly higher peak temperatures and pressures within the cycle compared to a stationary gas turbine. However, these conditions only need to be sustained for very brief durations, while the average temperature remains comparable to that of a gas turbine. Consequently, this leads to an increased thermal efficiency. Therefore, in order to limit the peak pressure in the piston engine, the pressure ratio in the turbocomponents are typically lower than in the conventional turbofan engines. This in turn leads to a lower exhaust temperature, $T_{5'}$. Also, in order to keep the efficiency as high as possible, the exit temperature $T_{4'}$ after the sequential combustor, which does the constant pressure combustion, is kept low. The free piston composite cycle concept that is investigated in this report, utilizes the composite cycle explained. Further detail on the the engine concept using this composite cycle will be presented in Section 2.4.

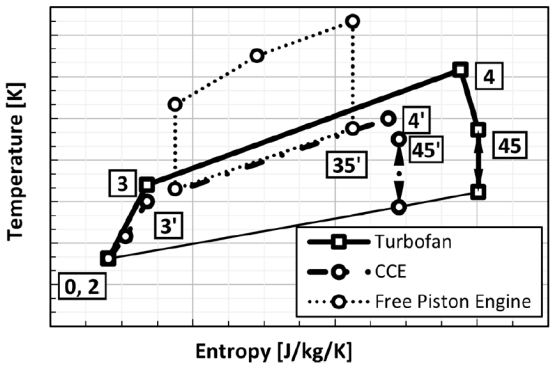

Figure 2.12: Enthalpy of entropy -diagram of the Composite Cycle and conventional Joule-Brayton Cycle[49]

2.4. Free Piston Composite Cycle Engine

In this section, the free piston composite cycle engine concept will be discussed. The composite cycle engine concept where a piston engine is used along with the turbofan was first introduced in paper by Kaiser et.al.[48]. In theory, this concept could achieve a higher core efficiency by employing discontinuous cycles for constant volume combustion, achieving an OPR above 100 (hecto-pressure ratio). In this study, it was determined that the this engine can reach peak pressure ratios above 300, provides an improvement in TSFC of 17.5% meanwhile leading to a 31% increase in weight. Moreover, it was argued that the CCE engine displays reduced emission index compared to the reference turbofan due to shorter residence times at high temperatures and pressures. A major contributor to lowered NOx emissions is the Joule/Brayton combustion chamber's decreased stoichiometric flame temperature. [48]

Kiaser compared three different thermodynamic cycles: conventional turbofan cycle as reference, composite cycle and cycle-integrated parallel hybrid [14]. These cycles were evaluated to assess their potential in reaching the emission targets set for 2035. The analysis was made on a short-to-medium range aircraft at Top of Climb (TOC) conditions. The piston engine characteristics were modelled for a two-stroke crankshaft engine using the Seiliger cycle. The piston system weight has been determined based on simple geometric representation of the piston engine setup and the volumetric efficiency. The mass of the piston and other components are taken into account using empirical relations. This report concluded that the composite cycle engine was most promising with providing 25.8% fuel burn over state-of-the art turbofan engines.

In [50], Kaiser et.al investigated the synergetic combination of the composite cycle engine with pistons and the Intercooled Recuperated engine that employs recuperators to utilize waste heat from the core engine exhaust, and intercooler to improve temperature levels for recuperation and to reduce compression work. After conducting a screening process for intercooler options, it was found that installing the intercooler in front of the piston system offers a notable benefit of up to 1.9% reduction in fuel.In this paper, it was concluded that only the application of an intercooler appears to provide a considerable benefit for the examined thermodynamic conditions.

Following the promising results obtained for the analysis made on the piston engine CCE concept, in this novel engine concept is analyzed to see how it would perform when the concept is applied to a year 2050 long range turbofan that uses the GTF configuration[51]. This paper evaluates aircraft engines within the context of an advanced tube and wing aircraft platform envisioned for 2050. In this paper, it was found that the baseline CCE concept improves the TSFC by 8.8% and increases the total engine weight by 41%. The advantages of the combination of intercooler with the CCE concept is also discussed in this paper. Firstly, there is an additional 2.5% fuel burn improvement while decreasing the engine weight. Secondly, the baseline CCE concept leads to a 15% higher NOx emissions than the conventional GTF. Meanwhile, the intercooled CCE has 12 % lower estimated NOx emissions on average than the GTF. Although, in cruise, simulated NOx emissions are 181 % higher than the GTF's for the CCE, and 97 % for the intercooled CCE.

In Grönstedt et al.[6], various concepts that were selected for the ULTIMATE project that will go into service in 2050 are evaluated.The results from this paper shows that compared to the reference performance values for 2050, various designs using constant volume combustion achieved double-digit fuel reductions. So, it was concluded that constant volume combustion could yield efficiency gains that very few radical concepts promise to deliver. Most of the increased efficiency is because isochoric combustion generates less entropy compared to isobaric combustion. In addition, in this paper, the three concepts that aim to decrease combustor irreversibility (piston engine CCE, nutating disc, pulse detonation) were compared. It was concluded that the piston CCE engine is closest to market, because of vast experience with four stroke diesel engines in the automotive sector. In addition, it was mentioned that the findings imply that while transitioning beyond the tube-and-wing architecture is essential, merely doing so may not be adequate. A greater level of integration between the airframe and innovative propulsion systems is necessary to align with the ACARE 2050 targets.

In 2020, Kaiser published a PhD thesis on Multidisciplinary Design of Aeronautical Composite Cycle Engines[21] which is the body of work that goes into the most detail about the CCE engine with pistons. The engine architecture considered in this report is constructed considering kerosene combustion.

The first time in this report, the free piston engine concept is considered for the CCE architecture. The free piston simulation in this report is conducted by making certain assumptions about the free piston performance compared to the baseline crankshaft engine in terms of change in power, mean

piston velocity and transmission efficiency. The thermodynamics of the free piston engine is solved using the same method as the pistons with the crankshaft. So, in this study, the details of the free piston is not considered. It was determined that the crankshaft configuration engines do not reach the CO2 emission reduction targets set for 2035, but has potential to reach them with minor improvements in propulsive efficiency. Meanwhile, the free-piston gas generator concept led to fuel burn improvement of 9.6%, exceeding the efficiency targets for 2035.

In the article by [49], the concept and the design choices of the free piston composite cycle engine (FP-CCE) is explained further. In Figure 2.13, a schematic illustration of a potential implementation of the FP-CCE concept is presented. Similar to a conventional turbofan, the flow is separated after the fan as bypass and core flow. The assembly can be considered as a self-powered gas generator as the gained usable power from the combustion process drives the piston compressor. The free-piston gas generator supplies high-temperature and high-pressure gas to the gas turbine core engine. Subsequently, the exhaust gas from the free-piston enters the combustion chamber of the gas turbine to further increase the temperature at the turbine inlet. The downstream components are typical of a turbofan engine, with turbines driving both the fan and the upstream compressor[49].

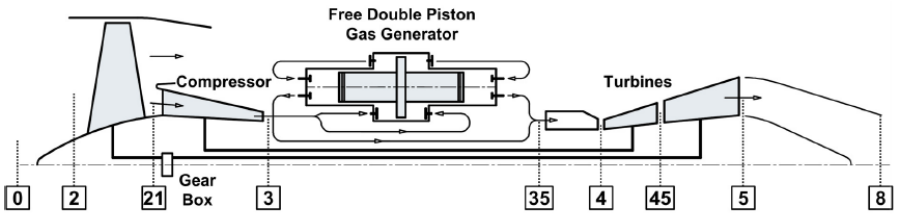

Figure 2.13: Scheme of a half-side arrangement of the proposed free-piston composite cycle engine concept supplemented with standard engine station nomenclature[49]

Firstly, the free piston concept offers a much more lightweight solution compared to the crankshaft bound piston engine concept as many mechanical components are taken out[49]. Secondly, in a free-piston engine, the mechanical forces are highly reduced, as no lateral forces are present apart from the piston weight.Mechanical losses in crankshaft bound piston engines are in the order of 5-10%, while losses conventional turbofan engines are in the order of 1-2%[49]. This disadvantage is eliminated by the free piston concept as the losses due to the lateral forces caused by the connecting rod are eliminated. Therefore, the free-piston concept offers significant advantage in eliminating mechanical losses. In turn higher mean piston velocities can be achieved compared to crankshaft bound piston engines and more energy can be extracted from the piston engine. So, for a given mass flow rate and power output, a smaller piston can be used, which will result in a lighter and more compact design. On the other hand, because the kinematics of the pistons are not bounded by the crankshaft but are controlled by the forces acting on the pistons, the control of the free-piston engine is more challenging.Looking at scavenging losses, they are quite similar between a crankshaft bound piston engine and the free piston engine. On the other hand, free piston engine requires an external source to provide auxiliary power for various systems such as fuel injection and valve actuation. For crankshaft bound piston engines this is not necessary. So, the required mechanical power for take-off is higher for the free piston engine[49].

In [21], two-stroke is compared 4-stroke operation for the composite cycle engine concept. It was found that, compared to the four-stroke engine, using two-stroke engines leads to a 3.7% decrease in efficiency, while decreasing mass by 23.2%. It is stated that this decrease in masss leads to an additional 1.1% fuel burn improvement. Furthermore, the overall pressure ratio is higher for the two-stroke engine, while the combustor exit temperature is similar. Due to higher temperatures being reached within the pistons, the NOx emissions increase by around 50 %. The total CO2 emissions of an aircraft are directly linked to the amount of fuel burned during its mission. A previous study evaluated the potential fuel savings compared to a turbofan engine of a similar technological level, estimating a reduction of around 15%. This improvement was achieved through a 14% decrease in TSFC, an 11% increase in engine weight, and subsequent cascading effects on the aircraft level due to the reduced fuel weight that needs to be carried. Due to the higher peak temperatures and pressures in the piston engines, NOx emissions are a challenge. The FP-CCE concept is expected to have higher NOx emissions than future turbofan engines with lean-burn combustor technology[21].Furthermore, If the constant volume

combustion cycle is realized, it is very likely to be used together with intercooling, possibly optimized to minimize NOx. Variable intercooling could be used to minimize NOx emissions. Furthermore, the power needed for compression within the piston compressor decreases. Therefore, can contribute positively to the weight of piston engines. However, this advantage comes with a slight decrease in efficiency and the inclusion of the intercooler's weight.[21]

In the paper by Nickl.et al released in 2022[52], the applied time resolved 0D piston engine performance simulation model of the CCE is adapted for hydrogen combustion. To model the free piston engine The BHL-inhouse piston simulation program PEPSI was modified. In this study, the free piston engine is not considered. Instead, a piston with crankshaft is simulated for hydrogen combustion. This report presents a senstivity analysis for showing the effect of valve timing and piston cylinder geometry. Furthermore, the piston engine specifics used in this simulation are for a generic piston engine rather than the piston engine that will be able to be integrated in the FP-CCE concept. The input data is quite limited whereas the output data for the piston is not given except the relative changes to the performance data. Therefore, this study does not consider the effects of free piston combustion with hydrogen, and the integration of the piston using hydrogen fuel into an aircraft engine architecture. In this paper, it was identified that the piston peak pressure level is the technological limiting factor for the development of the CCE design. The effects caused by the combustion characteristics of hydrogen will result in higher peak pressures higher heat losses occurring to the piston wall compared to when kerosene is used as fuel. Lastly, this report concludes that the intercooling technology will be expected to be synergistic with H2-CCEs.

2.5. Free Piston Engines

A free-piston engine (FPE) is a new type of energy converter, which eliminates the crankshaft and connecting rod mechanism. The free piston engine is a unique thermal hybrid propulsion machine inherently with a higher thermal efficiency than its counterpart, the Conventional Reciprocating Piston Engine (CPE)[53]. The piston motion of the FPE is not kinematically constrained like the CPE with a crankshaft. The piston motion only depends on the pressure differences that develop when the piston reaches either dead center. The piston operates without any mechanical constraints and undergoes unique strokes with each movement. Therefore, the stroke length and the compression ratio can vary almost instantaneously in each cycle. This allows, for the optimization of the compression ratio with different fuels and operating conditions, without major hardware modifications [53][54][55]. With the ability of the FPE to use various fuels with different compression ratios and indicated power, system efficiency of a FPE can be significantly improved by optimizing the thermodynamic cycle[56]. The free piston engine's structural simplicity enables it to achieve a higher power density due to the reduced number of moving parts, resulting in decreased weight and space requirements. Additionally, this design leads to lower friction loss and eliminates side forces caused by the crank mechanism.[54]In addition, the absence of the conventional kinematics to constrain the piston motion allows the systems dynamics to influence its trajectory, now directly via its coupled translational loads. Moreover, the dynamically constrained FPE can inherently explore an extensive range of piston motion profiles and trajectories during its development and operation, which may be vital in reducing and, in part eliminating in-cylinder combustion emissions[57].

2.5.1. Configurations

Free-piston engines can typically be classified into three groups according to their piston arrangement. Another classification, known as free-piston gas generators, distinguishes engines where the load is exclusively derived from an exhaust turbine rather than a mechanically coupled load device connected to the engine. The distinct characteristics of each FPE architecture will be presented in this section.

Single-Piston

The single-piston is a relatively simple architecture with moderately easy control. The single-piston architecture is visualized in Figure 2.14a. This engine essentially consists of three parts: a combustion cylinder, a load device, and a rebound device to store the energy required to compress the next cylinder charge. The main advantage of the single-piston design compared to the other free piston engine configurations is the high controllability. The rebound device allows for accurate control of the amount of energy put in the compression process, therefore, regulates the compression ratio and stroke length[55].

Studies suggest that effective management of compression ratios can result in reduced in-cylinder emissions and improved Brake Specific Fuel Consumption[53]. Furthermore, the single piston engine has advantages regarding costs, efficiency, control, and the simplicity of its construction. The evaluation also shows that the single piston concept has no disadvantages regarding vibrations, not even when the piston stroke is not balanced with a counter weight[58].

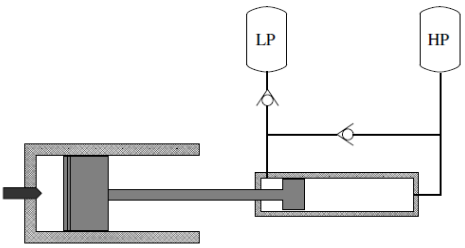

(a) Single piston hydraulic free-piston engine[55]

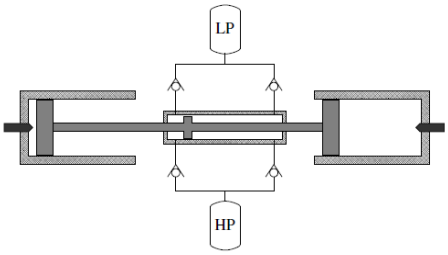

(b) Hydraulic dual piston free-piston engine [55]

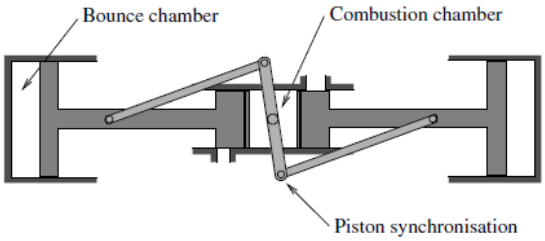

(c) Illustration of an opposed piston free-piston engine with piston synchronisation mechanism.[55]

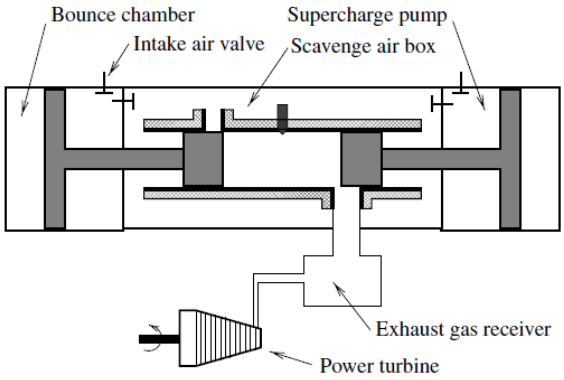

(d) Illustration of a free-piston gas generator [55]

Figure 2.14: Various Piston Engine Configurations

Dual Piston

The dual piston engine configuration is shown in Figure 2.14b. In this configuration, the rebound device is not required since the working piston itself generates the force needed to drive the compression process in the other cylinder. Therefore, this design allows for a simpler and more compact device with a higher power-to-weight ratio. On the other hand, having no rebound device produces certain disadvantages. The control of the stroke length and compression ratio becomes more difficult. This is because the combustion process that occurs in one cylinder, drives the compression in the other cylinder. So, even small irregularities in the combustion process can have a large influence on the next compression process. Therefore, the combustion process and the piston motion needs to be controlled and optimized for high efficiency and low emissions. Furthermore, research has shown that the dual piston configuration is highly sensitive to load differences and large variations for each cycle[55]. Lastly, dual piston engines have vibrations challenges to address if it is not combined with a second engine to provide a balanced design[53].

Opposed-Piston

The opposed piston free piston configuration has two single piston units, connected by a common combustion chamber. Each piston has a rebound device. Also, a load device can be coupled to one or both of the pistons. In Figure 2.14c, an opposed piston free-piston engine, with a mechanical piston synchronisation mechanism is shown.

The primary advantage of the opposed piston configuration is its perfectly balanced and vibration-free design. This characteristic sets it apart from other free-piston configurations that require additional methods to control vibrations. Another advantage of the opposed piston design is the reduction in heat transfer losses due to the absence of a cylinder head. This design also enables the use of uniflow scavenging, leading to high scavenging efficiency[55].The most important disadvantage of the opposed piston design is the requirement for a piston synchronisation mechanism. Considering also the need for a dual set of the main components, the engine becomes complicated and bulky[58].

Free Piston Gas Generator

Free-piston gas generators are engines that supply hot gas to a power turbine without any mechanical load on the engine itself, except for supercharging the intake air. The work output is solely derived from the power turbine. In Figure 2.15 an opposed piston free-piston gas generator plant is illustrated.

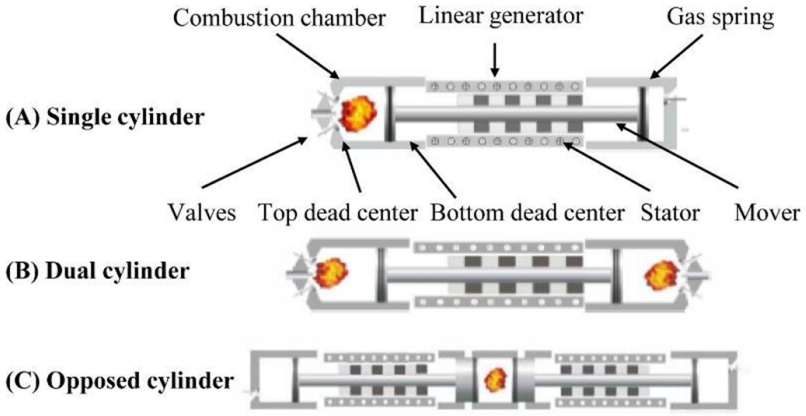

Figure 2.15: Illustration of a free-piston gas generator[59]

In comparison to conventional gas turbines, free-piston gas generators offers higher compression and pressure ratios. Additionally, they differ in the way the work required to compress the intake air is already extracted from the gas before it is supplied to the power turbine. As a result, the gas entering the turbine has a lower temperature, which reduces material requirements and allows the turbine to be positioned farther away from the combustor, minimizing heat transfer losses. The operational characteristics of a free-piston gas generator closely resemble those of other free-piston engines of the same configuration[55]. Based on the count of combustion chambers, available free piston gas generators can primarily be categorized into three groups: single-cylinder, twin-cylinder, and opposing-cylinder configurations[59].

The single-cylinder configuration typically includes a rebound device for pushing the piston from BDC to TDC. Combined with a controllable rebound device, the free-piston of single-cylinder FPLG can produce precise reciprocating motion which leads to better controllability. The dual-cylinder configuration is equipped with two combustion chambers. Under a two-stroke combustion cycle, each stroke of the free-piston motion is a power stroke. While one chamber is in the combustion stroke, the other is in the compression stroke that is immediately followed by the combustion. Hence, the combustion state at one end can directly affect the position of TDC on the other side. The dual-cylinder configuration can be designed in a compact size for higher output power. Compared with the single-cylinder, it is more difficult to ensure the consistency of the piston motion and dead centers.In the opposed cylinder configuration, the combustion chamber is placed in between the two pistons. When the fuel burns, the pistons on both sides are simultaneously pushed. The explosive force produced by combustion at each piston can be counteracted by the opposite direction of forces. However, the compression ratio is determined by the synchronized motion of the pistons, therefore, the motion has a significant effect on

the combustion process. The opposed piston structure is well-balanced but the piston synchronization control is quite complex[59]. The most recent developments on the free piston technology has been mostly on the dual-piston configuration, with approximately 80 % of the papers reviewed by Brosnan considers dual-cylinder engines[53]

2.5.2. Ignition Methods

Another important characteristic in a reciprocating engine is the method of ignition. Reciprocating engines can either work with spark ignition or compression ignition [25].

Spark Ignition

In the conventional spark ignition engine, fuel is injected into the intake port right before the intake valve (multi-point injection). This process allows a combination of air and fuel to enter and be compressed once the intake valve is closed. Prior to reaching the top dead center, the compressed mixture is ignited using a spark plug therefore it is called spark ignition. Since both intake and compression strokes are used for mixing fuel and air, the mixture is nearly homogeneous at the end of the compression stroke.

The amount of inducted air is regulated through valves, measured and the fuel is injected proportional to the amount of air that is available.Usually, this is done so that the medium air ratio $\lambda_a = 1$ is maintained. Therefore, the mixture is quantity regulated in spark ignition engines. In order to prevent auto-ignition in the compressed air fuel mixture, the compression ratio is restricted. In **??**, the engine map of a four-stroke spark ignition engine is shown. The characteristic map is limited by the idle and limit speeds as well as by the maximal torque line. Since the pressure is proportional to the torque times the engine speed, the constant performance lines are hyperbolas in the engine map. These lines, chondiodal curves, represent lines of constant specific fuel consumption.

Compression Ignition

The conventional diesel engine uses compression ignition. Furthermore, in the diesel engine, only air is taken in and compressed. Fuel is injected to the compressed air right before TDC.

At that point, the temperature of the compressed air is is higher than the autoignition temperature of the fuel. After a short time, the ignition lag time, autoignition occurs. Contrary to the spark ignition engine, the mixture is not homogeneous during ignition. Due to the short time between start of injection to autoignition, fuel and air can not mix fully, there the combustion proceeds in partial simultaneity. Therefore, the combustion process does not occur in a uniform way.

Compared to the SI engine, speed is in a narrower range and the actual medium pressure is higher. The control of the diesel engine is determined by the quantity of injected fuel, which is commonly referred to as fuel quantity regulation.While in the conventional SI engine the air ratio is always $\lambda = 1$, in the case of the diesel engine it varies with the load and changes between $1.1 \leq \lambda \leq 10$.

Another novel way of using compression ignition is the Homogeneous Charge Compression Ignition (HCCI). Essentially, HCCI combustion operates without the need for spark plugs or injectors to initiate the combustion process. Instead, combustion occurs spontaneously at multiple points once the mixture reaches its activation energy. This combustion method is noticeably faster than both compression ignition (CI) and spark ignition (SI) combustion. HCCI offers improved thermal efficiency and reduced emissions by modifying both CI and SI engines. It is compatible with a wide range of fuels, fuel combinations, and alternative fuels. However, there are challenges to overcome, such as controlling the combustion phase, dealing with limited operating range and cold starts, managing high noise levels, and preparing a homogeneous charge. Successful operation of HCCI engines requires addressing these issues[60]. The thermal efficiency of conventional diesel (CI) engine is around 30–40%; however, if diesel is used in HCCI engine, it increases thermal efficiency to 40–45% [61]. In conclusion, HCCI combustion can be implemented in existing CI engines with modifications, resulting in lower emissions of NOx and soot while maintaining comparable performance to CI combustion. Nissan is developing this technology further for commercial applications[62].

In the paper by Goldsborough and Van Blarigan[63], the numerical analysis on a free piston internal combustion engine operating on HCCI has been made. The engine considered in this paper operates in two-stroke mode and uses hydrogen as fuel. The conclusions from this paper can be summarized as follows. Firstly, the operating compression ratio in this engine can be adjusted based on various factors, allowing for control over thermal efficiency and performance. These factors can be equivalence ratio, scavenging efficiency, intake temperature etc. Secondly, the rapid and near-constant-volume

combustion process in HCCI eliminates burn duration as a limitation to achieving high efficiency with high compression ratios. Thirdly, HCCI combustion enables significant reduction in NOx emissions due to low equivalence ratio homogeneous charge combustion, potentially eliminating the need for exhaust gas after-treatment. Finally, proper piston dynamics are crucial for complete combustion and minimizing NOx emissions in the HCCI process, requiring careful control of piston motion near TDC.The success of the free piston engine depends on optimizing the scavenging process to prevent limitations on the achievable compression ratio and fuel loss through the exhaust port.

2.5.3. Free Piston Engine Modelling

There are various efforts to model various free piston configurations, yet, an opposed free piston model that uses HCCI combustion for hydrogen has only been investigated experimentally by Sandia Labs [64] . Furthermore, There are various efforts in literature modelling free piston engines[56][63][65][66] [67]. The free piston HCCI is modelled by Alrbai [68] and Goldsborough [65]. Sandia Labs experimental study on the free opposed piston model with H2 HCCI combustion that can operate at an high compression ratios (around 30) and at low equivalence ratios (around 0.35). The results of the experiment showed that this engine can reach indicated thermal efficiency higher than 50% with a design power output of 30 kW. Thus engine was motored with a pneumatic drive system utilizing bounce chambers. Furthermore, the use of linear alternator to generate electricity and control the compression ratio was also explored in these experiments.

Goldsborough and Van Blarigan modelled and analyzed the steady-state operation of a dual-cylinder free piston engine generator that uses hydrogen as fuel to reach HCCI combustion[63]. This analysis utilized a zero-dimensional thermodynamic model incorporating detailed chemical kinetics, as well as empirical models for scavenging, heat transfer, and friction components. This engine was also designed to operate for lean hydrogen combustion (phi around 0.3) at high compression ratios (30). Their simulation results showed that high indicated thermal efficiency and low NOx can be achieved using free piston HCCI combustion with hydrogen. Alrbai investigated the performance of a single cylinder free piston HCCI engine [68]. Zhu investigated the performance of an opposed free piston engine with SI combustion [67]. In this report, it was also found that a use of an alternator system was necessary in order to control the compression ratio which varies over time if not controlled.

In general, there are two main factors that is considered in modelling the free piston: the connection between the piston kinematics to thermodynamics, the heat losses and friction losses. One commonly used heat transfer relation is the Woschni-Vogel correlation to estimate the wall heat transfer coefficient [69].The main processes to be modelled in the free piston engine are compression of the intake charge, combustion of the mixture, expansion of the combustion products and scavenging. There are various models to describe the in-cylinder processes. A common simple model is the Seiliger cycle. The Seiliger cycle approach is too simplistic as it cannot predict efficiency, power and peak temperatures accurately. This is because the Seiliger cycle does not resolve the scavenging process, superposition of heat addition and expansion[21]. Another approach to model the piston is by using chemical kinetics. The chemical kinetics approach can solve the compression, combustion and expansion processes simultaneously. There are various models that are chemical kinetics models: 0-dimensional (0-D) thermo-kinetics, quasi-dimensional thermo-kinetics, segregated, sequential fluid mechanics –thermo-kinetics multi-zone approach and multidimensional fluid mechanics with coupled kinetics. The 0-D model is the simplest model that uses chemical kinetics[68]. In this model, the processes are modelled as a single zone. It is assumed that the homogneous mixture of gasses are ideal gasses and the first law of thermodynamics is imposed on the gasses. With the 0-D model, main characteristics of the engine such as work output, combustion time, peak pressure and peak temperature can be obtained. Meanwhile, this model cannot predict wall temperature effects accurately. Therefore, it is insufficient in predicting emissions compared to multi zone models. Furthermore, this model cannot predict the mixing process during scavenging[68]. Golsborough [63] and Kaiser [21] also uses 0-D single zone model for the thermodynamics. In order to model the free piston, the kinematics and the thermodynamics have to be coupled. The methodology from Alrbai[68] and Goldsborough [63] both uses force balances to solve the kinematics and then connect it to the mixture chemical kinetics. The combustion defines the pressure force in the chamber which is one of the main forces that effect the piston motion. In the method by Alrbai, the chemical kinetics is solved by Cantera[70]. Furthermore, in the work carried out by Alrbai, the gas pressure force is modelled as a spring system.

3

Free Piston Modelling and Validation

3.1. Methodology

In this section, the methodology to be followed to model the opposed free piston engine will be presented.The engine will be modelled as a two-stroke HCCI engine.The free-opposed piston is modelled using a 0-D single zone combustion with a chemical kinetics approach. In this section, the thermodynamic and kinematic model used to model the free piston motion and in-cylinder dynamics will be elaborated. Furthermore, the models considering friction, alternator, heat transfer and scavenging will be elaborated.

The free piston engine cycle consists of four main processes: the compression of the charge until ignition, combustion of the gas, expansion of the combustion products and lastly, scavenging. These processes cycle will be solved using the chemical kinetics approach where all the processes can be coupled to each other. The chemical kinetics approach is more complex compared to empirical models but provide higher accuracy. Furthermore, the model consists of using a thermodynamic and a dynamic model. With the chemical kinetics approach, compression , combustion and expansion can be simulated simultaneously.To achieve this, the first law of thermodynamics, ideal gas law and the combustion rate equations are coupled and solved using the chemical kinetics solver Cantera [70]. In this method, Cantera is coupled with the dynamic model in a Python simulation environment. The free piston model consists mainly of two parts, the thermodynamic model and the dynamics model. These two sub-models are coupled such that the pressures calculated from the thermodynamic model is inputted to the dynamic model to calculate the acceleration and velocity. In the meantime, the acceleration calculated by the dynamic model influences the piston wall velocity. So, the simulation advances in an iterative fashion. Furthermore, the reaction mechanism used to simulate the reactions greatly impact the properties and behaviour of the model. Species reaction equations pose challenges in terms of stiffness and sensitivity, requiring a specific solver. The nature of these reactions depends on the mechanism employed, with the option to choose between full or reduced mechanisms based on considerations such as result sensitivity and computational cost.

3.1.1. Opposed Piston Engine Schematic/ Configuration

The schematic opposed piston engine investigated in this study is shown in Figure 3.1. The combustion chamber, where all the in-cylinder processes are defined, is confined between two pistons. The movement of the piston is governed by the forces due to the bounce chamber gases, in-cylinder gas, friction and linear alternators. The pistons move towards the top dead center due to the pressure force exerted by the gas in the bounce chambers. Then, at top dead center, near constant volume combustion occurs and the piston is pushed towards the bottom dead center by the in-cylinder gas forces. It is desirable to have combustion at the top dead center as under-compression can lead to incomplete combustion and over-compression can lead to a significant increase in the NOx emissions [63]. Achieving constant volume combustion is quite difficult in reality. In order to come close to the desired point of ignition, the compression ratio is controlled using the linear alternator [68]. The control of the compression ratio using the linear alternator will be detailed in the coming sections. When the pistons reach the port locations, scavenging occurs. For this engine, loop scavenging is employed in order to have easier

control of the two pistons. The port locations are located symmetric to the x and y axis. This way, the two pistons can operate in symmetry which makes it much easier to control the compression properties. More details on the scavenging process will be detailed further later in this section.

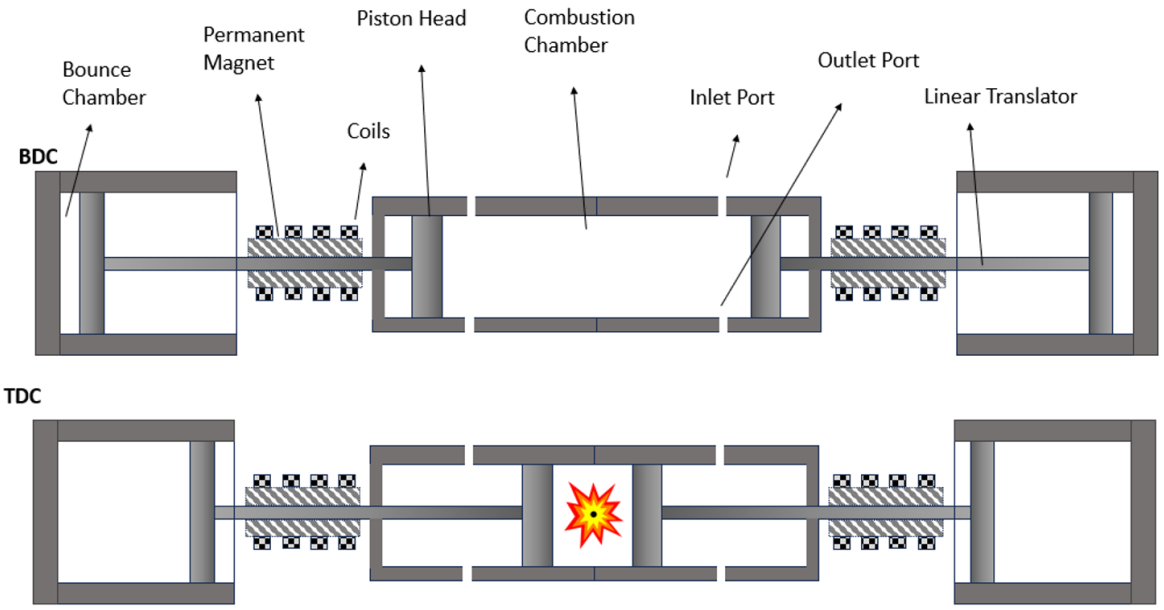

Figure 3.1: Schematic of the opposed-free piston engine with loop scavenging

3.1.2. Piston Dynamics

In a free-piston engine, the motion of the pistons are not prescribed like a crankshaft engine, but rather depends on the force balance on the piston. The force balance on the left piston is visualized in Figure 3.2. Due to the opposed piston configuration, the opposite force balance will be solved for pistons on both sides. This leads to the symmetric motion of the left and right piston. In this model, the motion is positive towards the right. The free piston dynamics can be solved using Newton's second law of motion.

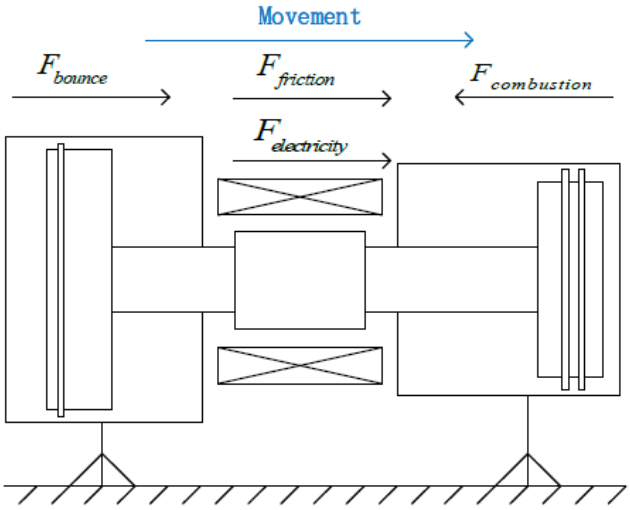

Figure 3.2: Force and kinetics analysis of the moving mass [67]

$$m_{piston}\frac{d^2x}{dt^2} = F_{bc} + F_{alt} + F_f + F_{cc} \tag{3.1}$$

The force balance acting on the left piston is given in Equation 3.1. The represented terms in this equation are the mass of the piston translator m_{piston}, the in-cylinder combustion chamber force, F_{cc}, the bounce chamber force, F_{bc}, the friction force, F_f, and the alternator force, F_w. The force balance is made for the pistons on each side. For the force balance on each side, m_{piston} is taken as the mass of the linear translator on that side. The bounce chamber acts like a spring system, pushing the pistons forward during compression and slowing them down during expansion. Meanwhile, the combustion chamber forces act on the opposite direction. The friction and alternator force act against the movement at all times, slowing down the piston. The alternator is mostly used in that way to keep a certain compression ratio.

Bounce Chamber Model

There are two main bounce chamber mechanisms that are commonly used for free piston engine applications. First method is using springs to control the motion of the free pistons where k is the spring stiffness and x_s is the spring neutral position [71]. Another method is using the gas force to control the motion of the pistons, also called the pneumatic bounce chambers [67] [72] . Using a pneumatic bounce chamber instead of springs are advantageous in terms of having a smaller mass and decreasing mechanical complexity of the system. In this method, the bounce chamber is filled with usually an inert gas. Inert gases are more feasible for bounce chamber applications because they do not go through chemical reactions at the prescribed temperature and pressure ranges. In the free piston model constructed by Alrbai, the pneumatic bounce chambers are utilized, but they are modelled as a spring system [68]. The pressure force exerted by the piston is simplified to a spring system as given in Equation 3.2.

$$\begin{aligned} &\textbf{\textit{penumatic}}: \quad F_P = A \cdot P_{bc} \\ &\textit{spring}: \quad F_P = k * (x - x_s) \end{aligned} \tag{3.2}$$

In the opposed piston engine design by Sandia, Helium is used in the bounce chamber gases [64]. In the reaction mechanisms used in the analysis did not include Helium. Therefore, Argon will be used in this analysis as it is the lightest inert gas after Helium. The bounce chamber gas is modelled as an ideal gas in this model. The pressure inside the gas is selected to achieve the desired compression and expansion characteristics. Looking at Figure 3.1, it can be seen that the there is also a gas on the other side of the bounce chambers. In reality, the force exerted from the bounce chambers to the piston is also effected by that gas force. In order to simplify the reactor network model in Cantera, the effect of that gas mass is not considered. Instead, just one pressure term for the bounce chamber is taken into account [67][73]. In future models, a reactor network that also takes that gas mass into account could be made. In the model proposed by Zhu, the pressure in the bounce chamber is also controlled by valves [67]. In the model used in this thesis, the mass of the gases in the bounce chambers are kept constant, with no leakage between the piston and the bounce chambers. 'The bounce chamber pressure will be varied in different simulations but the bounce chamber gas temperature is kept constant at $T = 300$K. Also, it is assumed that the bounce chambers do not experience heat loss to the environment.

Friction Model

The friction model used in thesis considers a dynamic and static friction term. This method was also used in various research made on free piston engines [63][67][68]. The friction model can be represented with Equation 3.3.

$$F_f = -sign(v_p) * f_1 + -v_p * f_2 \tag{3.3}$$

This approach to modelling friction offers a compromise between the simple model, where a constant value for friction is assumed, and the more complex models. An effort to model the friction in a free opposed piston engine is made by Jia[73]. In this paper, the free piston friction is broken down into components such as piston ring friction, friction due to valve train system and friction due to the losses in the linear electric generator. To calculate these friction components in more detail, more detail on the geometry of the model should be known. Since the geometry of the piston defined in this model is not defined in such detail, it was not feasible to use this approach. So, the model used in the thesis only

represents the piston ring-wall friction. In order to get realistic results for the friction force with the model represented in Equation 3.3, the coefficients have to be tuned. If there was experimental data available, the best approach would be to tune it to get close to the experimental values [63]. In the model created by Robinson et.al, the friction coefficients are selected to match the 7% friction loss presented by the researchers in DLR as a baseline value [74]. The same value is also used as a baseline to compare in the research made by Alrbai [68]. Therefore, it was decided that the friction coefficients would be tuned to get around 7% friction loss. This is a limitation of this research as this ratio of the friction loss could be different due to the different engine geometry and average piston speed between the engines. With more complex parameterisation of the piston model in the future, more detailed friction model can be applied.

Linear Alternator Model

Lastly, the force applied by the alternator is taken into account. The control of the free piston motion is vital in ensuring effective operation. Since the motion of the piston is not controlled by a crankshaft, it is much more difficult to reach the desired compression ratios consistently during operation. By using an alternator, the force applied to the pistons can be modified during operation to ensure that the desired compression ratios are reached [72]. In addition to that, the electromagnetic force generated in the linear alternators can be used to power other devices. In the case of aircraft engines, the power generated by the alternator can be used for avionics, on-board systems or even fed back to the propulsion system for next-gen hybrid electric propulsion systems.

The alternator force is generated by the alternator coils and resists the changes in the magnetic field. The change of magnetic flux through the coil, Φ, determines the induced voltage.

$$V_{\text{ind}} = -\frac{d\Phi}{dt} \tag{3.4}$$

By using the basic electronic circuit relation, the induced voltage can be written as given in Equation 3.5, where R_{coil} is the coil resistance. . Following this, the induced power can be found as presented in Equation 3.6.

$$V_{\text{ind}} = -\frac{d\Phi}{dt} = -\frac{d\Phi}{dx}\frac{dx}{dt} = iR_{coil} \tag{3.5}$$

$$P_{\text{ind}} = iV_{ind} = -i\frac{d\Phi}{dx}\frac{dx}{dt} \tag{3.6}$$

The induced power is equal to the power extracted from the piston by the electromagnetic force.

$$P_{\text{mech}} = F_{alt}\frac{dx}{dt} \tag{3.7}$$

Therefore, the alternator force can also be represented as a function of $\frac{d\Phi}{dt}$, which is a design parameter used for the alternator that depends on the properties of the magnet such as the magnetic strength, coil turns and gaps between the magnets [72]. In the efforts the model the free piston linear alternator engine by Sandia, this parameters is used as function of piston position for every single coil in the alternator.

$$F_{alt} = -i\frac{d\Phi}{dx} \tag{3.8}$$

Another method to model the alternator is by using a more simpler model where the electromagnetic characteristics of the alternator can be lumped into a single holistic parameter C_A and the alternator force is proportional to the piston velocity [72] [67] [63][68]. With this model, the force generated by the alterantor can be varied much more easily by just changing the coefficient C_A.

$$F_{alt} = -C_A * v_p \tag{3.9}$$

In the research made by Lee, the detailed model in the simple model are compared [72]. In their research, Lee found that the number of coils and magnets do not matter as long as the energy extracted by alternator is similar. When the simple model is used, the amount of power extracted can be modified much easily because the details of the complexity of the electrical components is not considered. This

makes the simple model much more computationally efficient and easy to alter compared to the detailed model.

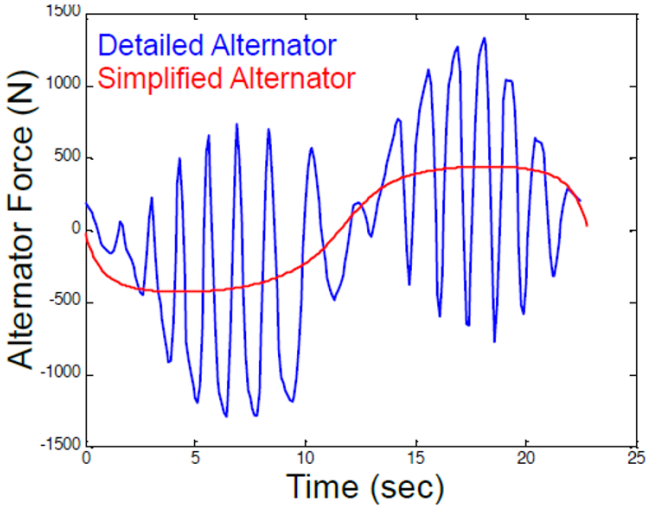

Figure 3.3: Alternator Force over time for one cycle [72]

The drawback is that the electromagnetic force behaves very differently between the models as presented in Figure 3.3. In the detailed model, the alternator force is oscillating many times within the stroke. This shows that the force is does not always do work against the piston motion during the stroke. The physics of electromagnetics within the magnet assembly leads to the magnetic flux to vary with the piston position. Hence, it is hypothesized that a constant value can be determined to accurately represent the average behavior of the actual alternator. Given the additional computational time required by the detailed alternator model,employing the simplified model to conveniently adjust the alternator output is preferred [72].Lastly, the current research does not encompass the rectifier circuit or battery model. The simplified alternator model given in Equation 3.9 is used in various free piston models in literature [63] [72] [67] [63][68]. In these models, the linear alternator is used to generate electrical power and control the compression ratio of the piston at the same time. Based on testing different combinations of coils and magnet numbers, the charging efficiency ranges from 85% to 92% [72]. The conservative estimate of 85% is designated as the ”alternator efficiency” to avoid overestimating efficiency.

3.1.3. Thermodynamic Model

The second sub-model is for the in-cylinder thermodynamics. The in-cylinder gas cycle is studied using a simple zero-dimensional chemical kinetics thermodynamic method, excluding fluid dynamics and spatial effects.The state of the in-cylinder gases is determined by applying the energy conservation equation to the cylinder’s control volume.

The energy conservation of the in-cylinder species are given in Equation 3.10

$$\frac{\mathrm{d}U}{\mathrm{d}t} = \frac{\mathrm{d}Q_{comb}}{\mathrm{d}t} - \frac{\mathrm{d}Q_{loss}}{\mathrm{d}t} - p\frac{\mathrm{d}V}{\mathrm{d}t} + \sum_i H_i - \sum_o H_o - \sum_l H_l \tag{3.10}$$

where U is the total internal energy of the combustion chamber, Q_{comb} is the combustion heat released due to the fuel, Q_{loss} is the heat transfer of the combustion chamber, H_i represents the total enthalpy of the air intake, H_o represents the total enthalpy of the air exhaust, H_l represents the total enthalpy of the air leakage.

The cylinder charge is represented as a perfectly mixed, ideal gas; compression and expansion are calculated with temperature dependent specific heat ratio and heat transfer between the gas and cylinder walls; combustion heat release is predicted with a chemical kinetics full reaction mechanism.The enthalpy flowing in and out of the combustion chamber are represented in this equation. The enthalpy

flow can be due to the scavenging process or leakage. In this thesis, the leaking flow from the chambers are not considered. The mass flow during the scavenging process can be controlled using the effective valve area, discharge coefficient, pressure ratio and the fluid conditions from the scavenging port. The compression, combustion and expansion phases are modelled differently compared to the scavenging process as there will be no change in mass during those processes. In this thesis, the perfect scavenging model is assumed and will be detailed later in this chapter. The reaction mechanism used in this study is the A2NOx reaction mechanism for kerosene [75]. This reaction mechanism was selected because it can models both hydrogen and kerosene combustion, which are needed to model the FP-CCE concepts.

Chemical kinetics governs the reactions of species within an in-cylinder Perfectly Stirred Reactor (PSR), where reactants mix thoroughly and combust uniformly. This reactor type is valuable for studying highly mixed internal combustion engines, residence time concerns, and high-temperature chemical kinetics. Cantera solves the time-dependent reaction equations that depict the evolution of the reactor's chemical and thermodynamic state. The combustion heat release rate is determined using the formula [68]:

$$\dot{Q}_{comb} = -V \cdot \sum_{i=1}^{N} (\dot{\omega}_i \cdot h_{i,m}) \tag{3.11}$$

Where $\dot{\omega}_i$ is the net production rate of the species i, $h_{i,m}$,is the molar enthalpy of the species i, and N is the total number of species involved in the reaction mechanism. The input energy to the system is the fuel energy added per cycle. The input fuel energy is shown in Equation 3.12.

$$Q_f = m_f * LHV \tag{3.12}$$

Heat Transfer correlation

For the free piston model, it is important to accurately estimate heat losses to have a realistic overview of the performance of the engine. The heat transfer between the walls and the in-cylinder gas can be expressed with Equation 3.13.

$$Q_{loss} = h \cdot A_{\text{wall}} \cdot (T - T_{\text{wall}}) \tag{3.13}$$

The heat transfer then depends on the instantaneous surface area of the cylinder (A_{wall}) and wall temperature (T_{wall}). In this study, the heat transfer correlation is estimated using the Hohenberg correlation given in Equation 3.14 [76].

$$h = 130V^{-0.06} \left(\frac{p}{1 \times 10^5} \right)^{0.8} T^{-0.4} (\bar{v_p} + 1.4)^{0.8} \tag{3.14}$$

where V is the in-cylinder volume, p and T are the in-cylinder pressure and temperature, and $\bar{v}$ is the average velocity of the moving piston mass.

There are various studies comparing the heat transfer models available that could be potentially used for HCCI combustion applications. In the study made by Hiaruttin et.al [77], a single-zone thermodynamics model was used to compare three different heat loss models: Woschni [78], modified Woschni[79], and Hohenberg correlations [76]. It was found that the difference in heat loss models leads to a big difference in the heat flux, with the modified Woschni model having the highest heat flux among these models. Furthermore, the effects of changing the scaling factor and characteristic velocity were also investigated. This study concludes that the most accurate results were produced by using the modified Woschni model. Meanwhile, the Woshcni and Hohenberg correlations require more rigorous scaling of the constants to match the experimental data. In another study made by Soyhan et.al, three heat transfer correlations, modified Woschni, Hohenberg and Assanis correlation [80] , are compared to assess their performance in predicting the heat transfer for HCCI combustion [81]. The results from their experiments are compared to the results obtained using each correlation. In the Woshcni correlation, there is a term representing the combustion compression velocity, which is defined as the bulk gas movement due to the compression of the unburned gases by an advancing flame front. It is argued that this term is not applicable to HCCI engines and can lead to overestimation of the gas velocity. This leads to an exaggeration of the heat transfer rates during combustion and expansion, and potentially an underestimation during compression. The Assanis correlation, a variation of the Woschni heat transfer correlation tailored for HCCI engines, addresses gas movement concerns

by empirically reducing the combustion compression velocity. This adjustment results in significantly lower heat transfer rates throughout the engine cycle in our HCCI engine, leading to an overestimation of peak pressures. It was found that, while the Assanis model can be aligned with the experimental data by tweaking the scaling coefficient, it is inconvenient to require significant coefficient adjustments for each unique HCCI engine. It was concluded that, the Hohenberg correlation gave the most realistic results without the need of a scaling factor, as it has no explicit combustion velocity term. Given that the HCCI free piston model at hand does not have any experimental values to scale the heat transfer correlations, the Hohenberg correlation was selected to be the most feasible for this study.

3.1.4. Scavenging

A cruical part of the free piston model is the scavenging model. The control and prediction of free piston dynamics is quite complex. In turn, this also makes the scavenging process complex as it depends on the port timings and usually, the pressure differences between in-cylinder and the reservoirs. This part of the free piston theory needs more attention in order to come up with smart methods to control scavenging in free piston operations. The free piston will inherently work in two-stroke operation. So, the gas exchange will happen as the piston are moving.

Perfect Scavenging

In order to simplify the modelling efforts, one of the methods implemented was the perfect scavenging method[68]. This assumption means that all the gases in the cylinder is changed from cycle to cycle.In this method, it is assumed that the simulation starts with the piston walls at port opening locations. When the piston walls reach the port opening locations again, the simulation stops with one cycle completed. With perfect scavenging, no cylinder gas is retained from cycle to cycle and all of the intake conditions return to the intake conditions. Meanwhile, velocity and acceleration continues with the cycles to have the dynamics module to work continuously.

Scavenging with Mass Flow Controllers

The change in enthalpy due to the gas exchange can be modelled using the equations below [67]:

$$\frac{\mathrm{d}m}{\mathrm{d}t} = \begin{cases} \frac{C_d A p_h}{(R_g T_{ph})^{\frac{1}{2}}} \left(\frac{p_l}{p_h}\right) \left\{ \frac{2\gamma}{\gamma-1} \left[1 - \left(\frac{p_l}{p_h}\right)^{\frac{\gamma-1}{\gamma}} \right] \right\}^{\frac{1}{2}}, \frac{p_l}{p_h} > [2/(\gamma+1)]^{\frac{\gamma}{\gamma-1}} \\ \frac{C_d A p_h}{(R_g T_{ph})^{\frac{1}{2}}} \gamma^{\frac{1}{2}} \left(\frac{2}{\gamma+1}\right)^{\frac{\gamma+1}{2(\gamma-1)}}, \frac{p_l}{p_h} \leq [2/(\gamma+1)]^{\frac{\gamma}{\gamma-1}} \end{cases} \tag{3.15}$$

$$C_d = 0.85 - 0.25 \left(\frac{p_l}{p_h}\right)^2 \tag{3.16}$$

where, C_d is the discharge coefficient, p_l is the pressure of the low pressure end, p_h is the pressure of the high pressure end, T_{ph} is the temperature of the high pressure end. This equation is applied to both inlet and the outlet port. Due to the high complexity of the scavenging model with massflow controllers, it was decided that the perfect scavenging method will be sufficient for this study.

3.1.5. Simulation Setup

In this section, the simulation setup for the free piston engine is presented. The simulation has an iterative nature where information is exchanged between the dynamic and chemical kinetics model. The set of inputs to the simulation consists of inputs that define the geometry of the piston and inputs that define the characteristics of the cycle to be simulated. The relevant inputs and the simulation procedure will be more detailed in this section.

The set of inputs for the cycle simulation are:

- N_{cycles}: number of cycles
- CR_{target}: Target compression ratio
- b: piston head bore
- $(b/s)_{max}$: maximum bore-to-stroke ratio
- R_{bdc}: bottom dead center ratio. The ratio of the bottom dead center to the total length of the combustion chamber module.

- R_{port}: port ratio. The ratio of the port location with respect to the total length of the combustion chamber module.
- m: translator mass for each piston
- T_i: cylinder inlet temperature
- P_i: cylinder inlet pressure
- P_{bc}: bounce chamber initial pressure
- C_A : alternator coefficient
- f_s,f_d: static and dynamic friction coefficient
- X_{fuel}: fuel composition
- X_{ox} : oxidizer composition
- ϕ: equivalence ratio

Geometry parameterisation
The free piston engine model to be investigated in this thesis in quite unique. The free opposed piston HCCI engine burning hydrogen is a very novel concept. Therefore, there is currently only one design in literature, presented by the report by Sandia [64]. In order to explore a wider design space, variables that define the geometry of the piston are created. In this thesis, the focus is to measure the effectiveness of the energizing of the flow rather than the detailed design or mechanics of the piston module. Therefore, a relatively simple parameterisation of the geometric variables were made. In a more detailed design, components such as the piston heads, bounce chambers and the valves could be defined in a more detailed geometry where lubrication could also be considered.

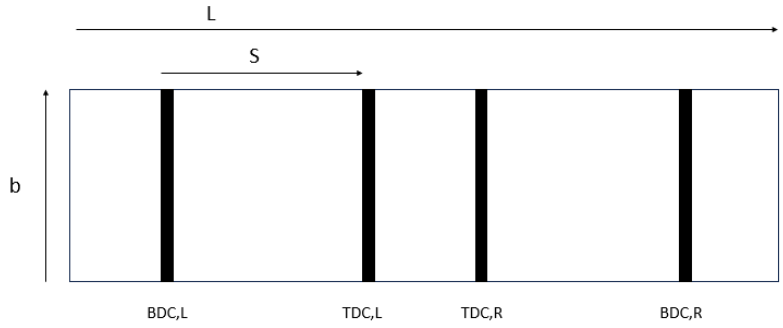

Figure 3.4: Simple Parameterisation of the Free Opposed Piston Engine

The geometry of the opposed free piston can be seen in Figure A.1. This simple paramatersiation is made mainly to calculate the total length of the engine. This step was necessary in order to accurately define the volumes in the simulated reactor network in Cantera. The selected variables for the geometry parameterisation are:

- CR_{target}: target compression ratio
- b: piston head bore [m]
- (b/s): stroke to bore ratio
- R_{bdc}: bottom dead center ratio. The ratio of the bottom dead center to the total length of the combustion chamber module.

where CR_{target} is defined as:

$$CR_{target} = \frac{V_i}{V_f} = \frac{A_{pistonhead}\, x_{BDC,R} - x_{BDC,L}}{A_{pistonhead}\, x_{TDC,R} - x_{TDC,L}} \tag{3.17}$$

The total length of the piston is determined by the stroke length and the maximum compression ratio. The total length of the piston engine is computed using Equation 3.18.The derivation of the total length equation is presented in Appendix A.

$$L = \frac{1}{(b/s)} * b * 2 * \frac{CR}{(CR-1) * (1 - 2 * R_{bdc})} \tag{3.18}$$

In order to understand the limits of the design parameterisation, a sensitivity analysis of Equation 3.18 has been made. In this analysis, the bore is kept constant at 0.06 meters. In Figure 3.5a, the change in total length for the changing target compression ratio and bore-to-stroke ratios are given. Firstly, the graph shows that the length of the piston module reaches a limit as compression ratio increases. The change in length going from a $CR_{target} = 20$ to $CR_{target} = 30$ only yields less than 1% difference in the total length. Therefore, for the same set of inputs for the variables that effect the forces on the piston, the compression ratio can only reach to a certain point. even though the CR_{target} is higher. Secondly, it can be observed that with the increasing bore-to-stroke ratio, the limiting compression ratio moves to higher values. So, with the same bore length, higher compression ratios can be reached because the piston module is longer. In Figure 3.5b, the change in total length for increased R_{BDC} is given. The total length goes go to infinity as R_{BDC} reaches 0.5. This is expected as the compressed volume cannot be zero. Furthermore, as R_{BDC} gets smaller, the total length decreases. This can be explained with the fact that the smaller the bottom dead center location for constant bore and stroke, smaller the length becomes.

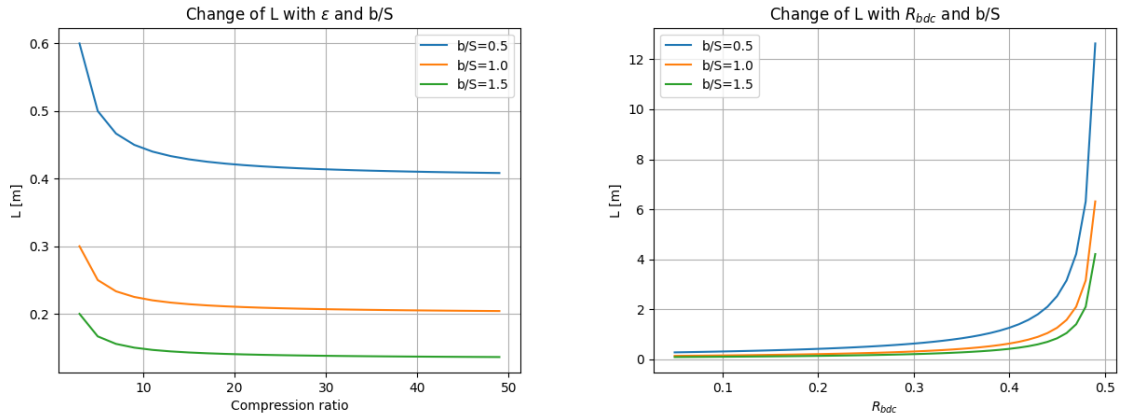

(a) Change in piston in-cylinder module length for changing compression ratio and bore-to-stroke ratio

(b) Change in piston in-cylinder module length for changing R_{BDC} and bore-to-stroke ratio

Figure 3.5: Piston dynamics for changing piston head mass

Simulation Procedure

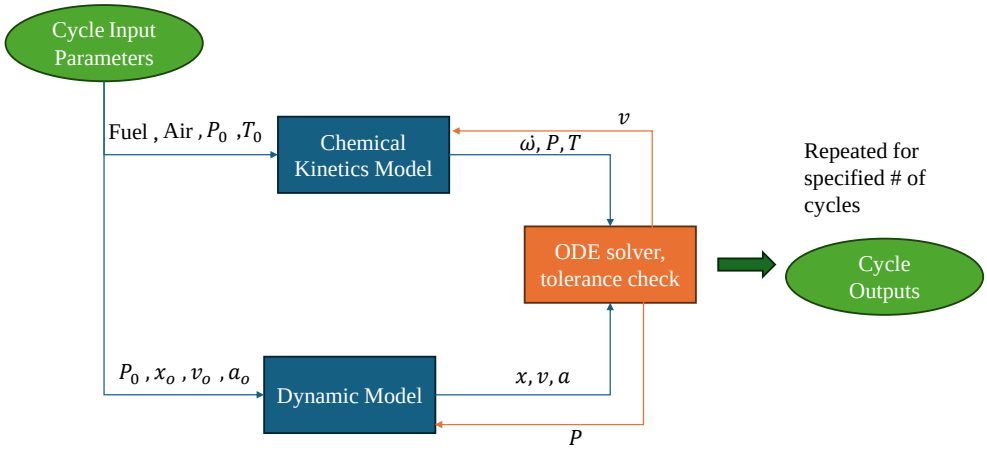

Figure 3.6: Simulation Procedure

The simulation procedure is similar to the approach taken by Alrbai, as Cantera is also in the model used in his study [68]. The simulation procedure can be seen in Figure 3.6. The simulation starts with defining the thermodynamic properties of the in-cylinder and bounce chamber gas and the dimensions of the piston engine. Then, the calculated pressure from Cantera goes to the dynamic model to calculate the acceleration from the net force and calculate the wall velocity. Then, this wall velocity is inputted to Cantera as the wall velocity. Then, the simulation advances by one time step to calculate the new location of the piston and the new thermodynamic properties at that location. Then, these thermodynamic properties are inputted back to the dynamic model to restart the loop. In the perfect scavenging model, all the thermodynamic properties of the model goes back to initial conditions.

The free piston control becomes especially complex during multi-cycle operations. The results from Zhu and Alrbai shows that without a controlling mechanism, the compression ratio increases as cycle moves on which leads to inefficiencies and even catastrophic failure. As a simple and robust solution, a PI controller was implemented [67][68].

The controller weight fluctuates within specified upper and lower bounds. The proportional part adjusts the controller weight according to the error between the actual and target CR. The integral part integrates the error over time, adding it to the proportional result. The controller uses the equations[68]:

$$\begin{aligned} F_a &= W_a \cdot C_a \cdot v \\ W_a &= 1 - K_P \cdot \text{ error } - K_I \cdot \int \text{ error } \cdot dt \\ \text{error } &= CR_{\text{Target}} - CR_{\text{Actual}} \end{aligned} \tag{3.19}$$

Where, W_e is the controller weight, K_p is the proportional component, K_I is the integral component, CR_{Target} is the target CR, CR_{Actual} is actual CR.

3.1.6. Baseline OFPE Design

The selected inputs for the piston engine simulation is based on the set of inputs provided by Goldsborough[63]. The engine used there is in dual-cylinder configuration but still aims to to HCCI combustion with hydrogen. Therefore, the inputs for the thermodynamic properties are taken from there. The bore is selected to be similar to the experiments provided by Sandia [64]. The bore-to-stroke ratio is taken

into account is taken as one, the square-stroke mode. The square-stroke mode is regarded as a good trade-off between high power and low mass [21]. The mass if the piston is selected to have a good overall synergy between being lightweight, requiring less force to push it towards TDC, and being heavy enough to stay in the TDC to have a more complete combustion [63]. More on this on the sensitivity analysis part. The static and dynamic friction coefficients are selected such that the friction loss could be around 7% [74]. The bounce chamber pressure and alternator coefficient is selected such that near constant volume combustion occurs near the TDC and the piston can travel back to the BDC. The alternator coefficient is also altered cycle to cycle to ensure that the compression ratios stay uniform during operation.

3.1.7. Scaled-up OFPE Design

In this section, the scaled-up design of the OPFPE is presented. In order to meet the performance requirements of a high bypass turbofan engine, the pistons have to accommodate for larger mass per cycle. As discussed before, the analysis made by Kaiser shows that there is currently no such design that can accommodate the performance requirements of state-of-the-art turbofan engines. In this study, the preliminary design of a large scale piston engine is conducted. This was necessary in order have an accurate estimation on the piston engine requirements of the FP-CCE concepts. In this section, the design choices made and the resulting performance characteristics of the design will be elaborated.

In order to have a feasible design for the FP-CCE concept, certain requirements were identified. The OFPE engine at hand will be used to integrate into the FP-CCE concept where the main goal is to combust at near constant volume conditions and energize the flow. The design requirements for the scaled-up piston is presented inTable 3.1. Firstly, the piston engine will be used to connect to the LEAP-1A26 engine. So, the engine has to accommodate enough mass flow, with a feasible number of pistons. To accommodate a higher mass per cycle, the bore of the piston heads are increased. The range identified is found to be around 0.1 to 0.5 m as the gas mass per cycle increases exponentially with increased bore.The number of pistons required is estimated with the relation given Equation 3.20. The estimated number of pistons is aimed to be between 8 to 24. This is also so that the pistons can be deployed possible in a V-12 or V-8 configuration[21]. In addition, the inlet pressure and temperature of the piston would be the values from the exit of the HPC of the aircraft engine.

$$N_{pistons} = \frac{\dot{m}_{core}}{m_{gas,p} * f_p} \tag{3.20}$$

There were a few more constraints identified in Kaiser in is analysis. For these constraints, the technological level of 2050 is taken into account by Kaiser[21]. The relevant constraints for this analysis are as follows. Firstly, it is stated that the mean piston velocity should be kept below 18 m/s. This is because the life-cycle of the piston gets deteriorated exponentially with the increased mechanical stress on piston and liner. Another requirement requirement identified by Kaiser, is that peak pressure is to be kept below 250 bar to limit peak mechanical loads. Initially, square-stroke mode was explored. It was seen that the required compression ratio for auto-ignition in this case was quite low in this case, around 4-5. From Figure 3.7, it can be seen that a lower compression ratio of 4 to 5 can be accommodated with a shorter length. In order to have a balance between a shorter engine and lower peak loads, $b/s = 1.5$ will be used.

Name	Value
N_{pistons}	[8-24]
P_i	$Pt_{3,\text{LEAP-1A}}$
T_i	$Tt_{3,\text{LEAP-1A}}$
v_{mean}	$<$ 18 m/s
P_{peak}	$<$ 250 bar
b/s	1.5
b	[0.1-0.5] m

Table 3.1: Scaled-up Piston Design Considerations

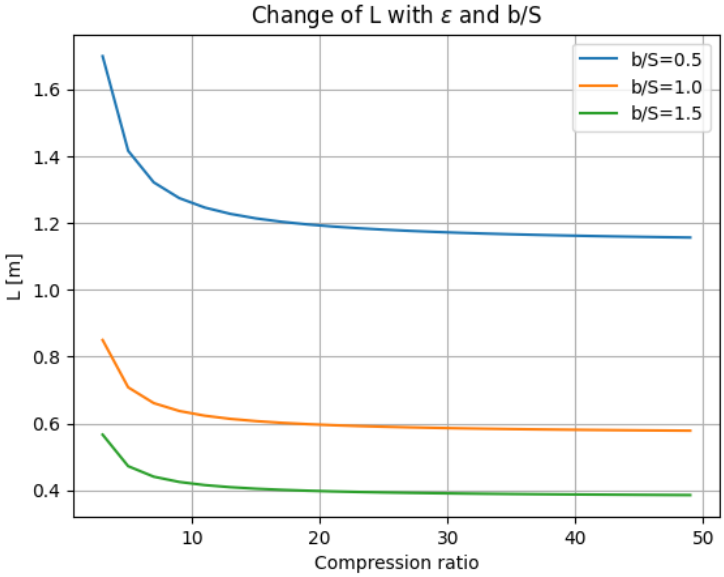

Figure 3.7: Change in piston in-cylinder module length for changing compression ratio ϵ and bore-to-stroke ratio b/s

A preliminary design is made considering the mentioned constraints. The model inputs were manually iterated to get a feasible design that would fit all the requirements, with having near TDC combustion.

3.2. Results and Discussion

3.2.1. Baseline Free Piston

In this section, the simulation the baseline free opposed piston engine is discussed. Firstly, the overview of the results from simulating the baseline free piston model will be presented, along with the relevant inputs. The baseline free piston engine is created to validate the free piston model, before scaling the piston up to meet the performance requirements for the LEAP-1A26 engine.The inputs are provided in Table 3.2.

Parameter	Value
b	0.06 m
b/s	1
CR	22
R_{bdc}	0.2
R_{port}	0.25
m	2 kg
C_A	80
f_s, f_d	80, 2
X_{fuel}	'H2:1'
X_{ox}	'O2:1.0, N2:3.76'
ϕ	0.38
T_i	400 K
P_i	1 bar
P_{bc}	15 bar
T_{wall}	700 K

Table 3.2: Baseline Inputs

Parameter	Value
Average frequency f	56 Hz
Average Compression Ratio CR	22
Final Temperature T_f	852 K
Final Pressure P_f	2 bar
Peak Temperature T_{max}	2410 K
Peak Pressure P_{max}	122 bar
Indicated thermal efficiency η_{ind}	40 %
Thermal efficiency η_{th}	27 %
Alternator Power P_{alt}	5 kW
Gas mass per cycle m_{gas}	0.22 g

Table 3.3: Baseline FP Results

Using these inputs provided in Table 3.2, the multi-cycle analysis of the free piston engine is conducted. For this analysis the piston is simulated for 100 cycles. The results for the baseline piston engine is as shown in Table 3.3. At the end of 100 cycles, the average frequency of the engine is found to be around 56 Hz, with an average compression ratio of 22.6. Figure 3.8, shows that after a few initial cycles, the compression ratio stayed around 22.8.

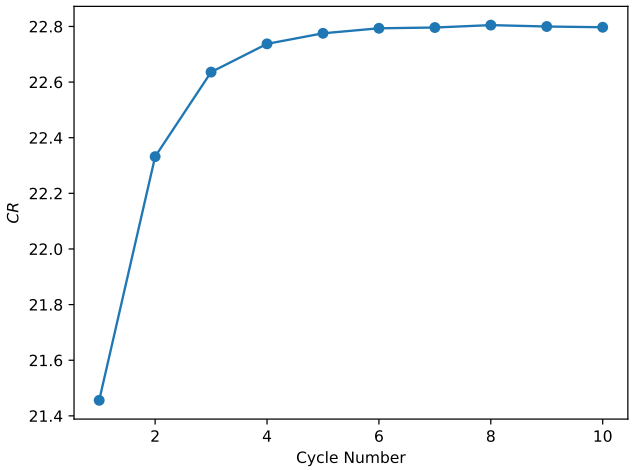

Figure 3.8: Compression Ratio over the first 10 cycles

The breakdown of input energy in the free piston engine can be seen in Figure 3.9. The input energy to the engine is defined as the energy of the fuel mass entering the piston module at every cycle. The input energy per cycle is determined using Equation 3.12. In this analysis, hydrogen is used as fuel. In this piston module, the useful extracted energy is the work done on the alternator, around 31.7%. The 5.6% alternator loss is due to the losses in the alternator in converting the work done on the alternator to useful energy. The alternator efficiency is taken as 85%. As a result, the alternator can generate around 90 J of work per cycle, corresponding to an average power of 5 kW over the whole operation. Looking at the losses, it can be seen that the largest percentage of the losses come from the heat loss to the walls. Using the Hohenberg loss correlation, the heat loss compared to the input energy was found to be around 24.8 % of the provided input energy. Furthermore, the friction loss is calculated to be around 7.9%. The energy that goes to heating the exhaust flow is not considered as useful energy in the context of the free piston module. Although, in the combined cycle application, the exhaust heat will be useful energy as the energized flow will be used for thrust. More details on this will be presented in the following chapters.

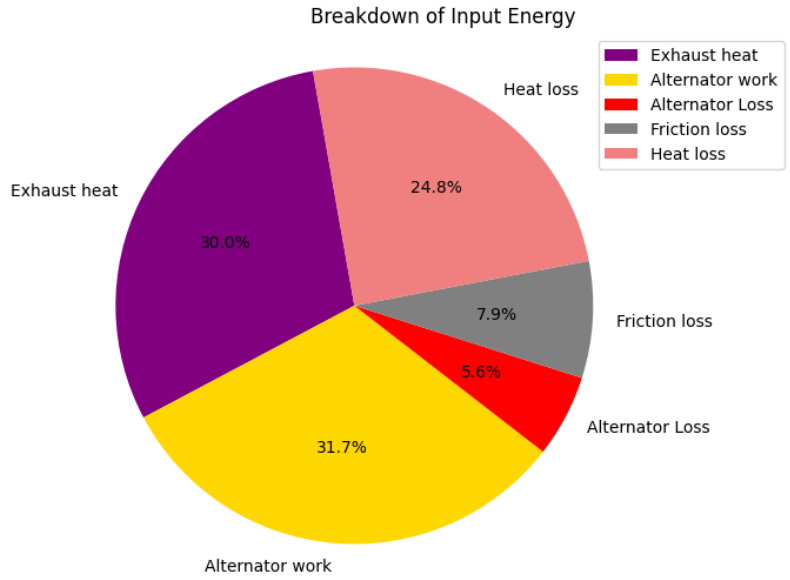

Figure 3.9: Breakdown of Input Energy for the Baseline Free Piston Engine

In Figure 3.10, the P-V diagram for the baseline free piston engine simulation for 5 cycles during operation is presented. In this figure, all the main processes involved in each cycle can be observed. Firstly, compression occurs. If the combustion gases are compressed to the auto-ignition point, HCCI combustion takes place. Furthermore, near the TDC, there is a region of adverse work. In this region, negative work occurs on the piston due to two phenomena. Firstly, HCCI combustion occurs slightly before the TDC is reached. So, the piston still slightly moves forward after combustion leading to negative work on the piston. Secondly, the rate of heat transfer through the walls is faster than the rate at which the in-cylinder pressure after combustion forcing the piston back towards the BDC.

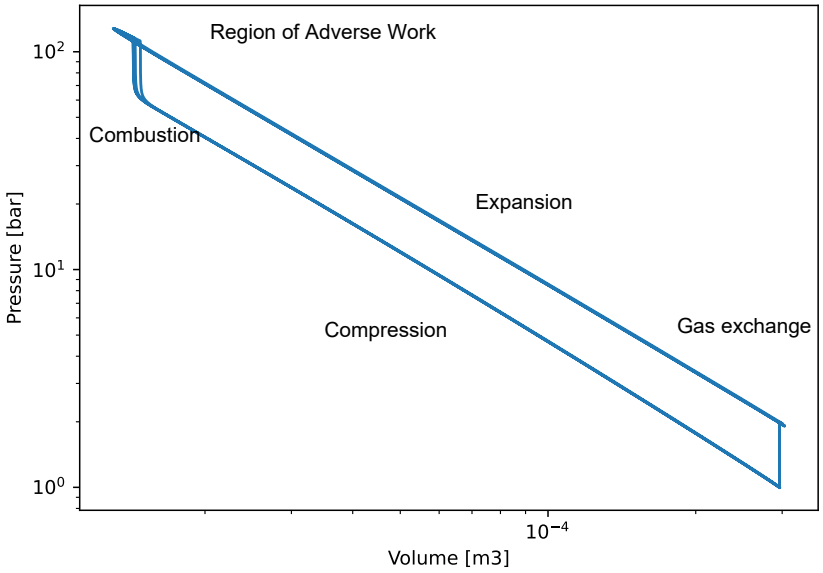

Figure 3.10: P-V diagram for the baseline OFPE for 5 cycles

In Figure 3.11, the T-s diagram for the piston engine operation over 5 cycles is given. It is important

to notice that there are zones where the entropy decreases in the T-s diagram. This is because of the heat loss function. When the rate at which heat transfer occurs is higher than the rate in which the compression does work on the flow, the change in entropy can be negative. In order to better visualize this effect, the T-s diagram when the heat loss function is turned off vs turned on is presented in Appendix A.

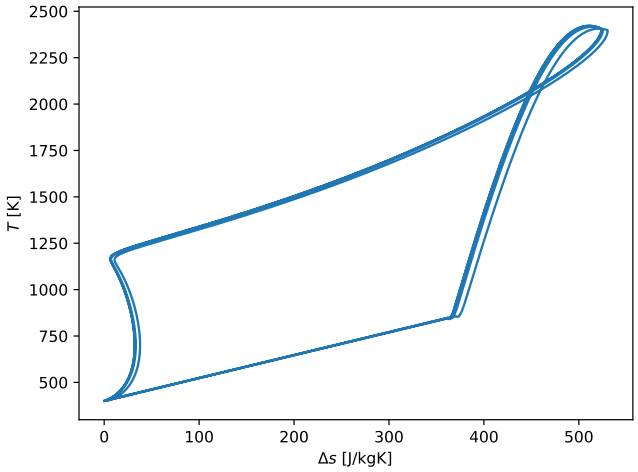

Figure 3.11: T-s diagram for 5 cycles for the baseline OFPE

The pressure and temperature profile during operation is given for 5 cycles in Figure 3.12. During operation, the temperature and pressure starts rapidly rising at at auto-ignition point around $T = 1150K$. This value is also recorded from the experiments of Cain, where the auto-ignition temperature of H2 is recorded for high pressures [82]. The moment of ignition can be also seen from the heat release rates over time given in Figure 3.13. The graphs shows that very rapid combustion for the auto-ignition process. The combustion duration is observed to be in the order of 10-50 μs. The results from this graph also supports the fact that free pistons could provide better performance than crankshaft engines due to not having any mechanical connection for the moving piston [63].

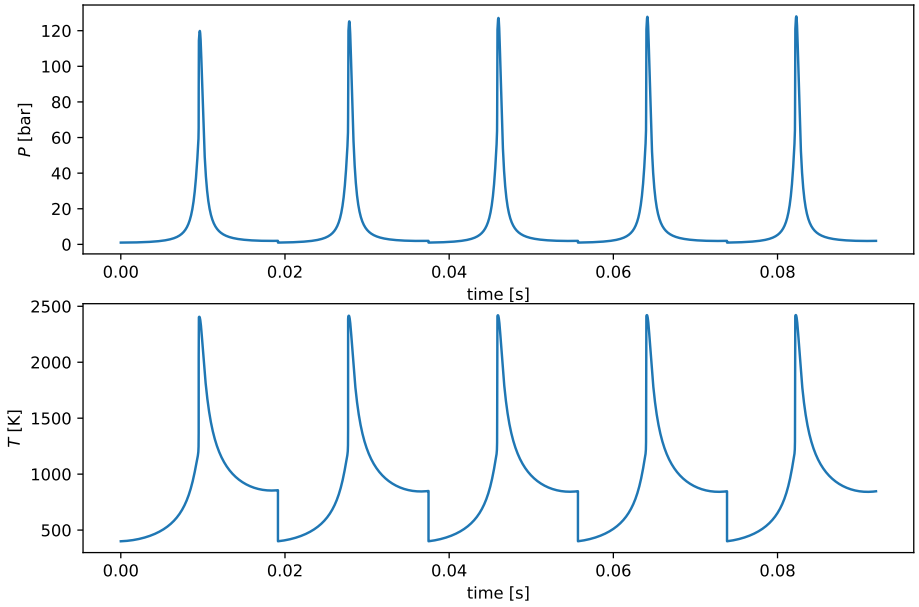

Figure 3.12: Pressure and Temperature over time for 5 cycles for the baseline OFPE

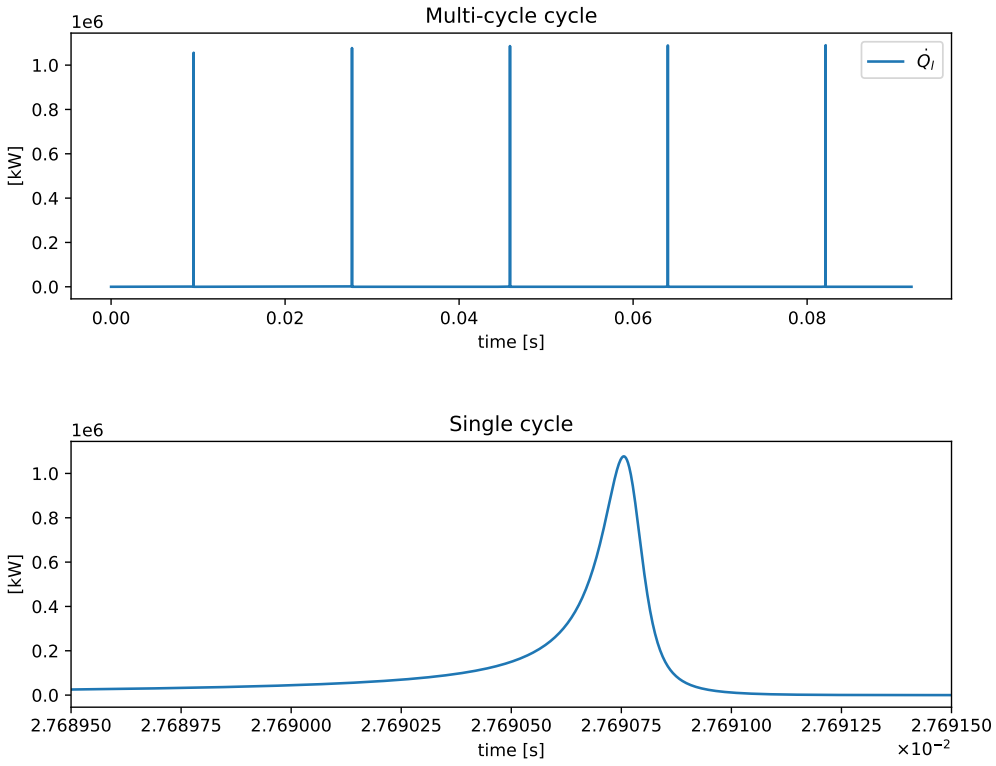

Figure 3.13: Heat Release Rate from the baseline OFPE

In Figure 3.14, the change in Hohenberg heat transfer coefficient over one cycle is presented. It

can be seen that the heat transfer coefficient follows a very similar trend with the pressure graph. The heat transfer rate peaks during auto-ignition with the rapid rise in pressure and temperature.

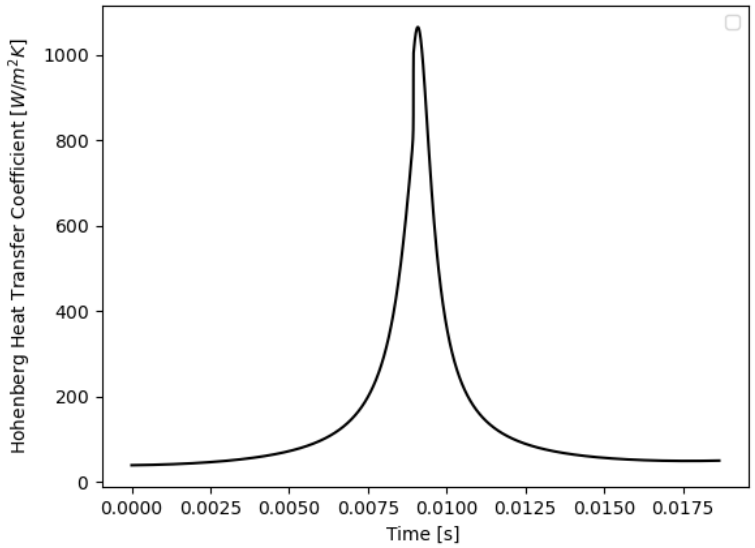

Figure 3.14: Hohenberg Heat Transfer coefficient over one cycle

The kinematics of the free piston is very important to analyze as the motion of the pistons are not prescribed. The steady-operation of the piston is highly dependent on the kinematics of the piston.

In Figure 3.15, the acceleration vs velocity for the multi-cycle simulation is presented. From the graph it can be seen that, the ignition that takes place right before velocity becomes zero near TDC, acceleration peaks. This is due to the sharp increase in the gas pressure exerted on the piston during ignition. Furthermore, the acceleration recorded at the TDC is much larger than the acceleration recorded at BDC. The rapid changes in the acceleration recorded in the BDC is also caused by the change in alternator load that occurs at BDC, at the start of each cycle.

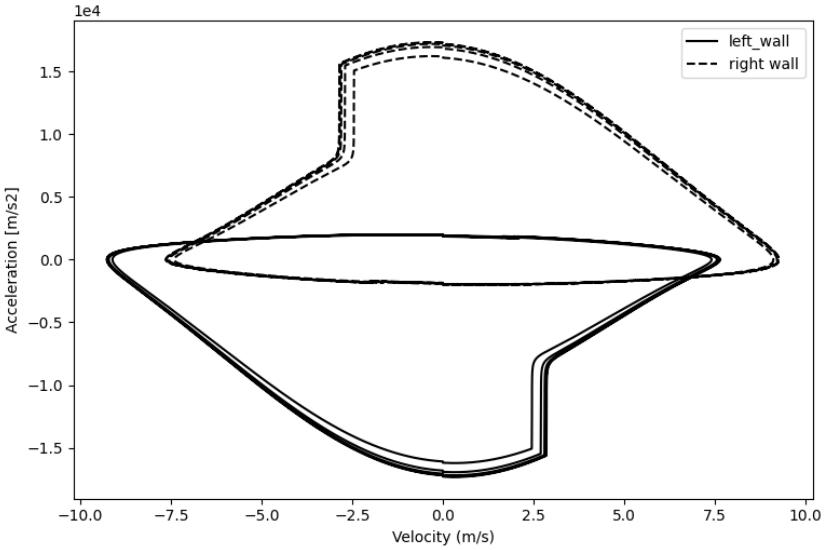

Figure 3.15: Acceleration vs velocity for the baseline OFPE

In Figure 3.16, the velocity over position for the pistons are presented. Looking at this figure, it can be seen that the velocity has an 'egg-shaped' profile. The piston has higher velocities near the TDC compared to the velocities near BDC. Another thing to notice is that the piston accelerates much quicker towards the other direction in the TDC compared to the BDC. This in turn shows the fact that in the opposed free piston engine, the pistons spend less time in the TDC compared to the BDC. This can also be observed when looking at Figure 3.17. The peaks near the TDC for both pistons have a shorter duration than the peaks during BDC. The fact that the pistons spend less time in the TDC makes this piston engine more advantageous than crankshaft engines as the heat losses in TDC and the NOx emissions are less. Furthermore, it can be seen that the velocities slightly increase during the first few cycles.

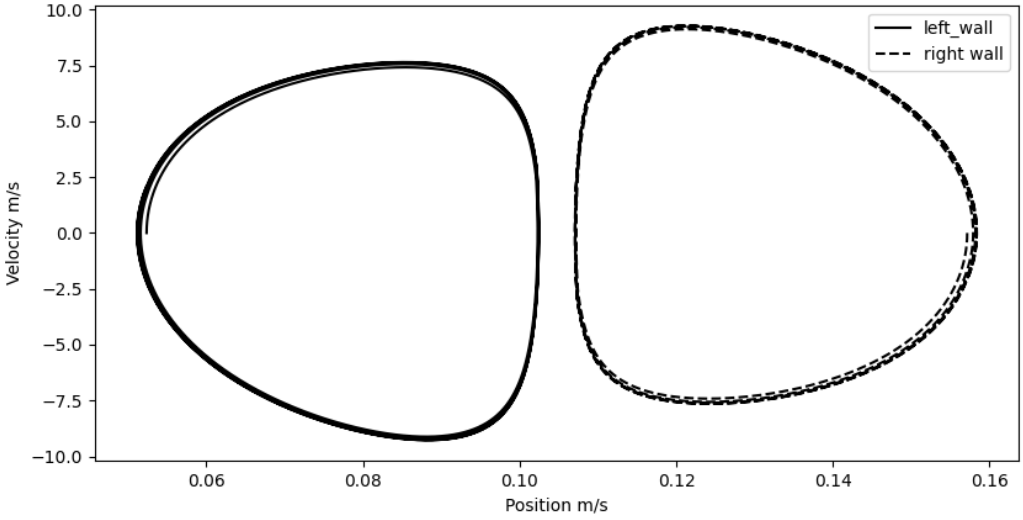

Figure 3.16: Velocity vs Position for the baseline OFPE

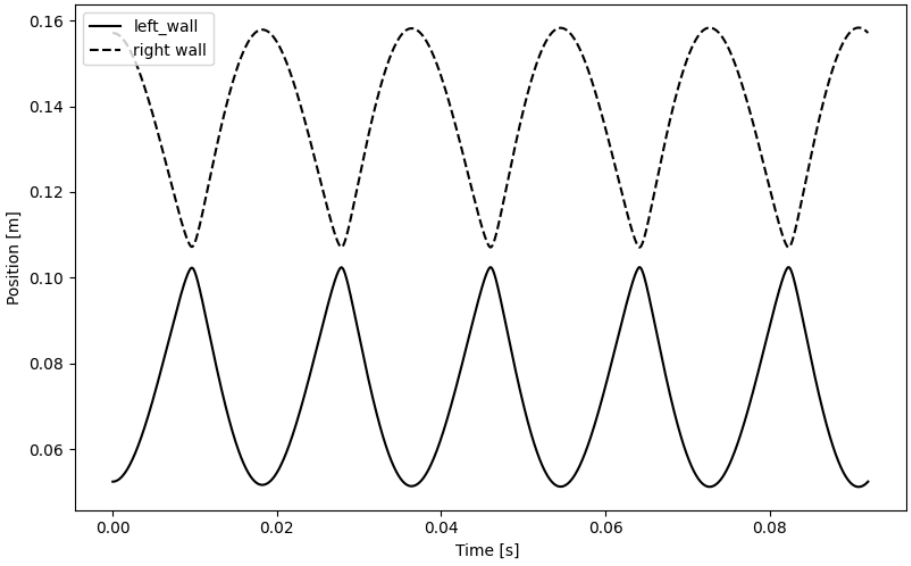

Figure 3.17: Position vs Time for the baseline OFPE

In Figure 3.18, the work done on the leftwards piston is presented. This figures illuminates the effect of the different forces that are acting on the piston. The overall net effect is very close to 0 but is slightly higher. If the compression ratios were constant at each cycle, then this net effect would always be zero. In this figure, it is clearly shown that the in-cylinder gas force and the bounce chamber gas force are acting always opposite of eachother. The bounce chamber always pushes the piston towards the TDC, while the in-cylinder pressure force always pushes the piston towards the BDC. So, during compression, the bounce chamber does work on the flow and during expansion, work is done by the piston on the bounce chamber, except the region of adverse work. Overall, the bounce chamber effect the system similar to a spring damping system. In contrast, the alternator and friction forces always work against the movement direction. Therefore, alternator and friction work is always work done by the piston.

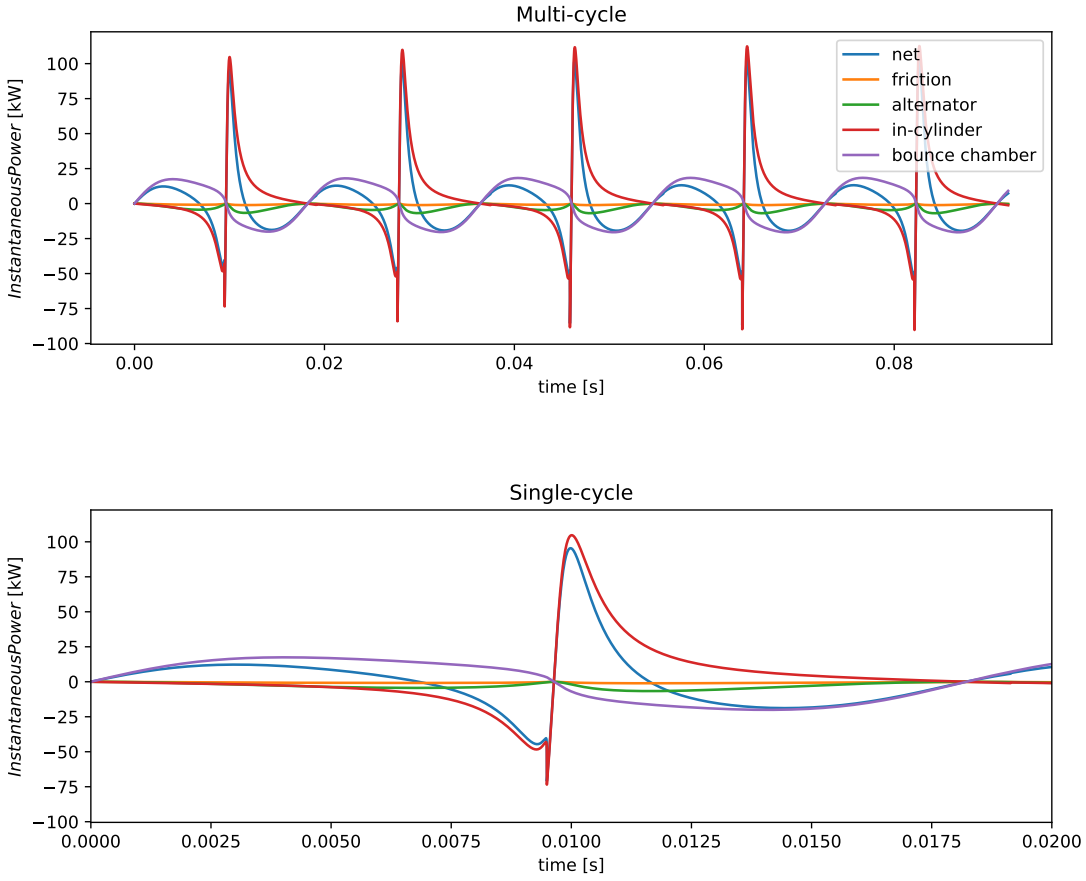

Figure 3.18: Work Balance on the Left Piston for the baseline OFPE

For the free piston engine at hand, it is very important to analyze the emission characteristics. As mentioned before, free piston engines offer better performance in terms of NOx production due to shorter residence times at TDC. The production of NOx for the first 5 cycles is presented in Figure 3.19 in terms of mass fraction and in Figure 3.20 in terms of mole fractions.

In this figure, the production of NOx is given in terms of the mass fraction. As expected, the production of NOx starts with ignition. The compression ratio slightly increases for the first few cycles. As a consequence, the piston spends more time at TDC with over-compression. This leads to an increased NOx production over the cycles. After conducting the multi-cycle analysis, it was found that the emission index for NO and NO2, defined as gram of specie over kg kilogram of fuel, was found to be: $EINOx = 163.3g/kg$.

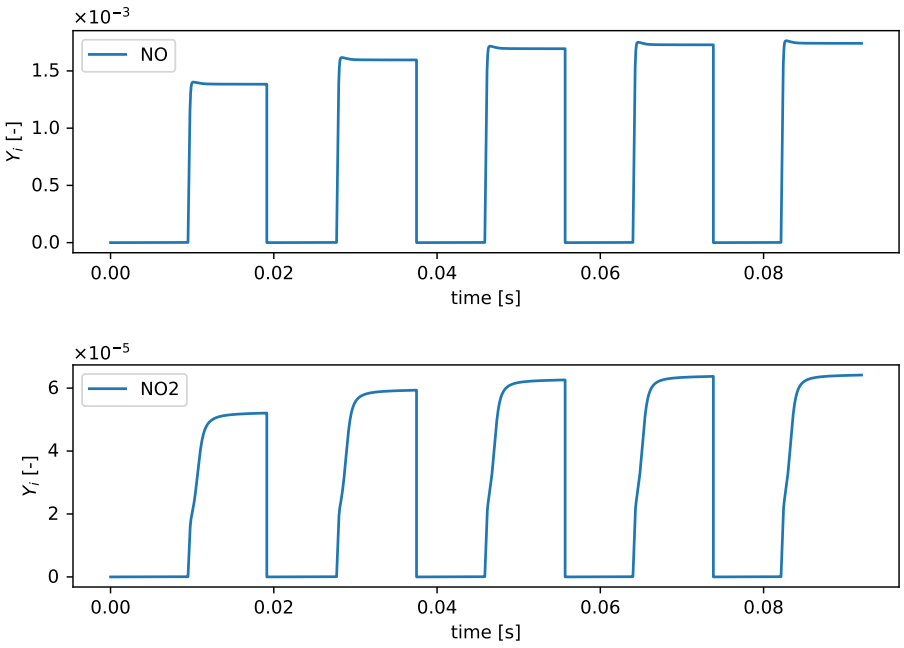

Figure 3.19: NOx emissions in mass fractions for the baseline OFPE

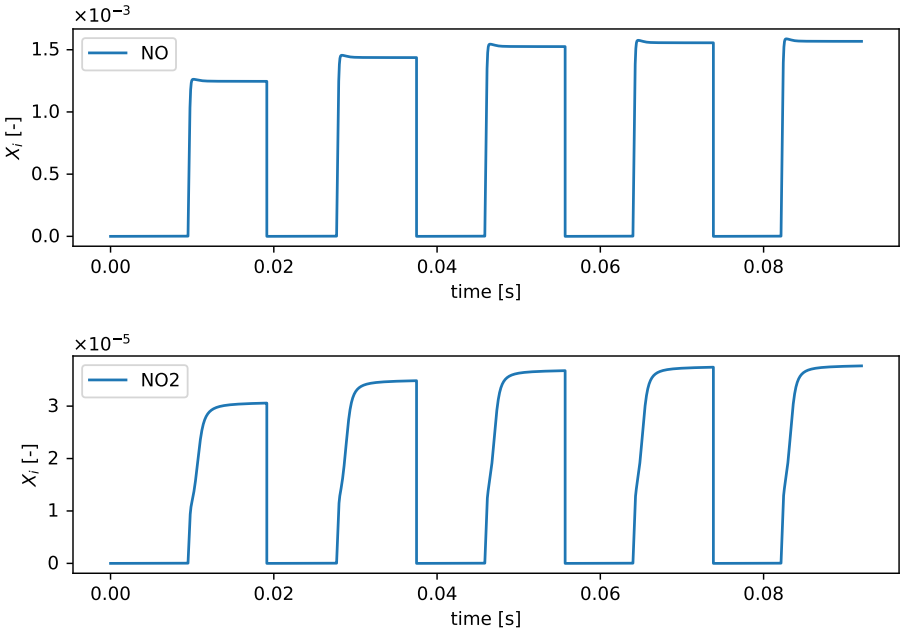

Figure 3.20: NOx emissions in molar fractions for the baseline OFPE

3.2.2. Sensitivity Analysis

In this subsection, the results of the sensitivity analysis conducted on the opposed free piston engine model will be presented. This allows a better understanding of the synergies of different parameters. For this analysis, the piston mass, inlet temperature and the equivalence ratio is varied. The results from the sensitivity analysis also was useful in scaling up the piston to a larger model. This would be further elaborated in the next section. In the sensitivity analysis conducted, the parameters that were varied are the piston head mass, in-cylinder inlet temperature and the equivalence ratio. In the

simulations made for each variable, every other input is kept constant. The inputs for the sensitivity analysis is provided in Table 3.4. The inputs for the variables that will be studied in the sensitivity analysis is given for both the baseline case and the ranges of values that are used in the study.

Parameter	Value
b	0.06 m
b/s	1
CR	22
R_{bdc}	0.2
R_{port}	0.25
m	**base:** 2kg, **sens**: [1,2,3,4] kg
C_A	70
f_s, f_d	210, 2
X_{fuel}	'H2:1'
X_{ox}	'O2:1.0, N2:3.76'
ϕ	**base:** 0.38, **sens**: 0.2-0.8
T_i	**base:** 400 K, **sens**: [300,400,500,600] K
P_i	1 bar
P_{bc}	15 bar
T_{wall}	700 K

Table 3.4: Inputs for the Piston Mass Sensitivity Analysis

Piston Mass

In this part, the effect of changing the piston head mass is discussed. In this analysis, all the inputs are constant except the piston mass which is analyzed for $m = [1, 2, 3, 4]$ kg. The overview of the simulations can be seen in Figure 3.21a and Figure 3.21a.For this study, the definition for the indicated thermal efficiency is used as the integration of the in-cylinder P-V curve over the fuel energy provided in the cycle [25]. Firstly, Figure 3.21a shows that when the piston mass is increased, the compression ratio increases. Meanwhile, Figure 3.21b shows a decrease in indicated thermal efficiency with increasing piston mass. This is because the piston undergoes over-compression. The over-compression on higher piston head masses for this case can be observed more clearly in Figure 3.22. In the cycle where $m = 1kg$, near constant volume combustion happens almost exactly at the TDC. The over-compression with increased piston mass is seen with the increase in adverse work zone. Therefore, even though the compression ratios are higher, the indicated thermal efficiency is lower.The reason why over-compression happens when only piston mass is increased in this case, is because higher the piston mass, higher the inertia. The rate at which heat is released is not fast enough to counteract the high inertia of the piston mass moving towards the TDC.

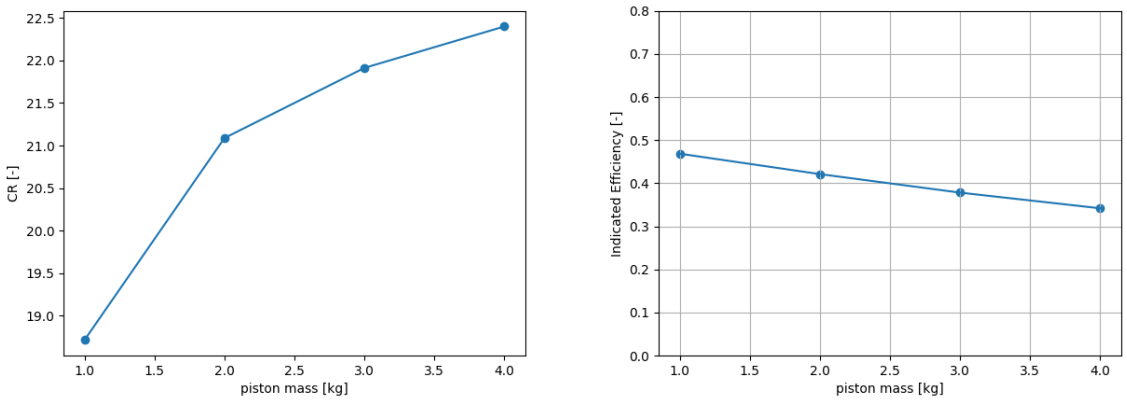

(a) Compression ratios

(b) Indicated Efficiency

Figure 3.21: Change in Performance for changing piston head mass

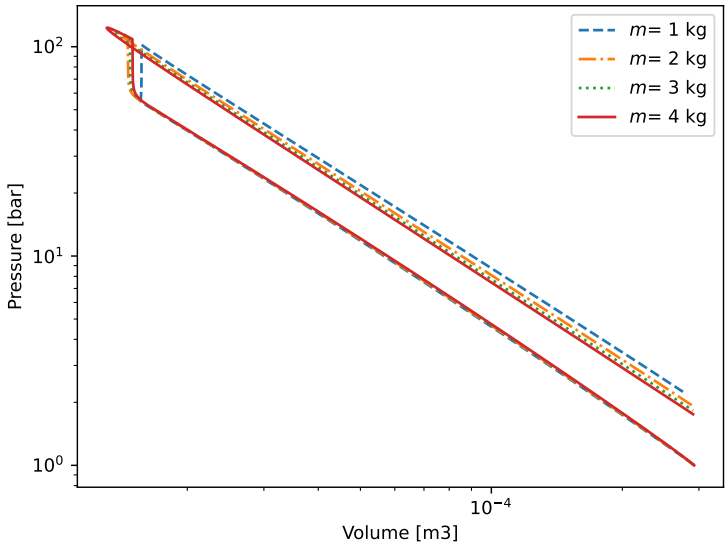

Figure 3.22: P-V diagram for changing piston head mass

In Figure 3.23a and Figure 3.23b, the temperature and pressure over one cycles for the different masses are presented. The higher compression ratios achieved with higher piston head mass is also observed in the pressure profile. Figure 3.23a shows that the peak pressures reached in the cycles are higher with the higher piston head mass. On the other hand, Figure 3.23b shows that the peak temperatures are somewhat constant. Due to the over-compression in this case, a higher compression ratio does not lead to a more complete combustion process. Therefore, the peak temperatures are similar in the simulations. Furthermore, the increased piston mass leads to an increased ignition delay. This is because, the higher piston mass leads to lower accelerations and therefore velocities.

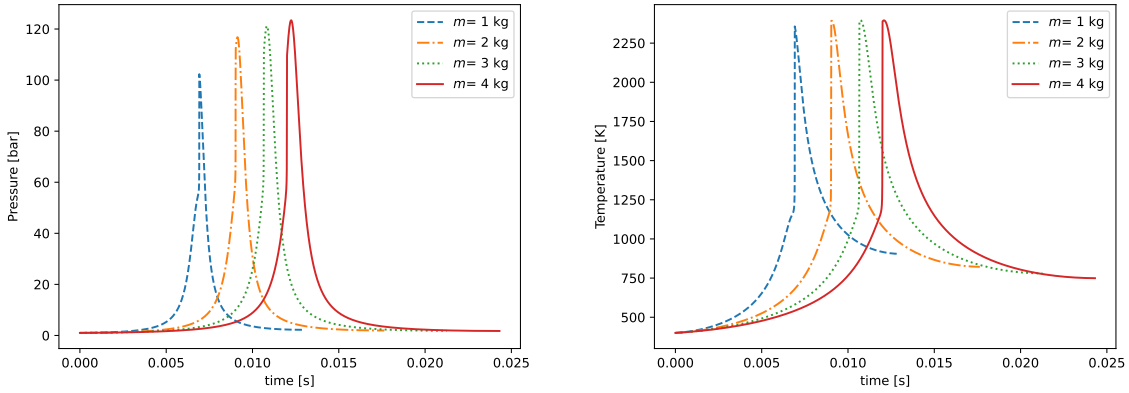

(a) Pressure over time

(b) Temperature over time

Figure 3.23: In-cylinder thermodynamics for changing piston head mass

The effect of changing the piston head mass on the dynamics of the piston can be seen in Figure 3.24a and Figure 3.24b. In Figure 3.24a, the increase in average piston velocity is observed, which confirms the higher accelerations. This is also observed with the fact that the cycles take much longer as also seen in Figure 3.24b. Another observation that could be made from Figure 3.24b is the fact that having a higher piston mass leads increased residence time near TDC during and after ignition. This is represented by the increased width of the peaks observed in Figure 3.24b.

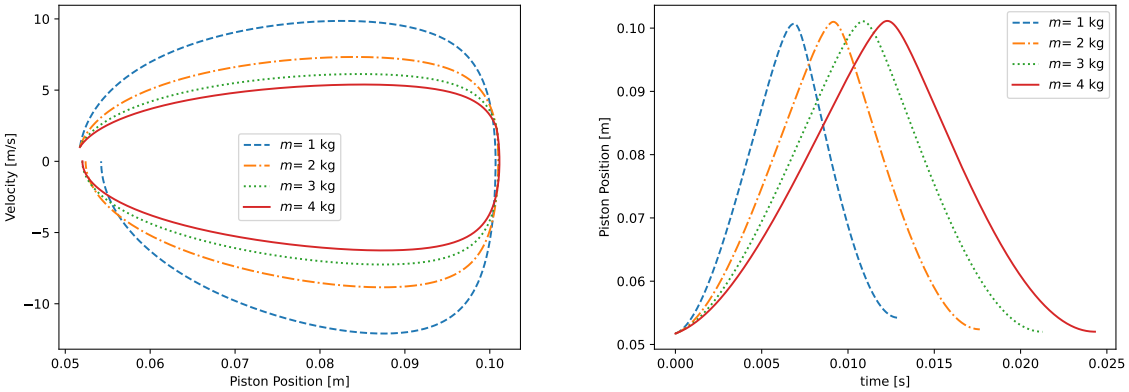

(a) Velocity over position

(b) Piston position over time

Figure 3.24: Piston dynamics for changing piston head mass

Higher residence times is expected to have higher NOx production [63]. Since an increased piston head mass leads to increased residence times, it is expected that the production of NOx will also be higher. Figure 3.25a and Figure 3.25b presents the production of NOx in terms of molar fractions over the cycle. As expected, the production of NOx starts at the point of ignition for each simulation. Furthermore, the increase in NOx production with increasing piston head mass is observed in both graphs. So, the effect of the piston head mass on the residence times is observed even more clearly from the NOx graphs. Furthermore, the Zeldovich mechanism for Thermal NOx production shows that the the production NOx increases with peak temperature [83].

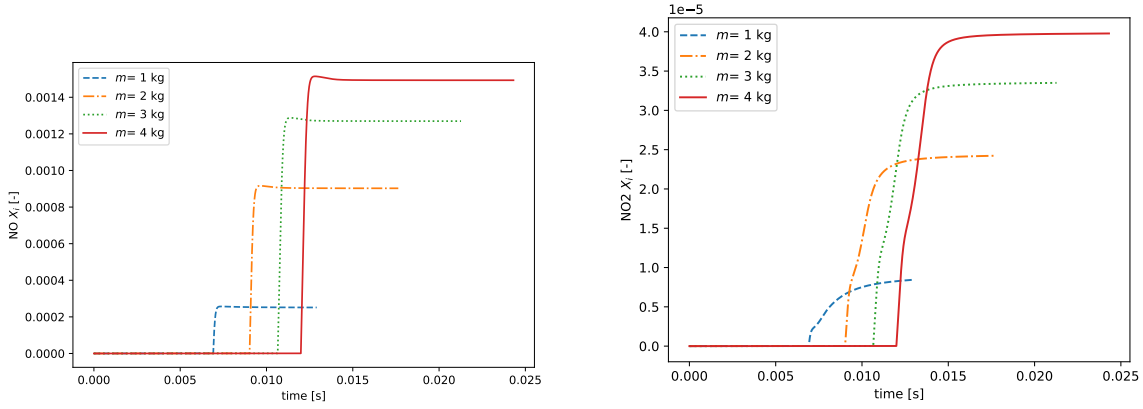

(a) NO molar concentrations

(b) NO2 molar concentrations

Figure 3.25: NOx emissions for changing piston head mass

Inlet Temperature

The next parameter that was explored was the inlet temperature. Again, keeping all the other inputs constant, the inlet temperature is varied as $T_0 = [300, 400, 500, 600]$ K. The inlet temperature and the performance of the engine are highly related. A higher inlet temperature will require less compression to reach the point of ignition. In Figure 3.26a, the compression ratios over changing inlet temperature is given. Overall, the observed trend shows a decrease in achieved compression ratio with increasing inlet temperature. Meanwhile, at $T_i = 300$ K, the compression ratio is lower than the case where $T_i = 400$ K. This can be better explained when examining Figure 3.26a as well. The fact that the indicated efficiency is almost zero when $T_i = 300$ K is because the flow does not undergo combustion. For the condition $T_i = 300$ K, the in-cylinder gas is under-compressed to achieve HCCI combustion. When $T_i = 400$ K, not only the required compression ratio for HCCI combustion is lower, but also the

actual compression ratio reached is also recorded to be higher. This can be explained by the fact that the mass of the in-cylinder gas for the cycle increases with increased temperature according to ideal gas law. With the increased gas mass, the inertia of the in-cylinder gas. This results in a similar effect of the increase in piston mass discussed previously. With the higher gas mass, the piston is pushed slightly further and ignition is achieved. For the $T_i = 500$ and $T_i = 600$, the required compression ratio is even lower as the temperatures are closer to the auto-ignition temperature of hydrogen. So, the in-cylinder gas goes through over-compression, which decreases indicated thermal efficiency of the cycle. The compression characteristics of the different conditions can be seen in more detail in P-V diagrams given in Figure 3.27.

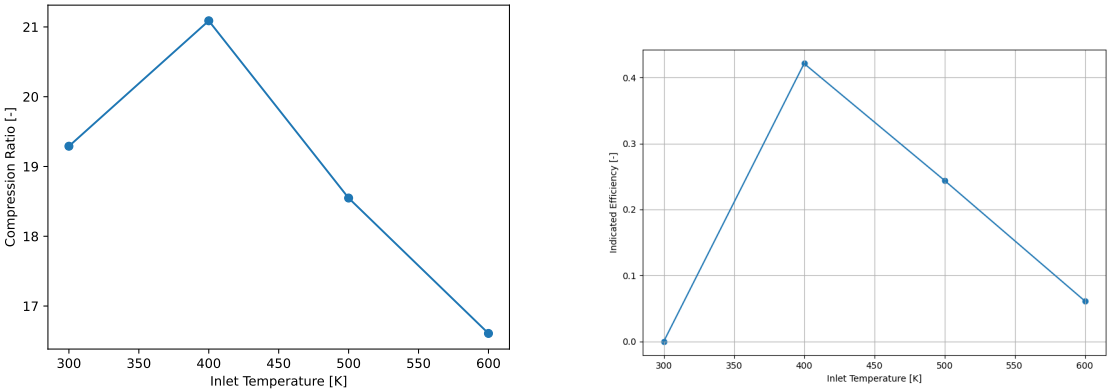

(a) Compression ratios

(b) Indicated Efficiency

Figure 3.26: Change in Performance for changing Inlet Temperature

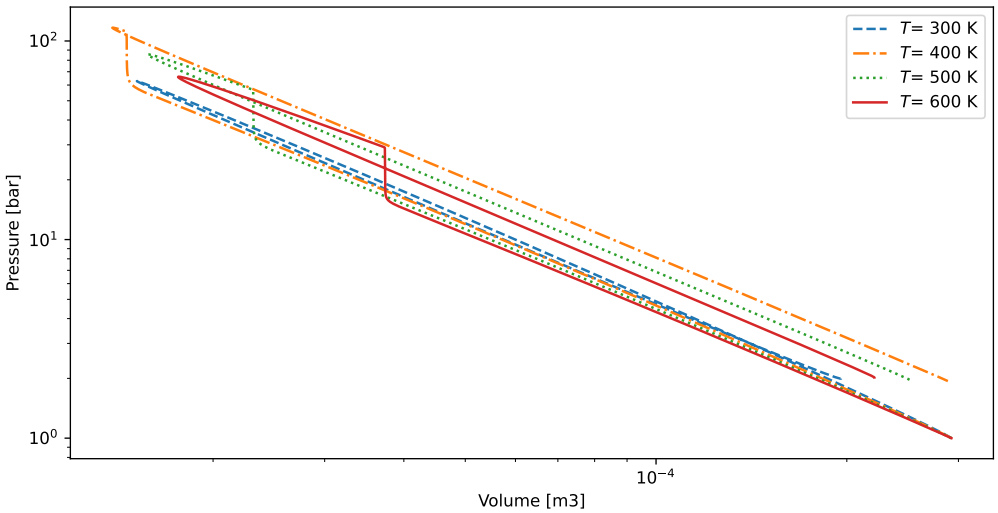

Figure 3.27: P-V diagram for changing Inlet Temperature

The change in in-cylinder pressure and temperature profiles are given in Figure 3.28a and Figure 3.28b. The cycle with $T_i = 300$ shows the lowest peak pressure and temperature. This is expected as there is no ignition in this cycle. Then, the highest peak pressure is reached in the cycle with $T_i = 400$. Since the compression ratio was highest in that cycle, the peak pressure is also the highest. Then, the peak pressures decrease with the increasing inlet temperatures, following the trend of the compression ratios. Meanwhile, the trend observed in the in-cylinder temperature profile is different. The tempera-

tures show an increase with the increase in inlet temperature. During over-compression, the time spent near TDC increases. This leads to a more complete combustion, therefore, higher peak temperatures.

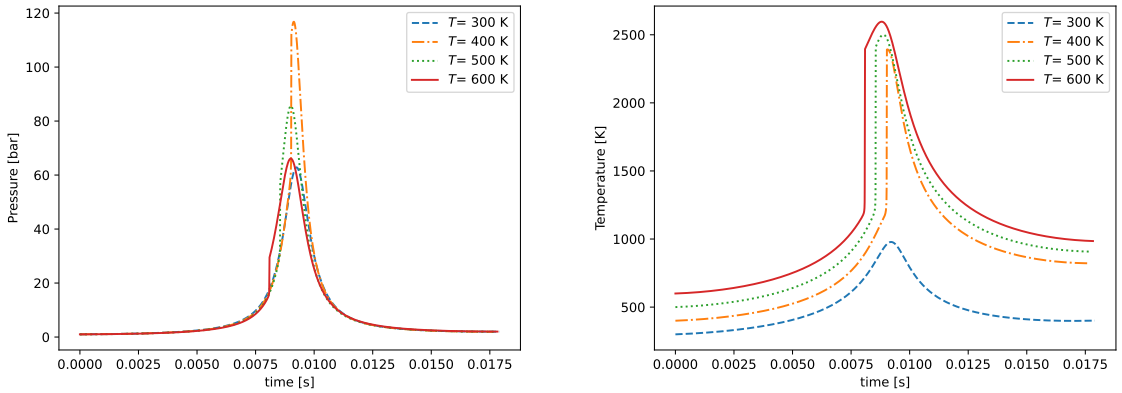

(a) Pressure over time

(b) Temperature over time

Figure 3.28: In-cylinder thermodynamics for Inlet Temperature

The effect of changing the in-cylinder inlet temperature on the piston dynamics is visualized in Figure 3.29a and Figure 3.29b. Looking at the widths of the peaks given Figure 3.29a, it can be seen that longest time spent at near TDC is by the cycle with $T_i = 300$K. Since there is no auto-ignition at that cycle, the in-cylinder gas does not rapidly start applying force to start the expansion stroke. With the cycle with $T_i = 400$K, the in-cylinder gases ignite, so there will be a higher force pushing the pistons to start the expansion stroke. As the inlet temperature increases, the cycles experience higher over-compression. Therefore, the residence time gets higher with increased inlet temperature in this case. Figure 3.29b, allows a better understanding of the behaviour of the piston for each condition. Looking at the right side of this graph, it can be seen that the cycle with $T_i = 400$ K has a slightly longer stroke than the cycle with $T_i = 300$K. This confirms the slightly higher compression ratio for the cycle with $T_i = 400$K compared to the cycle with $T_i = 300$ K. Furthermore, Figure 3.29b shows that, for the selected engine inputs, only the cycle with $T_i = 400$K reaches close to the desired BDC. The under-compressed cycle does not generate enough force at the end of the compression stroke to send the piston back to the BDC location. Meanwhile, over-compressed cycles lose some of the fuel energy on doing adverse work. So, not enough energy is left to push the piston back to the BDC.

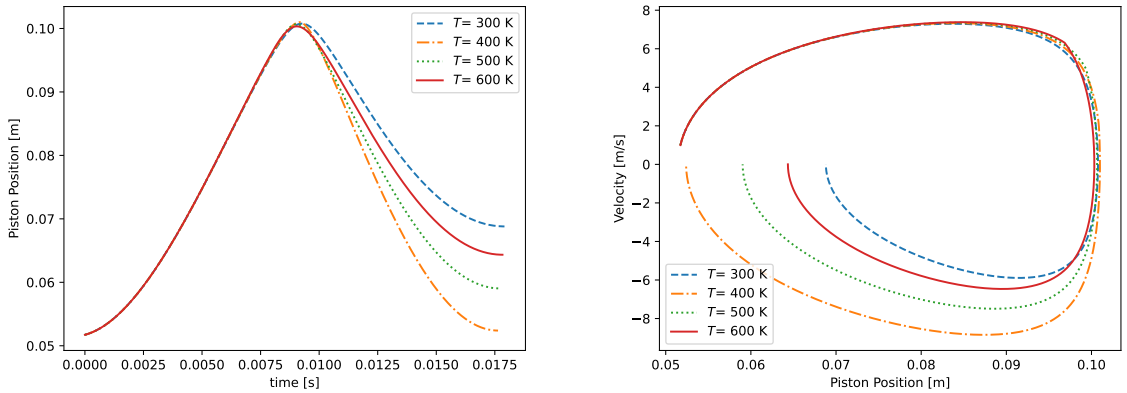

(a) Position over time

(b) Velocity over position

Figure 3.29: Piston dynamics for changing Inlet Temperature

The effect of the higher residence times during the increased over-compression with increased in-cylinder inlet temperature can be observed on the NOx formation. In Figure 3.30a and Figure 3.30b,

the production of NOx for the different conditions are presented. There is no NOx production with the cycle where $T_i = 300K$ because there is no auto-ignition. Looking at the other conditions, the trend in NOx production follows the trend of the residence times as expected. The more time spent at TDC due to over-compression increases the NOx production substantially.

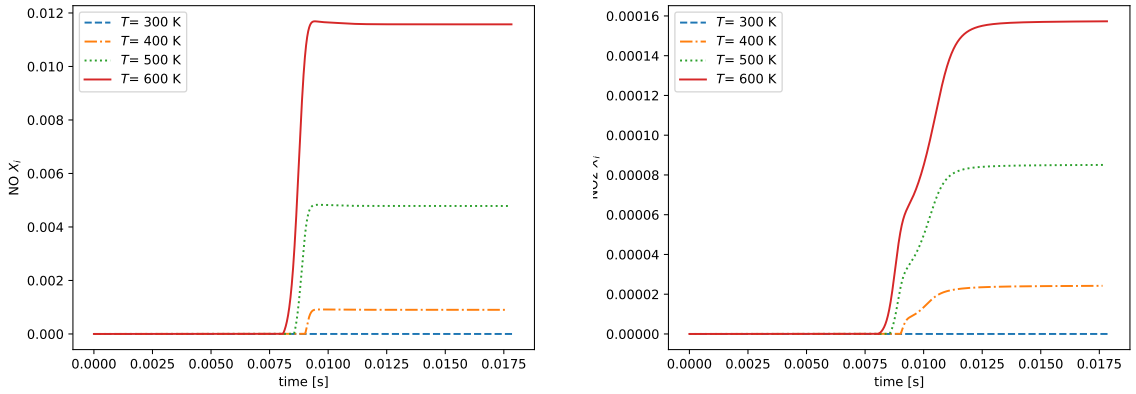

(a) NO emissions

(b) NO2 emissions

Figure 3.30: NOx emissions for changing Inlet Temperature

Equivalence Ratio

Lastly, the effect of changing the equivalence ratio, ϕ, is studied. Similar to the other sensitivity analysis studies made in the part, all other inputs except the equivalence ratio is kept constant. In Figure 3.31a, the achieved compression ratios are given for each value of equivalence ratio. The compression ratio decreases with increasing equivalence ratio. Meanwhile, Figure 3.31b shows that the indicated efficiency of the cycle peaks at around $\phi = 0.4$. In order to have a better understanding on the results of each cycle, the P-V diagrams given in Figure 3.32 are examined. The length of the compression strokes are in-line with the values of achieved compression ratio. The cycle with $\phi = 0.2$ is compressed to the furthest point, therefore has the highest compression ratio. This is because the cycles with higher equivalence ratio require a smaller compression ratio to reach auto-ignition[63].

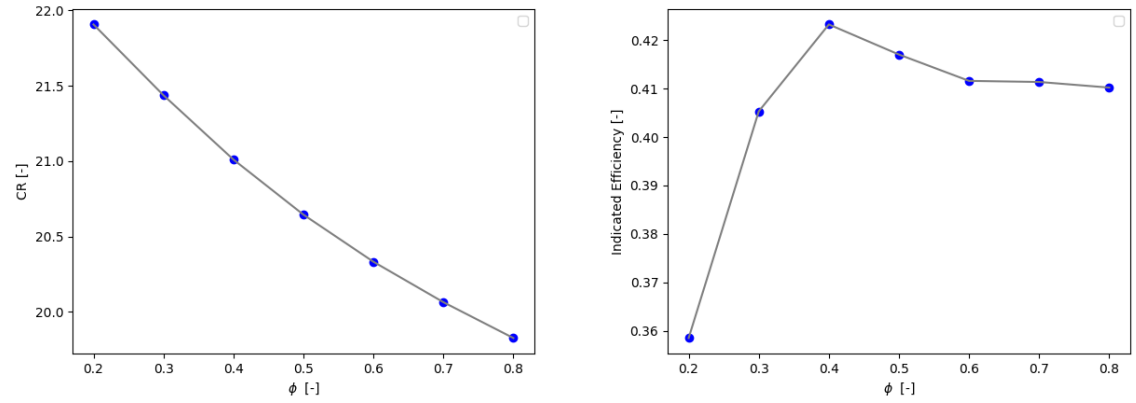

(a) Compression ratios

(b) Indicated Efficiency

Figure 3.31: Change in Performance for Equivalence Ratio

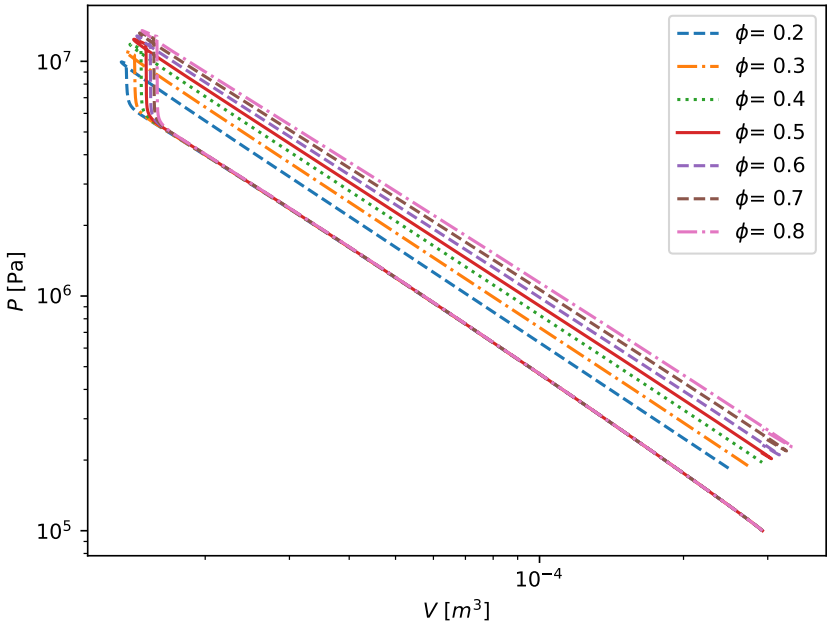

Figure 3.32: P-V diagram for changing Equivalence Ratio

Examining the combustion processes depicted in the P-V diagrams, it can be seen that the length of the constant volume combustion process is higher with increasing equivalence ratio. This is because as equivalence ratio is increased, the fuel energy packed in the in-cylinder gases increase. Therefore, a larger heat release can be achieved with higher equivalence ratio. Although, there is a larger heat release for the higher values of equivalence ratio, the indicated efficiencies are decreasing. This can be explained by two factors. Firstly, the larger heat release due to higher equivalence ratio leads to higher peak pressures and temperatures. Therefore, the heat losses at TDC due to combustion will be higher. This can also be observed in the pressure and temperature profiles given in Figure 3.33a and Figure 3.33b. The temperature and pressure profiles for each condition is quite similar except the peak values. Secondly, the over-compression achieved at higher equivalence ratio also deteriorate the indicated thermal efficiency.

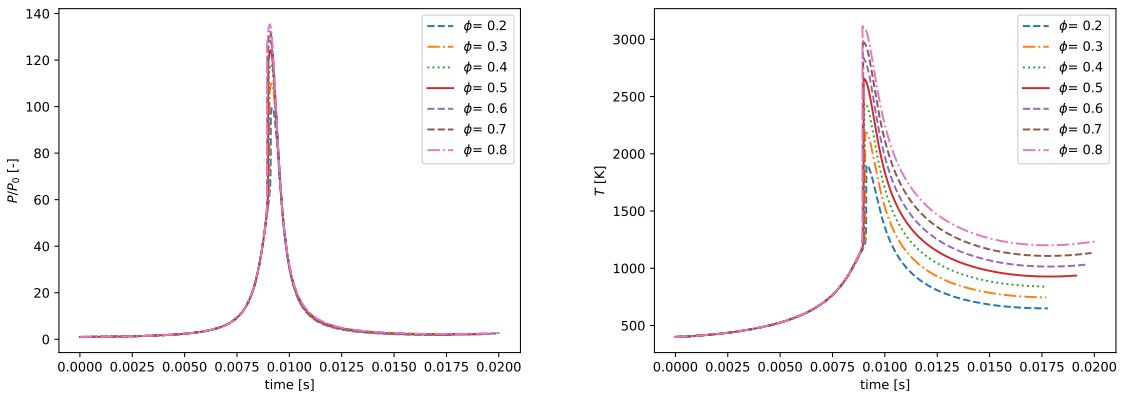

(a) Pressure over time

(b) Temperature over time

Figure 3.33: In-cylinder thermodynamics for changing Equivalence Ratio

In Figure 3.34a and Figure 3.34b, the effect of changing equivalence ratio on the piston dynam-

ics is presented. The effect of changing equivalence ratio has the largest impact on the expansion stroke. The higher peak pressures are reached during combustion with higher equivalence ratio. Consequently, a larger force is exerted on the pistons to move them towards the BDC at higher velocities. The force exerted by the in-cylinder gas after ignition should be high enough to reach the BDC. So, the increased equivalence ratio in this case, leads to a shorter residence time at TDC with having higher peak pressures. This leads to an interesting synergy in terms of the NOx production. In Figure 3.34a the production of NO over time and in Figure 3.34a production of NO2 over time is presented. In both graphs, the highest production of species does not correspond to the cycle with the highest peak temperature. The reason for this can be explained by the fact that the cycles with higher equivalence ratio values also spend less time near TDC. The time dependency of the production of NOx can also be seen in these graphs.

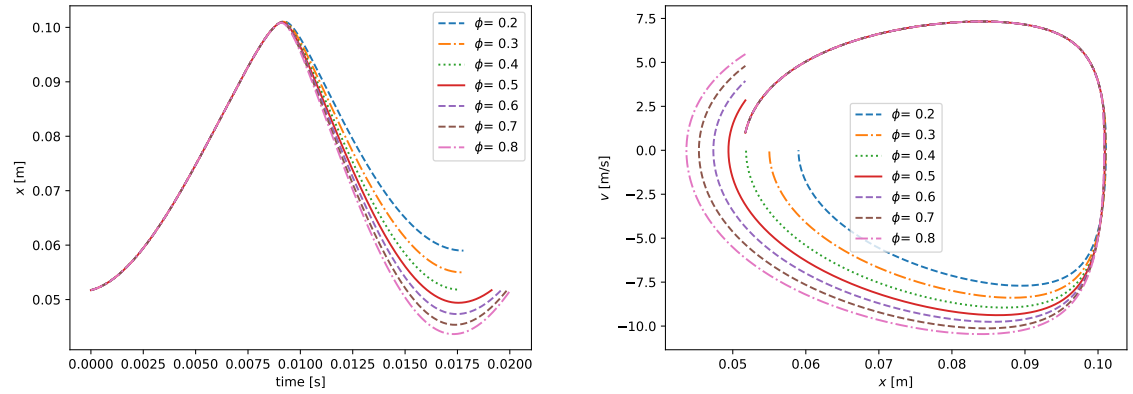

(a) Position over time

(b) Velocity over position

Figure 3.34: Piston dynamics for changing Equivalence Ratio

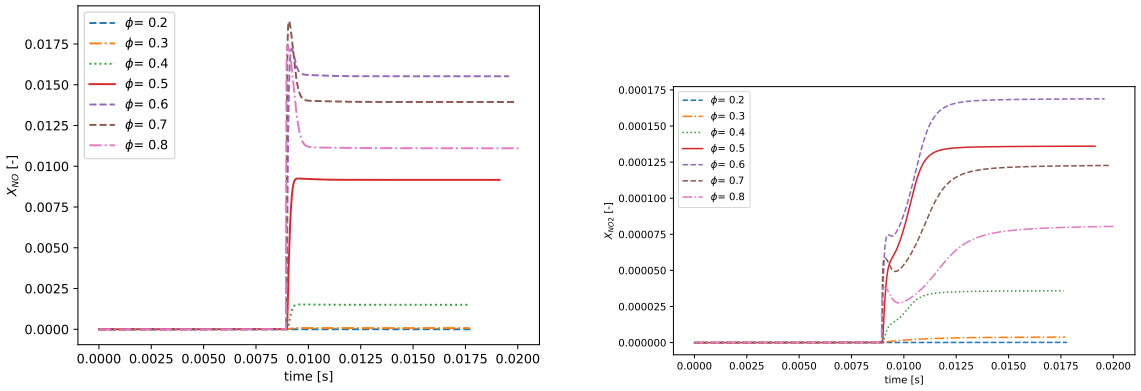

(a) NO emissions

(b) NO2 emissions

Figure 3.35: NOx emissions for changing Equivalence Ratio

3.2.3. Validation

The model for the opposed free piston engine has to be validated in order to ensure that the results are realistic. The validation of the engine analyzed in this study was a difficult task. Currently, there is no work available in literature that studies the modelling of an opposed free piston HCCI engine burning H2 using reactor networks. Therefore, validation of the model using an existing engine model was not possible. So, the different parts of the model had to be validated separately. The studies in literature that comes closest to the engine configuration at hand are the analysis on the dual-cylinder H2 HCCI

engine made by Goldsborough [63], the opposed free piston SI model created by Zhu [67] and the experiments made by Sandia [64]. The thermodynamics of the HCCI combustion with hydrogen can still be validated against Goldsborough's analysis. With similar inputs as Goldsborough, the cycle is simulated. The inputs for the cycle is given Table 3.5.

Parameter	Value
T_i	300 K
P_i	1.5 bar
T_{wall}	700 K
b	0.07 m
m_{piston}	2.7 kg
ϕ	0.38
CR	17

Table 3.5: Inputs from Golsborough[63] used in the validation study

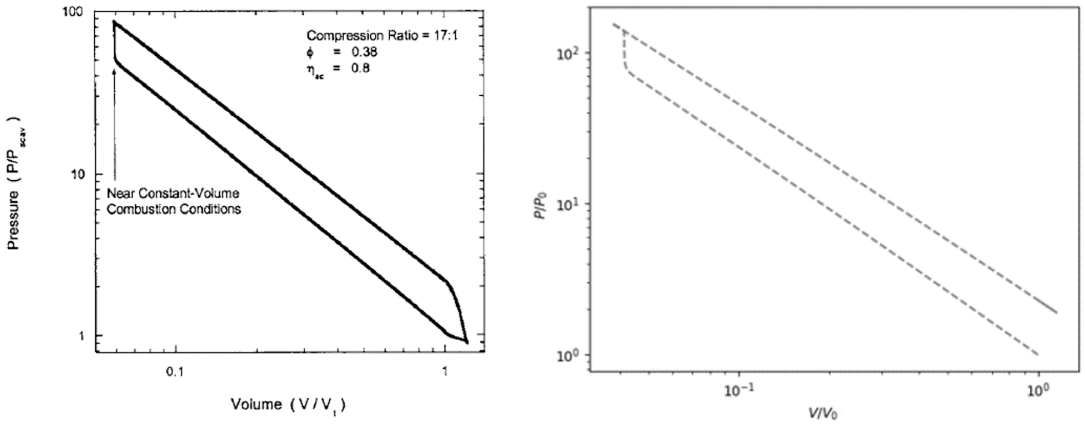

(a) P-V diagram from Goldsborough[63]

(b) P-V diagram from simulation

Figure 3.36: P-V diagram validation

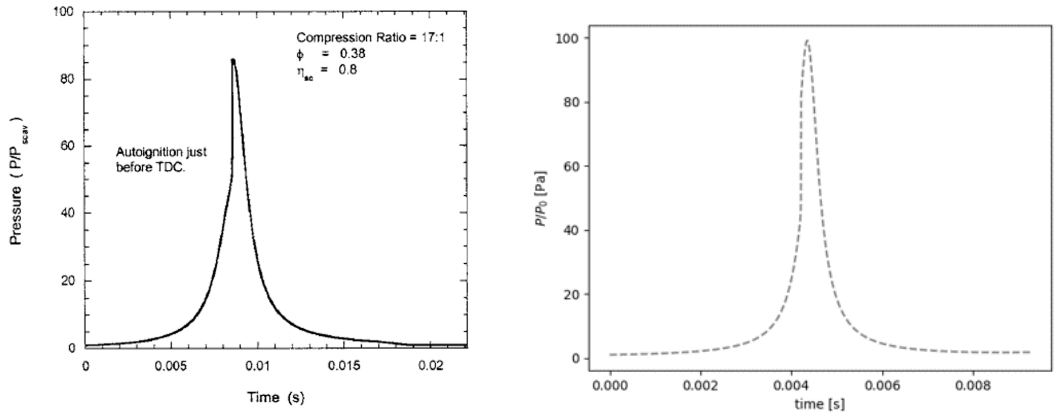

(a) Pressure over time from Goldsborough [63]

(b) Pressure over time from simulation

Figure 3.37: Pressure over time validation

Firstly, the P-V diagrams are compared looking at Figure 3.36b and Figure 3.36a. The trend of the P-V diagram is quite similar as there is near constant-volume combustion in the TDC. There is a small difference in the P-V diagrams where the results from the simulation show a slight over-compression whereas Goldsborough's results shows that the flow is compressed at an ideal compression ratio.

The pressure profiles for both simulations are given in Figure 3.37a and Figure 3.37b. The peak pressure for both cases are quite similar to eachother, with the simulated piston having slightly higher pressure than the results of Goldsborough. This is in-line with the P-V diagram showing the slight over-compression. Furthermore, cause of the rapid pressure rise due to the released fuel energy is captured in both cases. Lastly, the cycle of Goldsborough takes slightly longer than the cycle results from the piston simulation. Yet, the combustion duration in both simulations are very similar around 5-10 μs. The difference in the results can be explained by the difference in configurations as Goldsborough is a dual-cylinder engine and different reaction mechanism used in both cases. This is also apparent when looking at the cycle duration. In Figure 3.38, the P-V diagram recorded from the simulations of Sandia is presented. This graph also shows that the P-V diagram of the simulated opposed-free piston engine is close to the experimental results.

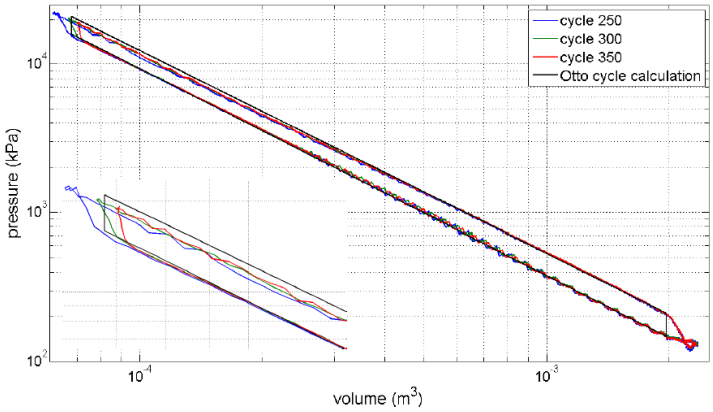

Figure 3.38: P-V diagram from Sandia [64]

The kinematics of the pistons have a large effect on the overall performance of the piston engine, therefore, it has to be validated. In addition, the piston dynamics depend highly on the thermodynamic properties of the in-cylinder gas. Therefore, validating the dynamics also will make the validation of the thermodynamics stronger. In Figure 3.39a, the position over time and in Figure 3.39b, the velocity over position is presented from the results of Goldsborough. The piston spends less time at TDC compared to the crankshaft configurations. Furthermore, the velocity profile is egg-shaped and moves faster in the TDC and BDC compared to the crankshaft configurations. Furthermore, the pistons move faster during the expansion stroke compared to the compression stroke in a HCCI free-piston engine[68][67]. This can be more clearly observed in the velocity-displacement curve by Zhu given in Figure 3.40. Lastly, the acceleration velocity profile from the study made by Alrbai is presented in Figure 3.41. The simulated acceleration profile is quite similar to the profile provided by Alrbai. The acceleration peaks with ignition and increases slightly when there is over-compression and starts decreasing as the expansion stroke starts. Furthermore, the step changes during gas exchange and BDC location are also presented in the simulated acceleration profile.

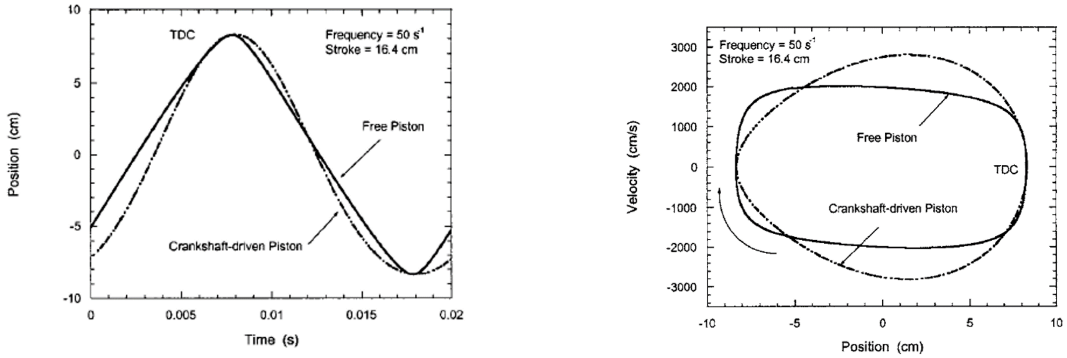

(a) Position over time

(b) Velocity over Position

Figure 3.39: Cycle results of piston dynamics from Goldsborough[63]

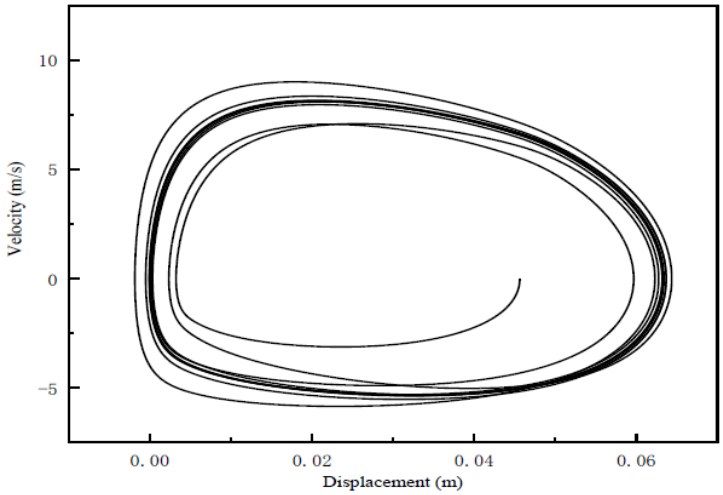

Figure 3.40: Velocity over Position from Zhu[67]

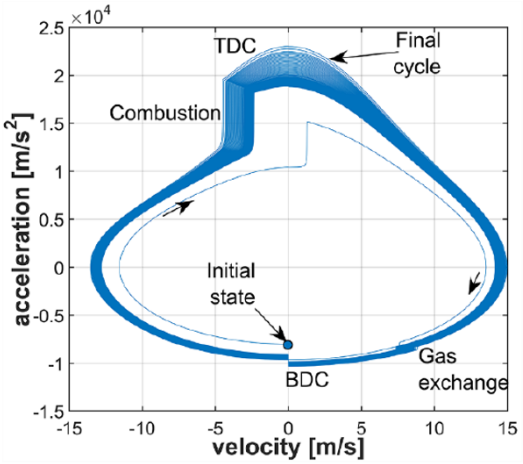

Figure 3.41: Acceleration vs velocity from Alrbai [68]

In Figure 3.42, the required compression ratio over various equivalence ratios are given from the analysis made by Goldsborough. The graph shows decreasing required compression ratio with increasing equivalence ratio. During the sensitivity analysis made, it was also observed that increasing

the equivalence ratio and keeping everything else constant would lead to over-compression. So, the sensitivity analysis results are in-line with the results of this graph. Furthermore, in Figure 3.44, the combustion pressure is presented for varying piston masses. Similar to the results found in the sensitivity analysis, the peak pressure of the combustion chamber increases with the heavier moving mass. In addition, the peaks move slighlty to the right because of the decreased piston velocity. This trend is also observed in the sensitivity analysis.In conclusion, the thermodynamics and kinematics of the free opposed piston HCCI combustion model is validated.

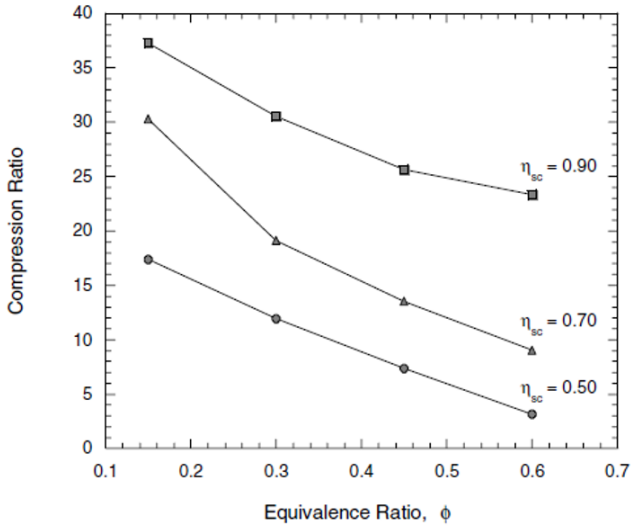

Figure 3.42: Compression Ratio over Equivalence ratio from Goldsborough [63]

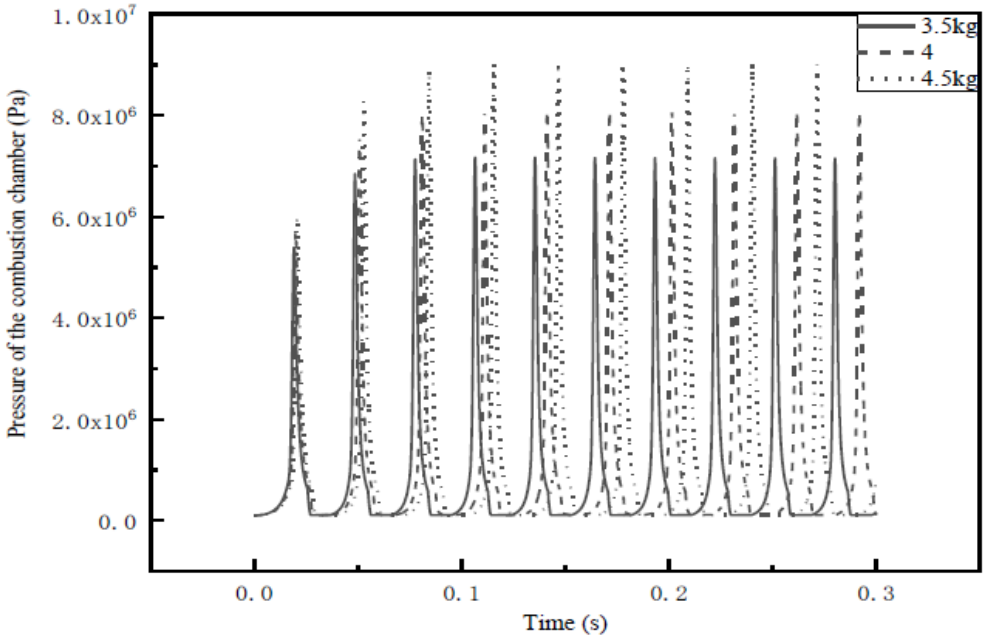

Figure 3.43: Changing piston mass effect on pressure profile from Zhu [67]

3.2.4. Scaled-up Piston

The multi-cycle analysis of the free piston engine is conducted. For this analysis the piston is simulated for 50 cycles. The overview of the results are presented in Table 3.7.

The results from the scaled-up engine will be compared to the baseline engine. An average frequency of 58 Hz and compression ratio reaches around 4.1 found over the cycles. The mass charge per cycle increased almost by 100 times. This allows for around 10 piston engine modules required to accommodate the mass flow requirement of LEAP-1A26. Since this is a high charging engine, the compression ratio of 4.5 was found to be sufficient to auto-ignite the gases. The bore-to-stroke ratio is shorter for the scaled-up engine compared to the baseline engine. This is also because the inlet temperature for the scaled-up engine is higher than the inlet temperature of the baseline engine. Therefore, the required compression ratio to reach the auto-ignition point of $T = 1150K$ is lower. Furthermore, since a lower compression ratio is needed, the stroke does not have to be as long. Although the initial temperature and pressure is quite similar for both scaled-up and the baseline engine, the peak pressure and temperature values are quite close. Since the compression ratio is lower for the scaled-up piston, the ratio of the peak value to the initial value for the temperature and pressure is lower. The value of the peak pressure is lower than the required 250 bar. In addition, even though the power generated by the alternator is much higher, the energy conversion efficiency is lower than the baseline engine. Furthermore, the indicated efficiency is also lower. The inputs of scaled up model is given in Table 3.6.

Parameter	Value
b	0.17 m
b/s	1.5
CR_{target}	4.5
R_{bdc}	0.2
R_{port}	0.25
m	25 kg
C_A	1200
f_s, f_d	1500, 300
X_{fuel}	'H2:1'
X_{ox}	'O2:1.0, N2:3.76'
ϕ	0.38
T_i	720 K
P_i	1 bar
P_{bc}	50 bar
T_{wall}	1000 K

Table 3.6: Inputs for the Scaled-up Engine

Parameter	Value
Average frequency f	58 Hz
Average Compression Ratio CR	4
Final Temperature T_f	1336 K
Final Pressure P_f	17 bar
Peak Temperature T_{max}	2342 K
Peak Pressure P_{max}	140 bar
Indicated thermal efficiency η_{ind}	23.8 %
Thermal efficiency η_{th}	14.3 %
Alternator Power P_{alt}	114 kW
Gas mass per cycle m_{gas}	23.86 g
Number of piston engines N_{pistons}	10

Table 3.7: Scaled-up FP Results

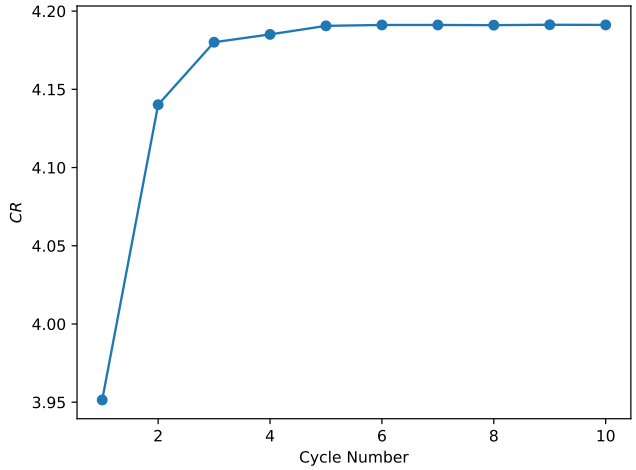

Figure 3.44: Compression Ratio over the first 10 cycles for the Scaled-up engine

To get a better understanding on the changes in the efficiency, the energy breakdown will be analyzed. The breakdown of input energy for the scaled-up piston is given in Figure 3.45. It can be seen that the percentages of the heat loss and friction loss are quite similar between the two models. Meanwhile, a much larger proportion of energy goes to the exhaust heat compared to the baseline engine. In the scaled-up engine, b/s is higher. This results in a shorter stroke. Since the alternator generates energy as the piston moves between TDC and BDC, it is less effective. In turn, less of the input fuel energy is used by the alternator. In this engine, most of the input fuel energy is used to heat up the flow. So, by having a longer stroke, the portion of energy that is used by the alternator increases and the exhaust heat decreases.

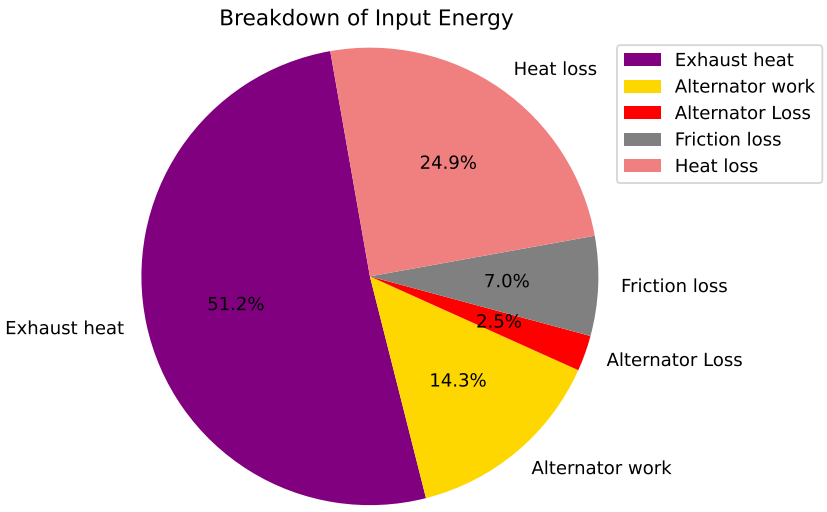

Figure 3.45: Breakdown of Input Energy

The thermodynamic characteristics of the scaled-up piston will be analyzed. This is important to understand the effects of the piston operation on the in-cylinder gas. In Figure 3.46, the P-V diagram for the scaled-up design is presented. The first cycle starts with a smaller compression and increases in the next cycles, causing slight over-compression. With the PI Controller, the compression ratio is controlled. The T-S diagram for the scaled-up design is presented in Figure 3.47. The difference between the initial

and later cycles are seen more apparent in the T-S diagram of the scaled-up engine vs the baseline engine. Again, due to the heat losses, the entropy seem to decrease during the compression and expansion strokes. In Figure 3.48, the in-cylinder pressure and temperature profile for the scaled-up piston is presented. The characteristic profiles for H2 HCCI combustion are also captured for the scaled-up piston. The auto-ignition temperature is around 1150 K, similar to the baseline piston. The peak pressure is slightly lower in the first cycle and slightly increases in the next cycles, following the trend of the compression ratios.

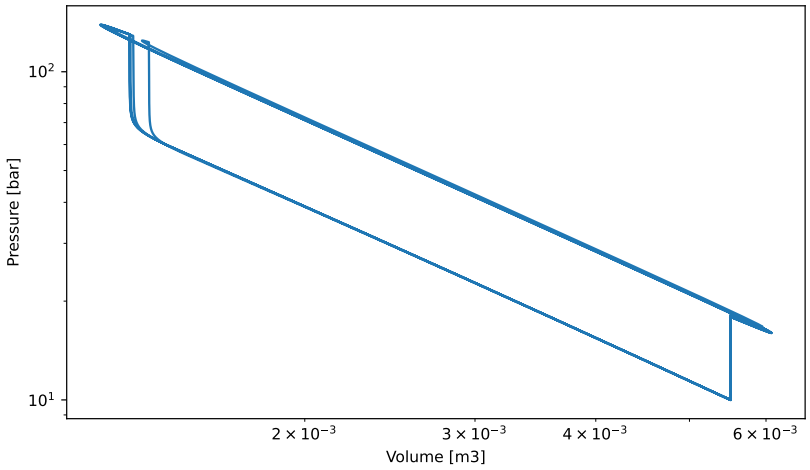

Figure 3.46: P-V diagram for the Scaled-up Piston Model over 5 cycles

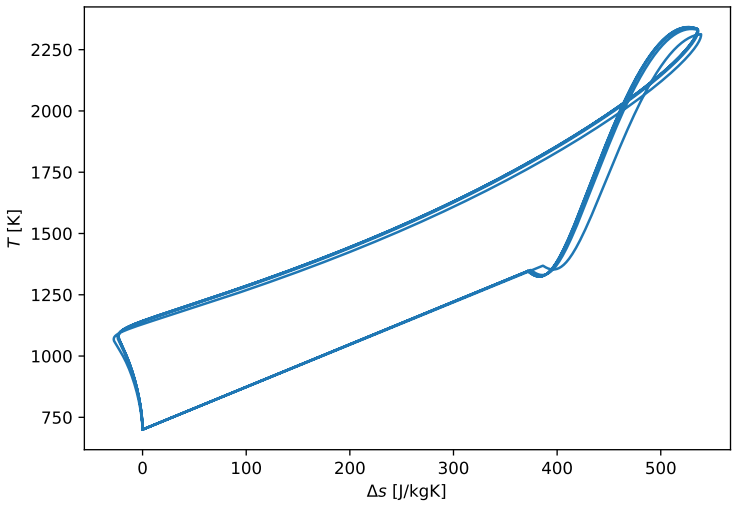

Figure 3.47: T-s diagram for the Scaled-up Piston model over 5 cycles

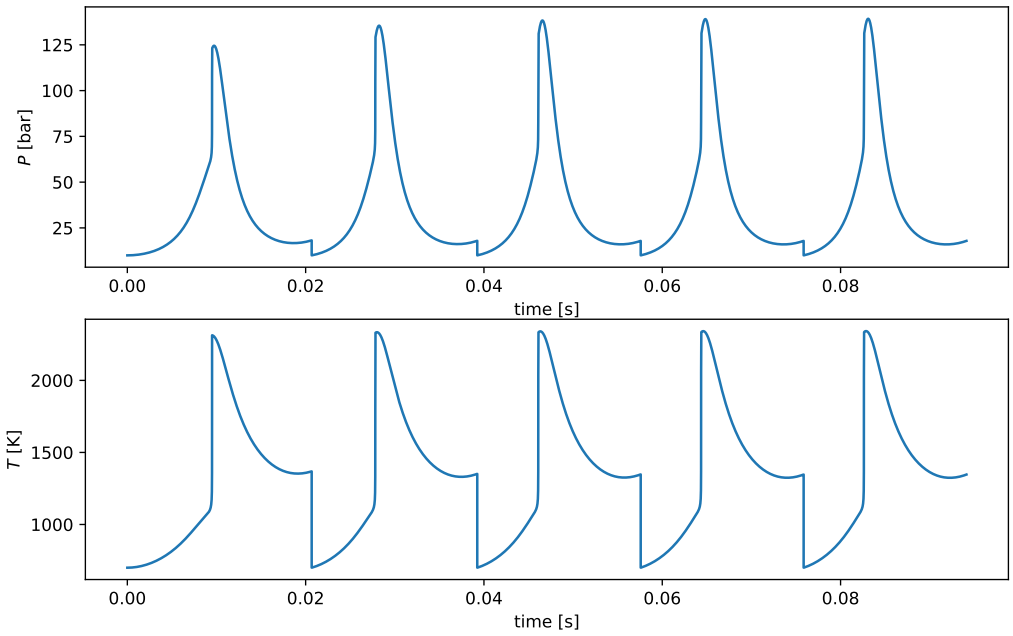

Figure 3.48: Pressure and Temperature over time the Scaled-up Piston model over 5 cycles

The piston kinematics for the scaled-up piston also has to be analyzed to see if the requirements are met. In Figure 3.49, the position over time graph for the scaled up piston is presented. The characteristic motion profile of a free piston is also observed in the scaled-up model. The piston spends less time at TDC compared to the BDC.

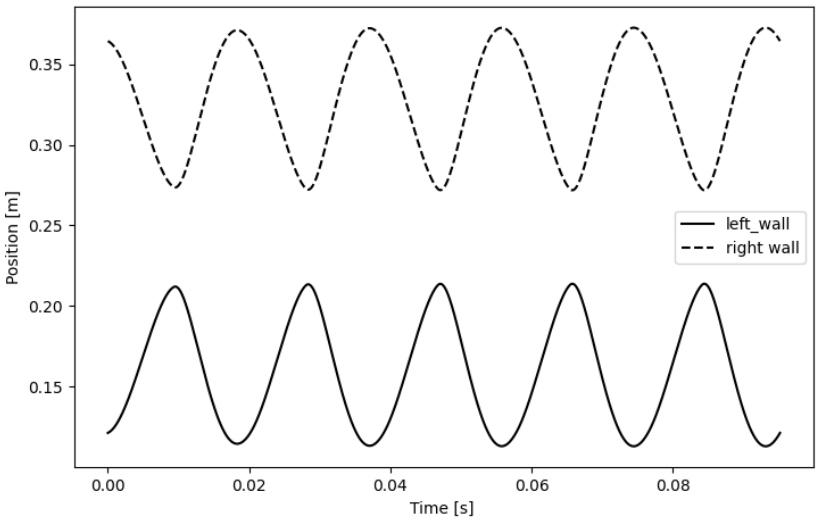

Figure 3.49: position over time the Scaled-up Piston model over 5 cycles

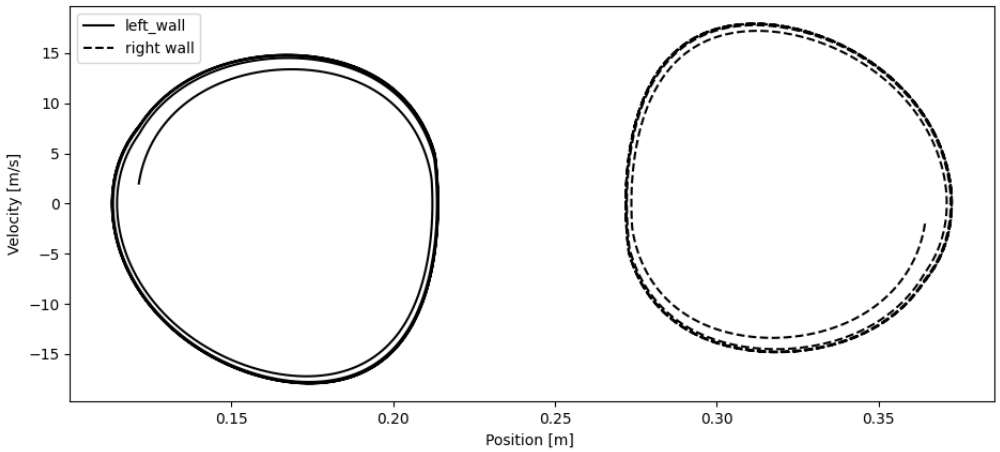

Figure 3.50: velocity over position the Scaled-up Piston model over 5 cycles

In Figure 3.50, velocity over position for the scaled-up model is presented. The egg-shaped profile is also apparent in this figure. Compared to the baseline engine, the scaled-up piston has a higher piston speed. Meanwhile, the maximum mean velocity of 18 m/s is not exceeded in this design. The higher velocities arise due to the lower b/s and higher bore length. Lower stroke lengths leads to higher accelerations and peak loads in the piston engine. The bore directly effects the force exerted by the gas pressure forces. Therefore, the recorded velocities are higher. The acceleration profile for the scaled-up piston is given in Figure 3.51. Comparing the acceleration profiles of the scaled-up to the baseline piston, a few observations can be made. Firstly, it can be seen that the accelerations starting from the BDC are much higher in the scaled-up piston until the piston reaches TDC. Then, the peak acceleration recorded in the scaled-up piston is actually lower than the baseline piston. This is because the compression ratio reached in the baseline piston is higher. So, the difference between the bounce chamber gas pressure and the in-cylinder gas pressure is higher in the baseline case. Still, the overall acceleration is higher in the scaled-up case due to the higher accelerations in the rest of the cycle, which leads to higher velocities.

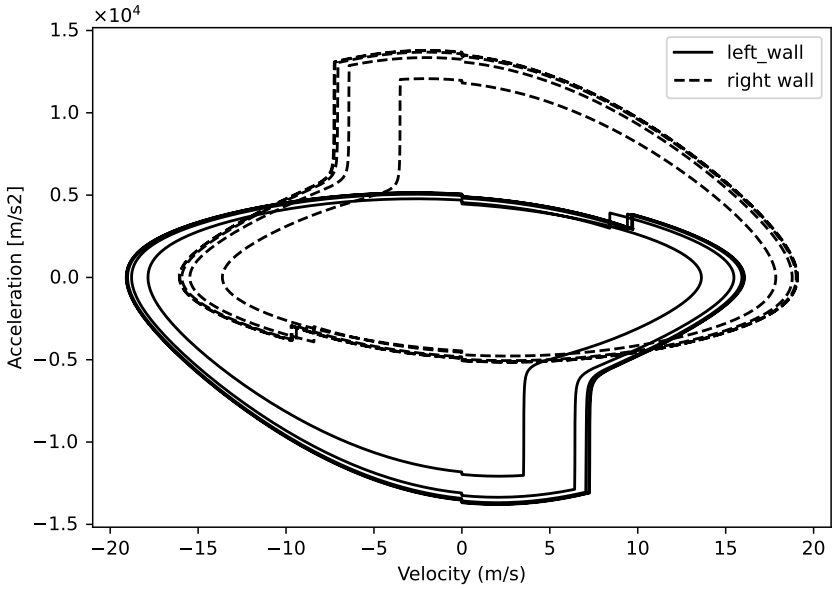

Figure 3.51: Acceleration over velocity the Scaled-up Piston model over 5 cycles

The NOx emissions are explored for the scaled-up piston design. The NOx emissions in terms of molar and mass fractions over time are presented in Figure 3.53 and Figure 3.52 . The emission trend is quite similar to the baseline engine model. The emission index for NO and NO2 are also calculated and found to be similar to the baseline piston engine where $EINOx = 233.76g/kg$. The NOX emissions from the scaled-up piston seems to be higher than the baseline concept. This can be attributed to a few reasons. Firstly, the density of the gas going into the scaled-up piston is higher than the baseline concept. This also explains why, given the same equivalence ratio, auto-ignition occurs in at a smaller compression ratio for the scaled-up piston. Furthermore, due to the higher piston head mass in the scaled-up piston, the residence time of the pistons at the TDC is higher compared to the residence time of the baseline piston. Therefore, higher NOx is recorded. The results shows that preliminary design of the scaled-up piston fulfills the requirements. The design can accommodate the performance and mass flow requirements for integration into LEAP-1A.

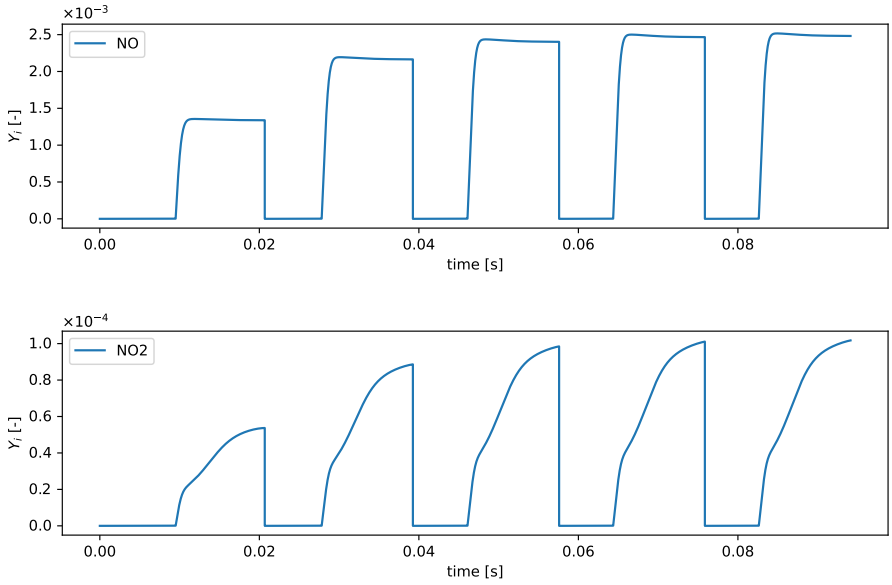

Figure 3.52: NOx emissions in mass fractions

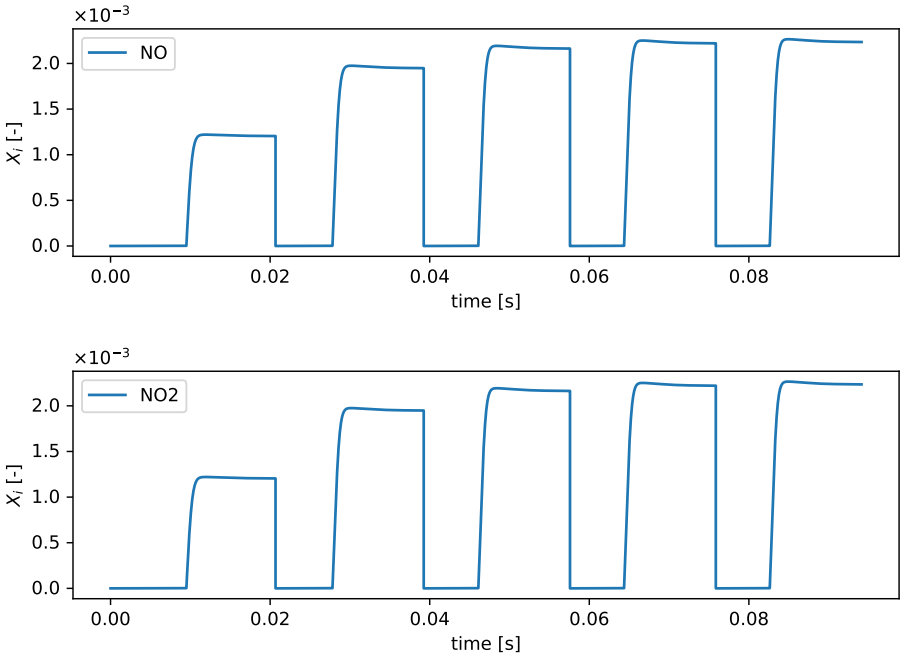

Figure 3.53: NOx emissions in molar fractions

4

Combined Cycle Aircraft Engine Modelling

4.1. Methodology

One of the most important tasks of during this thesis was to accurately model aircraft engine in which the pistons will be implemented. Therefore, a simple model of an existing aircraft had to be created. The FP-CCE concept is projected to be used in next generation short to medium range aircraft, such as the next generation Airbus A320Neo. Therefore, the LEAP-1A26CJ engine is used as the baseline aircraft engine, equipped in A320Neo. In this chapter, the modelling of the LEAP-1A26 engine and the validation of the results will be detailed.

In this study, the free piston engines will be implemented to work with the LEAP-1A26 engine that is utilized by A320Neo. LEAP-1A26CJ is a state-of-the-art high bypass turbofan engine that offers high efficiency and low emissions [84]. The data in order to model the LEAP-1A26 engine comprehensively, is not found in open sources as some of these data are proprietary knowledge for the company. Therefore, it is vital that the engine model is validated with the existing data. Initially, pyCycle would be used to model the FP-CCE engine [85]. Given the very limited documentation of pyCycle and lack of examples available, using pyCycle to integrate the piston engine would require more time and resources, outside of the scope of this project. Therefore, it was decided that the cruise condition and LTO cycle of the LEAP-1A26 engine will be modelled in pyCycle to have a validated model for the aircraft engine. Then, a custom aero engine code was created and this code was verified and validated against the LEAP-1A model. The integration of the free piston engine to the baseline aircraft was conducted using the custom aero engine code.

4.1.1. pyCycle Model

Initially, LEAP-1A26 is modelled in pyCycle. The initial conditions for the simulation and the engine inputs are set such that the design condition is cruise. The main objective of pyCycle is to serve as an efficient cycle analysis tool within the context of vehicle-level multidisciplinary optimization [85]. It aims to retain the modularity and flexibility of existing cycle analysis tools like NPSS. To achieve this goal, pyCycle combines modeling approaches and methods from two distinct fields: thermodynamic cycle analysis and multidisciplinary design and optimization (MDO).The capability of pyCycle to deliver precise and efficient derivative information for gradient-based optimization has proven to be highly advantageous for the overall optimization process. Compared to traditional finite difference methods used in existing tools, such as NPSS, pyCycle is at least seven times faster[85]. Furthermore, due to its highly modular nature and Pyhton supported environment, it is much easier to implement the piston engine to the code with pyCycle compared to GasTurb, GSP or PROOSIS. Also, it is open-source and free unlike NPSS. Therefore, The FP-CCE concept thermodynamic cycle analysis will be made using pyCycle. In pyCycle, cycle models are constructed by connecting modular cycle elements to form a comprehensive representation of the entire propulsion system. Given its modularity, using pyCycle is very advantageous in terms of implementing the piston engine model to the turbofan than other open source or commercial software's. The overview of the structure of the code of pyCycle is presented

in Figure 4.1. The code is made up of four main computational parts: Optimizer, Solver, Cycle, and Balance. These components interact by passing data between them, as indicated by gray lines in the diagram. The Cycle block is the main part of the code, containing thermodynamic properties and equations for the components. It consists of modular cycle elements like compressors, burners, or turbines, which can be combined for various engine designs. In the Balance block, implicit state variables and associated nonlinear residual equations makes sure the physical dependencies and the design conditions are satisfied. This convergence of these equations are handled by the Solver block. Lastly, the Optimizer adjusts design variable values to meet constraints and minimize specified objectives.

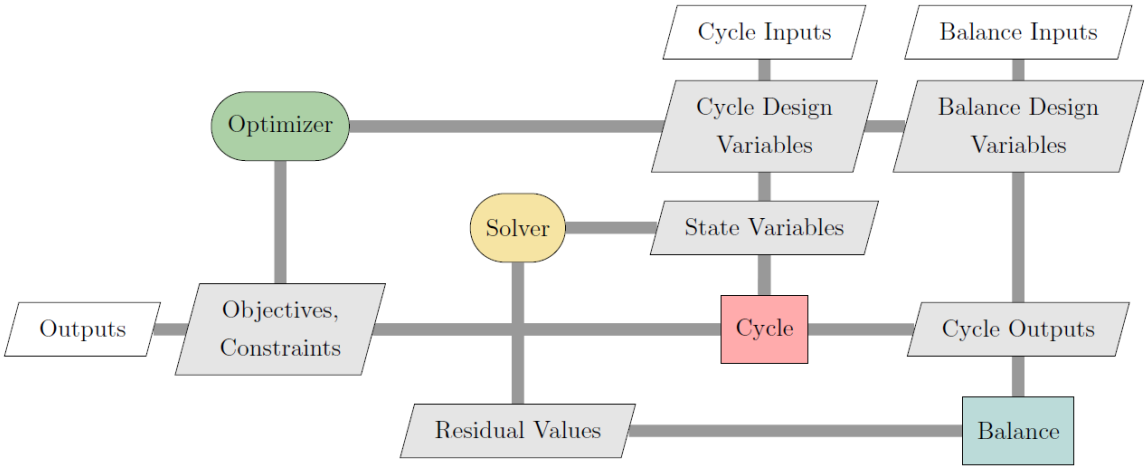

Figure 4.1: General cycle analysis tool structure[85]

The setup in pyCycle for the high bypass turbofan configuration can be seen in Figure 4.2. In this setup, the flow connections are shown with f. Furthermore, the shaft are connected by the rotational speed and the torque. Lastly, the performance element shown as ”Perf” will compute the final values of thrust and specific fuel consumption. More information on the modelling principles of pyCycle can be found in the papers provided by Hendricks and Gray [85].

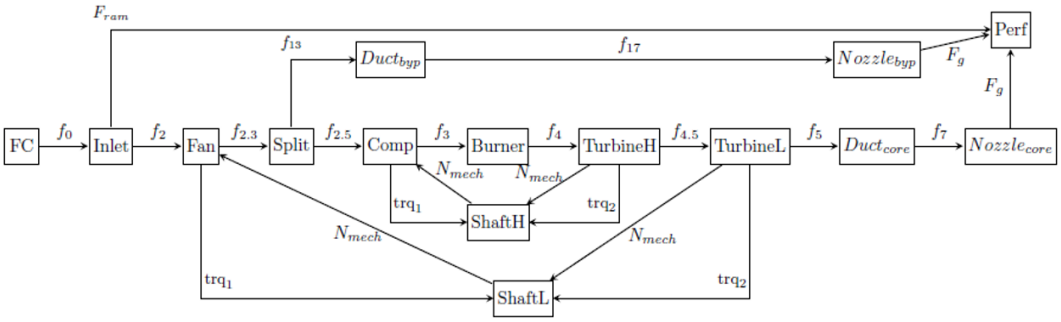

Figure 4.2: High Bypass Configuration used in pyCycle[85]

In the pyCycle model, the cruise condition and the conditions in the LTO cycle were simulated. The design case was selected to be the cruise condition. The input data for the cruise condition of LEAP-1A26 is retrieved from the GSP model provided by TU Delft and the data provided in the ICAO database [86].

4.1.2. Custom Aero Engine Model

The main objective of this thesis requires the analysis of the piston and the aircraft together. Due to the lack of documentation and support on pyCycle ’s code, limit on time and resources, an alternative

approach was needed. So, a more modular and less complex aero engine model was constructed. The results from pyCycle is still valuable as they validate the inputs that are used for the custom aero engine code. Due to the aero engine specifications usually being proprietary data, validating the inputs with pyCycle is a cruical step. The less complex aero engine cycle calculator will be regarded as custom code. In the custom code, in order to accurately represent the thermodynamic characteristics of the aero engine, Cantera is implemented. This way, the thermodynamic properties of the gases at each station could be determined. Furthermore, with the use of reaction mechanisms in the combustor, the CO, CO2 and NOx emissions could also be estimated. The engine cycle model is based in the law of conservation of mass, and first and second law of thermodynamics. The are certain assumptions made for the cycle simulations.

- The gases are modelled using the ideal gas assumption. The thermodynamic properties and the composition at every flow station is determined assuming perfectly stirred reactor .
- The compression and expansion processes are modelled as non-isentropic and losses are taken into account by the isentropic efficiency η_{is}
- Changes in potential energy between stations are neglected.
- Changes in kinetic energy between stations are taken into account by using total conditions
- Mechanical losses with transmission of expansion power to the compression process are accounted for through the use of the mechanical efficiency.
- Entering mass flow is taken in as real mass flow
- Entropy values are calculated from Cantera

Following the assumptions, the cycle calculations will be explained. The entering mass flow in the cycle calculations are taken as the real mass flow to follow the notation of the pyCycle outputs. The entering mass flow gets split in the fan as shown in Equation 4.1.

$$\dot{m}_{\text{core}} = \frac{\dot{m}_{\text{real}}}{BPR+1}, \quad \dot{m}_{\text{bypass}} = \frac{\dot{m}_{\text{real}} \cdot BPR}{BPR+1} \tag{4.1}$$

The ambient (a) to total conditions at the cruise altitude is determined using Equation 4.2.

$$\begin{aligned} Pt_a &= p_a \left(1 + \frac{\gamma-1}{2} M^2\right)^{\frac{\gamma}{\gamma-1}} \\ Tt_a &= T_a \left(1 + \frac{\gamma-1}{\gamma} M^2\right) \end{aligned} \tag{4.2}$$

During the compression side of the cycle, the pressures at each station are calculated by taking into account the pressure ratio defined for each station as presented in Equation 4.3 . The temperatures at the following stations are determined by the isentropic relation and isentropic efficiency. Finally, the work required for the fan and compressors can be calculated.

$$Pt_f = PR * Pt_i$$

$$Tt_f = Tt_i \left(1 + \frac{1}{\eta_{is}} \left[\left(\frac{Pt_f}{Pt_i}\right)^{\frac{\gamma-1}{\gamma}} - 1\right]\right) \tag{4.3}$$

$$W = \dot{m}_i c_{p,i} \left(Tt_f - Tt_i\right)$$

The results of the combustion process is determined using Cantera. In order to accomplish this, a function is created. The inputs for the combustor function are the target combustor exit temperature Tt_4, fuel composition X_{fuel}, inlet gas composition X_i, inlet total temperature Tt_i and inlet total pressure Pt_i. This function works by iterating over values of equivalence ratio, ϕ, and equilibrating the mixture at constant enthalpy and pressure in Cantera. The iteration continues until the right composition of input gases are found that would result in the target Tt_4. The combustor loss is then added as a percentage to the entering pressure. With this function, Tt_4 and the final composition of the gases are determined.

Then, the expansion part of the cycle is calculated as shown in Equation 4.4. The high pressure turbine drives the high pressure compressor, with taking mechanical efficiency,η_{mech}, into account. Then, the total temperature at the next station is found using the enthalpy balance with W_{HPT}. Finally, the total pressure at next station is determined using the isentropic efficiency, η_{is}.

$$\begin{aligned} W_{HPT} &= \frac{W_{HPC}}{\eta_{\text{mech}}} \\ W_{LPT} &= \frac{W_{LPC} + W_{fan}}{\eta_{\text{mech}}} \end{aligned}$$

$$Tt_f = Tt_i - \frac{W_{PT,i}}{\dot{m}_i c_{p,i}} \tag{4.4}$$

$$Pt_f = Pt_i \left(1 - \frac{1}{\eta_{is}} \left(1 - \frac{Tt_f}{Tt_i}\right)\right)^{\frac{\gamma_i}{\gamma_i}}$$

Following the LPT, the core nozzle calculations take place. Here, the pressure is checked against the critical pressure ratio to check whether either the bypass or the core nozzle is choked. In addition, a simple turbine cooling model is adopted, given in Equation 4.5 [87] .

$$\frac{\dot{m}_c c_{p,c}}{\dot{m}_g c_{p,g}} = b \left(\frac{T_4 - T_b}{T_b - T_{\text{cooling}}}\right)^s \tag{4.5}$$

In this study, the estimated values used are b = 0.06 and s = 1, with a metal temperature of Tb = 1450 K. The specific heats, for the gas entering the turbine and the cooling gas are determined using real gas property models. The turbine inlet temperature T_4 and coolant temperature T_{cooling} are sourced from the engine performance model. While modelling the cycles, if T_4 is less than 1450, no turbine cooling will be required.

Lastly, exit flow velocities and the thrust values are calculated. Furthermore, the final composition of the flow exiting the nozzle is known. So, the emissions coming out of the engine can be calculated. By using the mass fractions calculated in Cantera for each specie to track, the total emission index is calculated.

4.1.3. Modelling the FP-CCE

In this section, the methodology followed in implementing the free piston engine into the aircraft environment is explained.

Implementing the Piston into the aircraft

The piston engine code had to be implemented into the high bypass turbofan engine cycle simulation. To achieve this, the piston engine is added to the engine cycle simulations as station 35, between the HPC and the combustor. The final temperature, pressure, composition, gas mass per cycle and change in entropy is recorded from the outputs of the piston engine simulations and fed to the next station.

One of the most important aspects to consider is the connection between the instationary operation of the piston engine to the aircraft engine. The piston engine imposes pulsating conditions to the turbo components. The HPC is subject to pulsating outlet conditions, meanwhile, the HPT is subject to pulsating inlet conditions. In the methodology followed by Kaiser [21], the pulsating conditions are taken into account by deteriorating the efficiency and creating buffer volumes to the inlet and outlet of the piston engine. Considering the effect of the pulsating conditions on the turbine efficiency, the main influencing factors were determined to be the pulsation frequency f_{pulse} and pressure amplitude $\Delta p/p$[88]. In his thesis, Kaiser assumes that the losses mainly occur in the first stage and uses the simplified relation given in Equation 4.6[21]. In the case of the compressor, the pulsating exit conditions deteriorate the efficiency, again depending on the frequency and pressure amplitude[89]. The method used by Kaiser is given in Equation 4.7, where the efficiency deterioration depends on the quadratic pressure amplitude.

$$\Delta\eta_{\text{is,HPT}} = 13.4\% \cdot \frac{\Delta p}{p} \cdot \frac{2}{n_{\text{stages}}} \cdot \frac{f_{\text{pulse}}}{2500\ \text{Hz}} \tag{4.6}$$

$$\Delta\eta_{\text{is ,HPC}} = 150\% \cdot \left(\frac{\Delta p}{p}\right)^2 \cdot \frac{1}{n_{\text{stages}}} \tag{4.7}$$

The buffering volumes are places before and after the piston engine in order to reduce the oscillations observed by the turbo components. They are sized such that the efficiency deterioration is kept below 3%, therefore, negligible. Additional volumes such as ducting and combustor also contribute to decreasing the efficiency deterioration but are neglected for sizing in the method by Kaiser[21]. In this study, the sizing of the buffering volumes are not considered. Therefore, an assumed efficiency deterioration of 3% is assumed for both the HPT and LPT.

FP-CCE Designs
The FP-CCE concept is explored for three different designs in this study to compare the results of different FP-CCE configurations. The three different design concepts are:

1. **C1-FP-CCE - Piston(H2) & Combustor (Jet-A1)**: Employs both the piston burning hydrogen and the combustor burning Jet-A1
2. **C2- FP-CCE - Piston(H2) & Combustor (H2)**: Employs both the piston burning hydrogen and the combustor burning hydrogen
3. **C3- FPCCE - Only Piston(H2)**: Employs only the piston burning hydrogen

The first concept (C1) is when the piston burning hydrogen is directly implemented into the aircraft engine burning Jet-A1. This design will shed light on the multi-fuel synergy between the piston and combustor for the LEAP-1A engine. This design provides insight into the potential performance improvement expected when integrating the piston directly into the LEAP-1A26 engine. The second concept (C2) is created to assess the FP-CCE design when burning only hydrogen. Since the future aircraft concepts work to eliminate CO2 emissions by hydrogen combustion, this concept would be interesting to compare against the multi-fuel concept. For this design, it is assumed that the combustor can accommodate hydrogen combustion. Lastly, the third concept (C3), where combustion occurs only in the piston engines, is explored. This design offers an alternative to the combined cycle concept. In this study, the details of the flow path generation is not considered. When using hydrogen instead of Jet-A1, different fuel storage methods are needed which will overall alter the mass of the aircraft, and therefore the mass of the engine. This is not considered in this analysis. In addition, it is expected that adding the piston engine to the aircraft engine will also lead to an increased thrust requirement due to cascading effects. The specific of the free piston engine is still not as developed for a sizing analysis. Therefore, the cascading effects of adding the pistons are not considered in this study. The relevant thermodynamic performance and emissions will be discussed.

Optimiziation
In order to converge to a feasible design, optimizations studies are conducted using the Optuna python module. For a fair comparison with the baseline LEAP-1A26 engine, the concepts are configured such that the net thrust is close to $F_{net,0} = 18.3kN$. The goal for the CCE concepts are to achieve higher core thermal efficiency so the optimization is set such that each design has results in 18.3 kN thrust with highest thermal efficiency possible. Therefore, the objective function to minimize is given as presented in Equation 4.8. The weights of the optimization function were selected to give a higher priority to achieving the same thrust for the sake of fair comparison.

$$f = 0.8 * abs(F_{net,i}/F_{net,0} - 1) + 0.2 * \eta_{th}/\eta_{th,0} \tag{4.8}$$

The design variables used in this optimization are the BPR, PR_{HPC}, Tt_4, P_{bc} and ϕ_{piston} as presented in Table 4.1. The design variables are normalized in order to simplify the design space and increase the efficiency of the optimization process. The bounds for the design variables are also presented in Table 4.1.

In this design, the properties of the bypass flow is kept constant to minimize the effect on propulsive efficiency. Then, only the core thrust will be edited to the required thrust level. So, with the changing BPR, the bypass mass flow is kept constant, but the core mass flow altered. The $HPCPR$ is selected because the piston engine also increases the pressure of core flow, so less shaft work is required from

Table 4.1: Variables and Bounds for Optimization Problem

Variables	Bounds
1	$0.8 \leq \frac{BPR}{BPR_0} \leq 1.2$
2	$0.75 \leq \frac{HPCPR}{HPCPR_0} \leq 1.25$
3	$0.8 \leq \frac{Tt_4}{Tt_{4,0}} \leq 1.2$
4	$0.8 \leq \frac{P_{bc,i}}{P_{bci,0}} \leq 1.2$
5	$0.75 \leq \frac{\phi_{\text{piston}}}{\phi_{\text{piston},0}} \leq 1.2$

the compressor. So, the $HPCPR$ could be decreased to get a similar pressure rise at the end of the compression part of the aero engine cycle. Tt_4 is altered because it effects the fuel consumption, emissions and the core thrust. Moreover, the initial bounce chamber pressure $P_{bc,0}$ is altered. This was done to see whether a different compression ratio could result in better performance and to match the changes in $HPCPR$ which would effect the inlet pressure of the piston. Lastly, ϕ_{piston} is varied in the design process. The equivalence ratio of gas going into the piston has a large effect on the compression ratio and peak temperature in the piston engine cycle and therefore, the NOx formation and the thermal efficiency. The initial values for each design is selected by doing a manual iteration to converge to a design point where the thrust is close to 18.3 kN. These values would serve as the baseline values going into the optimization for each model. The trial study is conducted 100 times by Optuna's solver for each of the design concepts. The resulting designs are presented in the next section.

4.2. Results and Discussion

4.2.1. pyCycle

The results for simulating the baseline LEAP-1A26 engine is presented.The summary of the inputs used for modelling the cruise condition in pyCycle is given in Table 4.2.The summary of the results of the cruise condition for LEAP-1A26 are presented in Table 4.3.

	value	unit
$\dot{m}$	177	[kg/s]
M_0	0.78	[ ]
h	35000	[ft]
BPR	11.1	[-]
OPR	37	[-]
N_{LPC}	3663	[rpm]
N_{HPC}	16312	[rpm]
T_4	1550	[K]

Table 4.2: Inputs Cruise Condition for LEAP-1A26 from pyCycle

	value	unit
F_{net}	18.3	[kN]
m_{fuel}	0.2667	[kg/s]
FAR	0.02338	[-]
P_{t3}	12.8	[bar]
T_{t3}	722	[K]
$TSFC$	14.73	[g/s-kN]

Table 4.3: Results Cruise Condition for LEAP-1A26 from pyCycle

The T-S diagram for the cruise condition is constructed using the temperature and entropy outputs from pyCycle. This T-S diagram is presented in Figure 4.3.

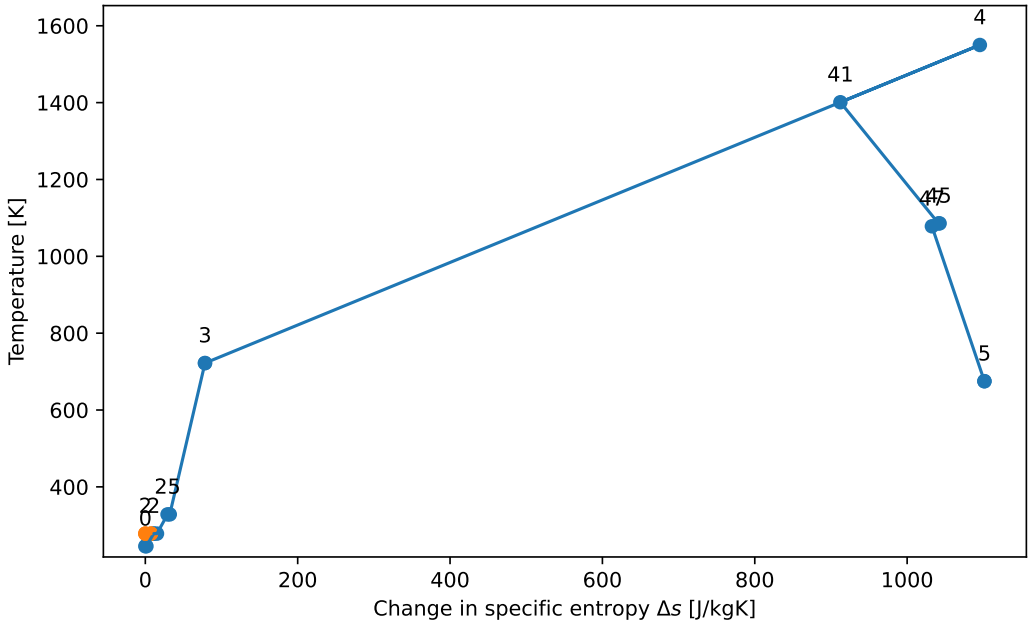

Figure 4.3: T-s Diagram for the LEAP-1A26 model made in pyCycle

In order to ensure that the cruise condition model is accurate, the off-design conditions are also modelled. So, validation can be done using the results of the different conditions in the LTO cycle. The fuel flow for the LTO cycle is provided in the ICAO database. For each condition in the cycle, a different thrust setting is applied. Since the maximum thrust setting is given in the ICAO database [86], the thrust value for the other conditions can be determined by assuming a thrust setting value. The assumed thrust setting values are the taken from the report provided by ICAO [86].

In Table 4.4, the comparison between the outputs from pyCycle and the ICAO database is presented. From this table it can be observed that the pyCycle simulation outputs differ less than 5 % compared to the ICAO data. Only the overall pressure ratio at take off shows a higher error. Since the pressure ratios were taken from the validated GSP model, it can be assumed that the error in overall pressure ratio is trivial.

Take-off (100%)	pyCycle	ICAO	unit	error (%)
BPR	10.9	11.1	[-]	-1.5
OPR	35.8	33.3	[-]	+7.5
F_{net}	118.2	120.6	[kN]	-2
m_f	0.894	0.861	[kg/g]	+4
Climb-out (85%)				
F_{net}	100.5	102.5	[kN]	-2
m_f	0.730	0.710	[kg/s]	+2.8
Approach (30%)				
F_{net}	35.5	36.2	[kN]	-2
m_f	0.244	0.244	[kg/s]	0
Idle (7%)				
F_{net}	8.3	8.4	[kN]	-1.2
m_f	0.088	0.091	[kg/s]	-3

Table 4.4: LTO-cycle results for baseline LEAP-1A from pyCycle against ICAO data

4.2.2. Custom Aero Engine Model Validation

The baseline LEAP-1A26 engine is modelled using the custom aero engine code and compared to pyCycle. The results are shown in Table 4.5. The results from both simulations are quite close to eachother as shown. In the simulations, the maximum difference between the flow stations are recorded to be less than 3%.

	Custom	**pyCycle**	**unit**	error (%)
F_{net}	18.3	18.3	[kN]	0
m_{fuel}	0.2667	0.2667	[kg/s]	0
P_{t3}	12.8	12.8	[bar]	-2
T_{t3}	737	722	[K]	+2
T_{t4}	1550	1551	[K]	0.1
$TSFC$	14.55	14.73	[g/s-kN]	-1

Table 4.5: Comparison of Custom aero engine simulation to pycycle

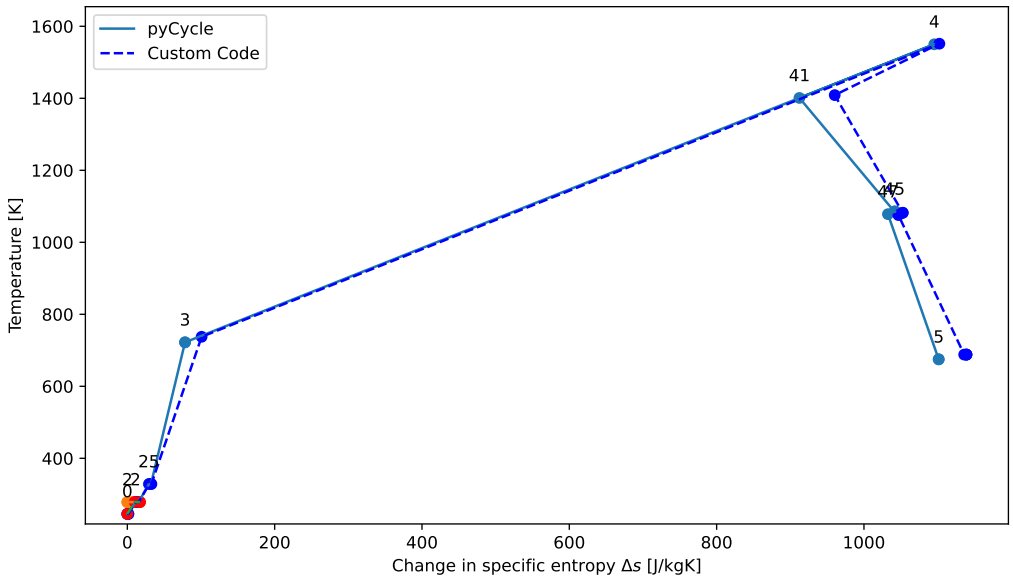

Figure 4.4: T-s Diagram for the LEAP-1A26 model made in pyCycle compared to the custom aero engine code

The comparison of the T-S diagrams are given in Figure 4.4. The processes seem to deviate more after the combustion process. This is because the cooling flows are modelled as only flowing enthalpies in my custom code. In the meantime, pycycle uses a more complex model, taking into account stage cooling. The resulting efficiencies found for the LEAP-1A26 model were found to be. $\eta_{th} = 46\%$ and $\eta_{prop} = 81\%$

In the custom aero engine code, the resulting emissions of the baseline LEAP-1A26 engine can also be analyzed. Therefore, the resulting emissions can be validated, which is vital for the emissions comparison considering the CCE designs. The resulting emissions from the Cantera simulation are found as:

- $EICO = 1.72 * 1e-2g/kg$
- $EICO_2 = 3.13kg/kg$
- $EINOx = 54.18g/kg$

In the paper by Saluja et.al, the emissions from LEAP-1A26 engine is evaluated [90]. For the Lean-Burn TAPS-II engine, the empirical relation for NOx production is determined as given in Equation 4.9

. This empirical relation gives the NOx index at sea level depending on Pt_3, Tt_3, FAR and the thrust setting. The cruise thrust is assumed to be above the 40% thrust setting. The sea level emissions can be corrected to get the cruise emissions by using Equation 4.10 [90].

$$\begin{aligned} EINO^{p}_{x,SLS} &= 0.0069 \cdot P_{t3}^{-2.7496} \cdot \exp\left(0.0216 \cdot T_{t3}\right) \cdot 9.773^{(13.3701 \cdot FAR)} && \text{F}_{\text{engine}} \leq 40\% \\ EINO^{p+m}_{x,SLS} &= \left(3.9072 \cdot 10^{-6}\right) \cdot P_{t3}^{-13.9974} \cdot \exp\left(0.0776 \cdot T_{t3}\right) \cdot 1.4697^{(86.8456 \cdot FAR)} && \text{F}_{\text{engine}} > 40\% \end{aligned} \tag{4.9}$$

$$EI_{\text{mass , cruise}} = EI_{\text{mass },SLS} \cdot \left(\frac{P_{t3,\text{ cruise}}}{P_{t3,SLS}}\right)^{1.35} \cdot \left(\frac{FAR_{\text{cruise}}}{FAR_{SLS}}\right)^{2.5} \tag{4.10}$$

When using this correlation, the emission index for NOx is calculated to be $EINO_X = 8.327$ g/kg. This shows that the results from Cantera over-predicts the emissions substantially compared to empirical correlation. One source of uncertainty is because of the fact that TAPS-II is a complex state-of-the art lean burn engine so it might have mechanisms to decrease NOx within the combustor that is not taken into account in Cantera. Also, the empirical correlation determined in the article by Saluja has an uncertainty of 10% with respect to the ICAO values [90]. In this article, the emission index for CO2 is also given as $EICO_2 = 3.15$ kg/kg. The $EICO_2$ determined at the end by Cantera falls within less than 1% of this value.

4.2.3. FP-CCE Results

In this section, the results of the different design concepts for the FP-CCE is presented. Firstly, the results from each design model is presented. Then, the designs are compared in terms of performance and emissions.

FP-CCE Multi-fuel

The results of the preliminary design for the FP-CCE Multi-fuel concept is presented here. The multi-fuel configuration uses H2 combustion in the piston and jet-A1 combustion in the combustor. The initial values of the design parameters and the final values from optuna are presented in Table 4.6.

Parameters	Leap-1A	Initial	Final
$HPCPR$	14.5	8	9.1
BPR	11.1	12.5	13
Tt_4	1550 K	1470 K	1248 K
P_{bc}	N/A	45 bar	53 bar
ϕ_{piston}	N/A	0.38	0.32

Table 4.6: Design Parameter Inputs for the Multi-Fuel Design

The results of the Multi-fuel FP-CCE concept is presented in Table 4.7. For the results, two thermal efficiencies are indicated. The second thermal efficiency, $eta_{thermal,alt}$, represents the thermal efficiency of the engine cycle when the alternator power is also considered. Total combined alternator power for 14 piston engines become 3.3 MW. The T-S diagram of the engine cycle is given in Figure 4.5.

	value	unit
F_{net}	18.3	[kN]
$m_{f,piston}$	0.1188	[kg/s]
ϕ_{piston}	0.32	[-]
CR_{piston}	6.5	[-]
f_{piston}	57	[Hz]
N_{piston}	14	[-]
P_{alt}	237	[kW/piston]
ϕ_{comb}	0.05	[-]
$m_{f,combustor}$	0.039	[kg/s]
P_{t3}	8.0	[bar]
T_{t3}	655	[K]
P_{t35}	14.3	[bar]
T_{t35}	1186	[K]
T_{t4}	1248	[K]
$TSFC$	10.19	[g/s-kN]
$\eta_{thermal}$	0.33	[-]
$\eta_{thermal,alt}$	0.54	[-]
η_{prop}	0.81	[-]

Table 4.7: Results Cruise Condition for Multi-fuel FP-CCE

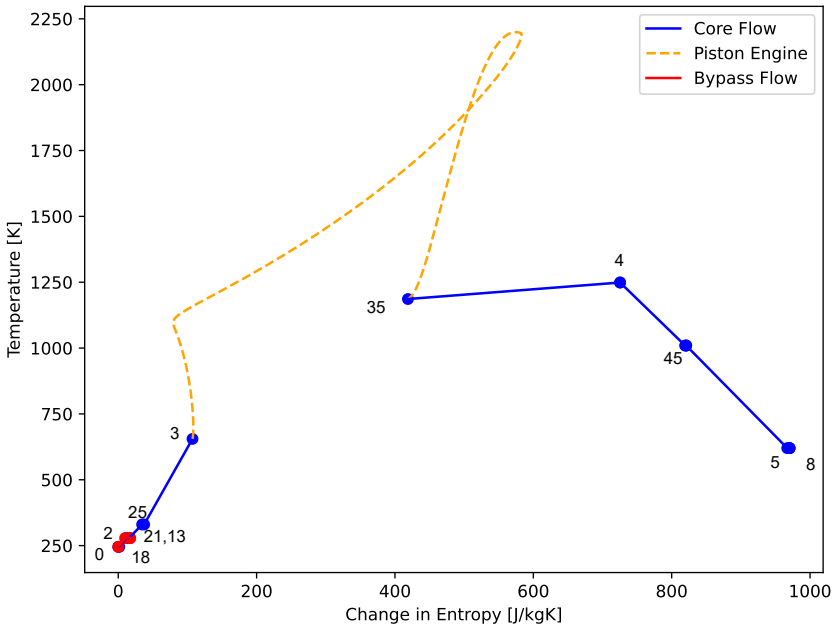

Figure 4.5: T-s Diagram for FP-CCE multi-fuel

The emissions from the Multi-fuel FP-CCE is calculated. The resulting emission index for the relevant species are presented below.

- $EICO = 1.35e-5 g/kg$
- $EICO_2 = 0.49 kg/kg$
- $EINOx = 18.23 g/kg$

FP-CCE H2

The results of the first iteration for the H2 FP-CCE concept is presented. The design variables determined by Optuna are presented in Table 4.8.

Parameters	Leap-1A	Initial	Final
$HPCPR$	14.5	8	6.6
BPR	11.1	12.5	14.4
Tt_4	1550 K	1470 K	1301 K
P_{bc}	N/A	45 bar	46.5 bar
ϕ_{piston}	N/A	0.38	0.29

Table 4.8: Design Parameter values for the H2 FP-CCE Design

The results from the H2 FP-CCE model is presented in Table 4.9. The T-S diagram for this engine cycle is presented in Figure 4.6.

	value	**unit**
F_{net}	18.4	[kN]
$m_{f,piston}$	0.095	[kg/s]
ϕ_{piston}	0.29	[-]
CR_{piston}	9.2	[-]
f_{piston}	59	[Hz]
N_{piston}	14	[Hz]
P_{alt}	265	[kW/piston]
ϕ_{comb}	0.175	[-]
$m_{f,combustor}$	0.058	[kg/s]
P_{t3}	5.8	[bar]
T_{t3}	595	[K]
P_{t35}	10.4 bar	[bar]
T_{t35}	1021	[K]
T_{t4}	1301	[K]
$TSFC$	8.33	[g/s-kN]
$\eta_{thermal}$	0.38	[-]
$\eta_{thermal,CCE}$	0.66	[-]
η_{prop}	0.81	[-]

Table 4.9: Results Cruise Condition for H2 FP-CCE

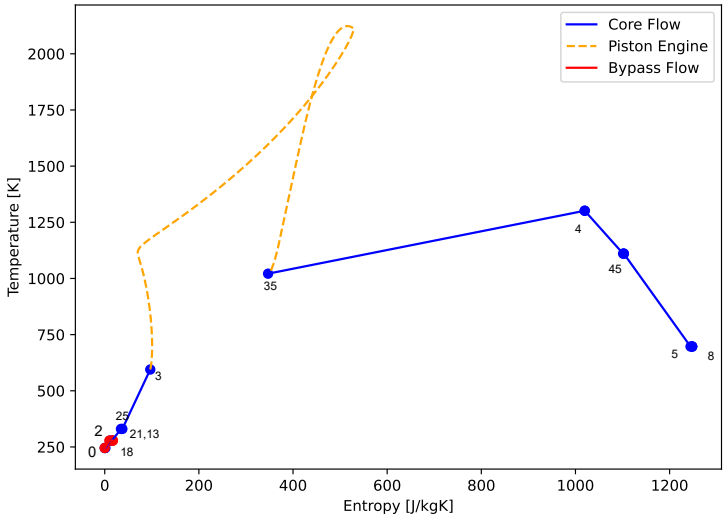

Figure 4.6: T-s Diagram for FP-CCE H2

The emissions from H2 FP-CCE is calculated. The resulting emission index for the relevant species are presented below.

- $EICO = 0g/kg$
- $EICO_2 = 0kg/kg$
- $EINOx = 22.68g/kg$

FP-CCE Only Free Piston Engine H2

The results of the first iteration for the H2 FP-CCE concept is presented. The design variables determined by Optuna are presented in Table 4.10. The results from the H2 FP-CCE model is presented in Table 4.11. The T-S diagram for this engine cycle is presented in Figure 4.7.

Parameters	Leap-1A	Initial	Final
$HPCPR$	14.5	8	11.3
BPR	11.1	12.5	13.3
P_{bc}	N/A	45 bar	48 bar
ϕ_{piston}	N/A	0.38	0.38

Table 4.10: Design Parameter Values for Only piston FP-CCE concept

	value	unit
F_{net}	18.6	[kN]
$m_{f,piston}$	0.136	[kg/s]
ϕ_{piston}	0.38	[-]
CR_{piston}	5.2	[-]
f_{piston}	49	[-]
N_{piston}	14	[-]
P_{alt}	205	[kW/piston]
$m_{f,combustor}$	0	[kg/s]
ϕ_{comb}	0	[-]
P_{t3}	9.96	[bar]
T_{t3}	699	[K]
$P_{t35} = P_{t4}$	17.5 bar	[bar]
$T_{t35} = T_{t4}$	1320	[K]
$TSFC$	7.300	[g/s-kN]
$\eta_{thermal}$	0.33	[-]
$\eta_{thermal,alt}$	0.50	[-]
η_{prop}	0.807	[-]

Table 4.11: Results Cruise Condition for Only Piston H2 FP-CCE

The results from the only piston FP-CCE model is presented in Table 4.11. The T-S diagram for this engine cycle is presented in Figure 4.7.

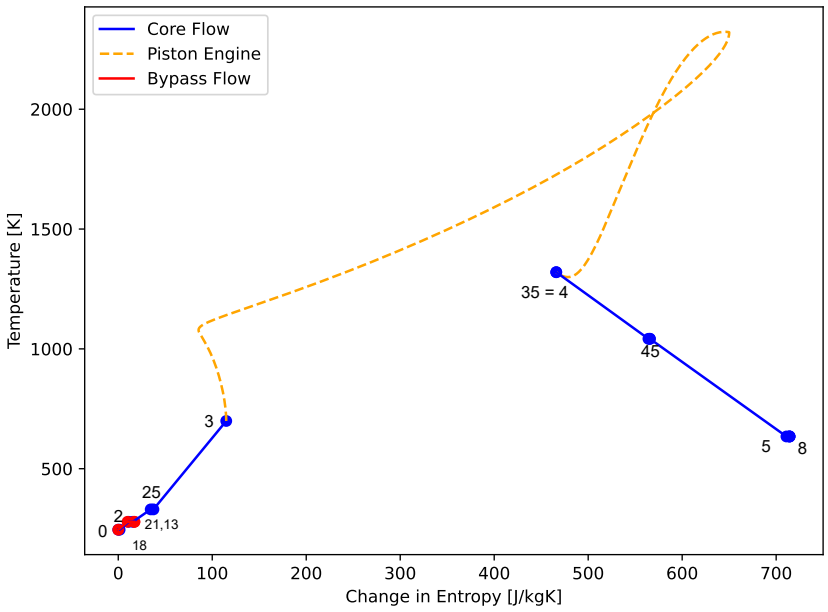

Figure 4.7: T-s Diagram for FP-CCE Only Piston H2

The emissions from only FP-CCE is calculated. The resulting emission index for the relevant species are presented below.

- $EICO = 0g/kg$
- $EICO_2 = 0kg/kg$
- $EINOx = 191.5g/kg$

4.2.4. Design Comparison and Selection

In this section, the different designs made for the FP-CCE concept are compared in terms of performance and emissions. The best designs for each category will be presented and the overall best performing design will be determined. In this study, the increase in the core thermal efficiencies of the high bypass turbofan engines are considered. The bypass flow characteristics are kept constant throughout the designs. Also, the same level of thrust is attempted to be generated by each design. As a result, the propulsive efficiency are almost exactly the same between the designs.

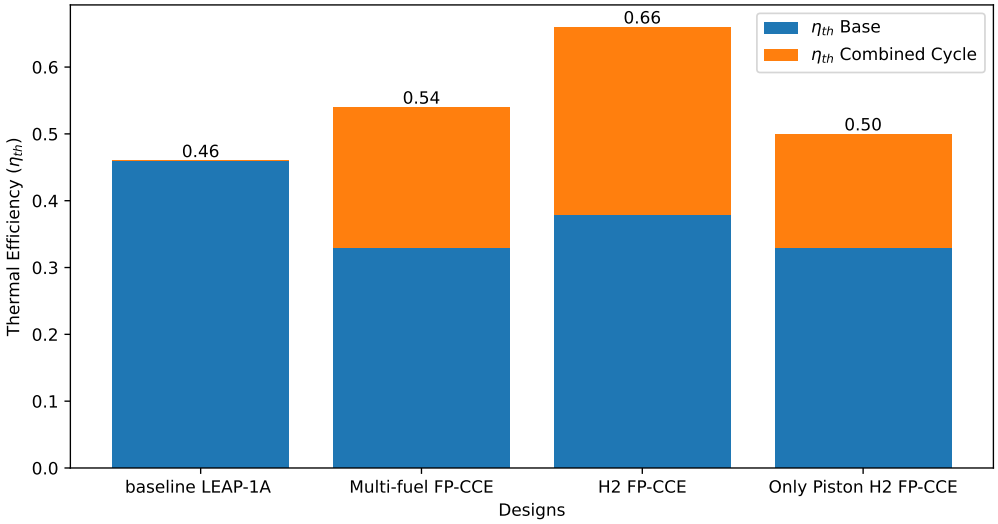

Figure 4.8: Thermal Efficiency Comparison

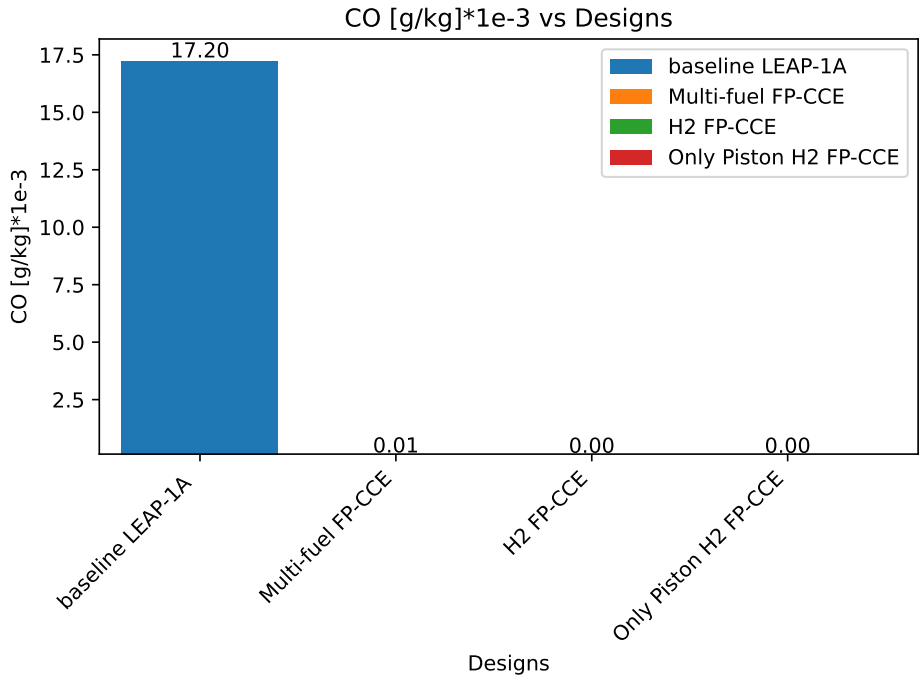

Figure 4.9: CO emissions comparison

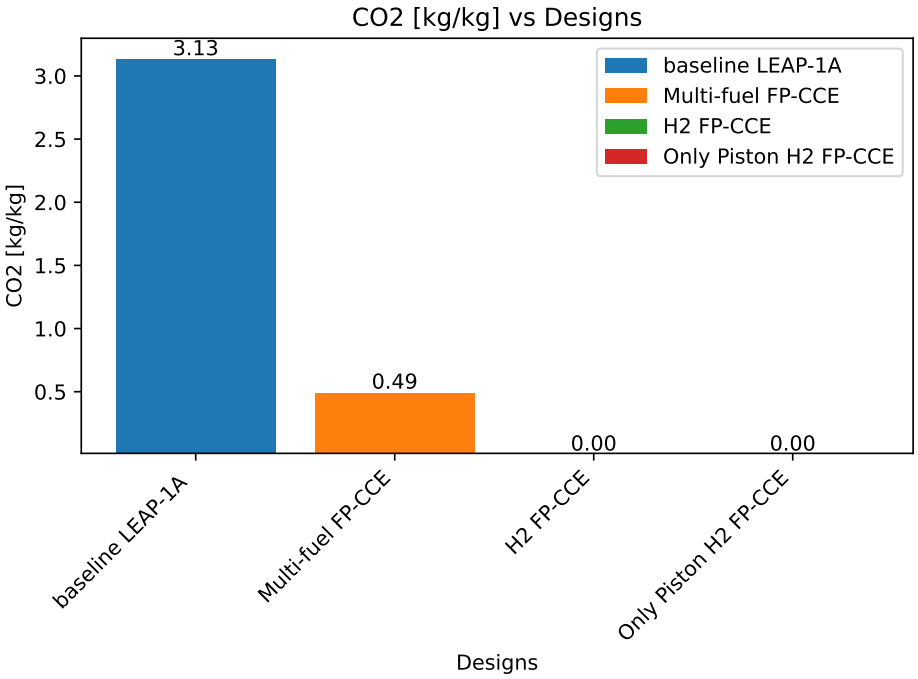

Figure 4.10: CO2 emissions comparison

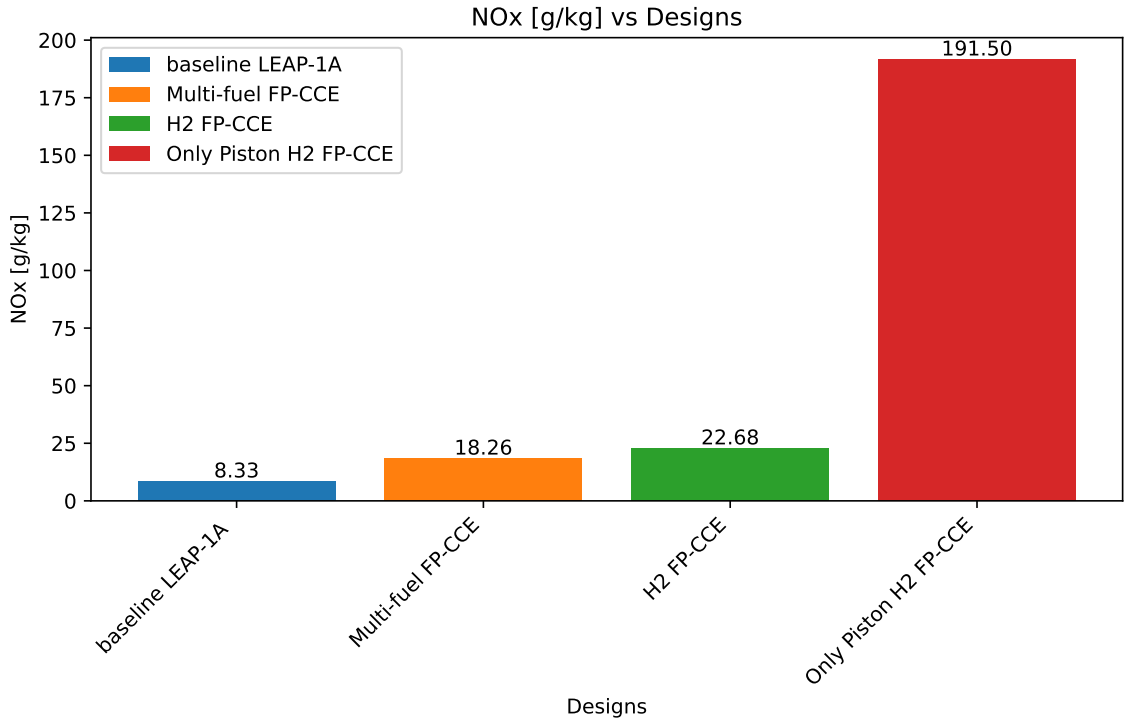

Figure 4.11: NOx emissions comparison

In Figure 4.8, the thermal efficiencies of the different concepts are presented. In this discussion, for the sake of clarity, the thermal efficiency considering only the energy that goes to create thrust

will be regarded as the base thermal efficiency and the thermal efficiency also considering the energy extracted from the alternators in the piston will be regarded as composite thermal efficiency.

Firstly, it can be seen that the baseline LEAP-1A concept has a higher base thermal efficiency than CCE concepts. Meanwhile, the base thermal efficiencies for CCE concepts were found to be close to each other around 33%. The lower base thermal efficiencies of the concepts can be explained by fact that H2 has a much higher LHV value than jet-A1. So, the fuel energy released is higher than the initial value of fuel energy release, even though the kinetic energy generated in the core is very close to each other due to the generated thrust. Comparing the multi-fuel concept to the H2 FP-CCE concept, it can be seen that when more of the combustion process is appointed to the combustor in the H2 FP-CCE concept due to the lower ϕ_{piston}. As a result, the base thermal efficiency is higher for the H2 FP-CCE concept. When the composite thermal efficiency considered, the highest thermal efficiency is reached by the H2 FP-CCE concept. Looking at the results, it can be seen that the H2 FP-CCE concept has the highest alternator power per piston. This can be explained by the higher compression ratio achieved by the free pistons in the H2 FP-CCE concept. Between the three concepts, the H2 FP-CCE design has the highest compression ratio with $CR = 9.5$. Compared to the other CCE concepts, the H2 FP-CCE concept uses a lower pressure ratio in the compressors. Therefore, the gas entering the piston combustion chamber has a lower pressure and mass. So, it can be compressed more. Since, the bore of pistons are kept constant in this analysis, the stroke length is increased for the H2 FP-CCE concept. With the higher stroke length, more power is generated by the alternators. So, the over-compression of the in-cylinder in this case help to increase the thermal efficiency by increasing the alternator work output. In reality, over-compression also causes inefficiencies in the piston cycle due to the adverse work region, but that seems to have less of an effect on the thermal efficiency of the cycle than the generated alternator power.The effect of the compression ratio on the alternator power generated can also be seen when the only Piston FP-CCE concept is examined. Even though it has a similar base thermal efficiency without the alternator power, compared to the other FP-CCE concepts, it has now a lower composite thermal efficiency as the other FP-CCE concepts. This can be explained by the the fact that the only piston FP-CCE concept has the lowest compression ratio with $CR = 5.2$. Consequently, it has the lowest alternator power per piston. As a result, the increase in thermal efficiency with the addition of alternator power is the lowest for the only piston FP-CCE concept.

The concepts are also compared in terms of the different emissions. The CO and CO2 emissions are presented in Figure 4.9 and Figure 4.10 respectively. With the concepts where only H2 is used as fuel, there is no CO or CO2 emissions recorded. The multi-fuel FP-CCE CO emissions are more than two orders of magnitude lower than the emissions of baseline LEAP-1A baseline LEAP-1A. Looking at the CO2 emissions, a similar trend is observed. The concepts burning hydrogen has no CO2 emissions. The multi-fuel FP-CCE concept also has a significantly lower CO2 output but the difference is less than the one for CO. So, in each concept, there is a significant decrease in carbon emissions.

In Figure 4.11, the NOx emission index for each concept are compared. The graphs show that the highest overall NOx production is by the only piston FP-CCE concept. This shows that the free opposed piston does not perform as well in terms of limiting NOx production. The lowest NOx production is still recorded for the baseline LEAP-1A. The CCE concepts using both the piston and the combustor have around 3 times higher NOX production than the baseline LEAP-1A concept.Kasier also recorded that the NOx production for the CCE cocnepts he explored resulted in 3 times higher NOx production compared to the state-of-the-art turbofan engines. The H2 FP-CCE concept has slightly higher NOx production than the multi-fuel concept. This expected due to the difference in types of fuels used in both concepts. Lastly, it is interesting to see that the NOX production for the CCE concepts using both piston and combustor are substantially lower than the Only piston concept. This shows an interesting synergy between the piston and the combustor. The combustor after the pistons works as an afterburner and burns away of a substantial amount of NOx produced during the combustion in the pistons. For example, for the multi-fuel CCE concept, the mass of NO recorded after the piston engine is recorded to be around 7.4 grams. Meanwhile, after the combustor, this value is recorded as 2.5 grams. So, more than 60% of the NOx are burned away according to the results of the simulation. So, using the combustor after the piston is quite beneficial in terms of lowering the NOx production. Although, a more accurate NOx model, for example using multiple zones, would be necessary to prove the NOx after burning.

The results of the comparison showed that the H2 FP-CCE concept showed the best performance overall. This concept burns only hydrogen and more of the combustion takes place in the combustor compared to the multi-fuel concept. This concept has the no carbon emissions with the highest com-

posite thermal efficiency. The drawback for this concept is that the NOx production is more than 3 times higher than the NOx production of the baseline LEAP-1A concept.

5

Discussion and Recommendations

In this chapter, the results of the study on the FP-CCE concept will be discussed.

Baseline and Scaled-up Piston Models

- **RQ1**: When scaled-up, is the opposed free piston engine still feasible to be used in the aircraft in terms of performance?

In order to correctly model the FP-CCE concepts, both the piston and the aircraft engine model had to be accurate and representative. The modelling of the free opposed piston model required the accurate modelling of reactor networks and the characteristics of the free piston processes. The free opposed piston with H2 HCCI combustion simulation model did not exist until this study. In addition, the model considered in this study uses reactor networks to track emissions, which is also not so common in the free piston models available in literature. The results of the free opposed piston was validated against other free piston models with H2 HCCI combustion. Furthermore, a sensitivity analysis is conducted to further examine the behaviour of the model against the changes in different variables. The effect of changing piston head mass, inlet temperature and equivalence ratio were important to explore before the design of the scaled-up engine was conducted. Following the validation and the sensitivity analysis it was concluded that created model accurately predict the characteristics of an OFPE with H2 HCCI combustion.

Compared to the other free piston models, the perfect scavenging model can be considered a limiting factor. The free opposed piston model considered in this study works in two-stroke operation mode. The performance deterioration in two-stroke engines due to the losses in scavenging is not considered in this design. In future designs, the scavenging model can be implemented in the engine to analyze the multi-cycle characteristics in more detail. Furthermore, as the design of the free piston is more realized, more complex geometry could be considered. This in turn would allow more complexity in the sub-models and geometric parameterisation.

The design of the scaled-up piston was a key step in the design process of the FP-CCE. The lack of designs that can accommodate the performance requirements of the state-of-the-art turbofan engines was identified by Kaiser. Therefore, first time in this study,the preliminary design of the free opposed piston HCCI model for an aircraft engine is conducted. The design constraints selected were identified by Kaiser considering the technology levels of 2050. With the additional performance requirements from LEAP-1A26CJ, the scaled-up piston design has been made. The resulting design showed that the long term requirements for the maximum pressure and the mean piston velocity could be reached. Furthermore, the bore size were adapted such that the number of piston modules never exceeded 16. It was also seen that the operational characteristics of the scaled-up engine was similar to the baseline engine in terms of frequency, mean piston speed and peak pressure. In Figure 5.1, the piston model used by Kaiser is compared to the state-of-the-art piston designs in terms of the displacement volume specific power over mean effective pressure. The identified design for the thesis from Kaiser is also indicated in this graph. It can be seen that the design of the FP-CCE in this thesis falls within the expected ranges identified by Kaiser. Furthermore, since the design of the scaled-up engine fits

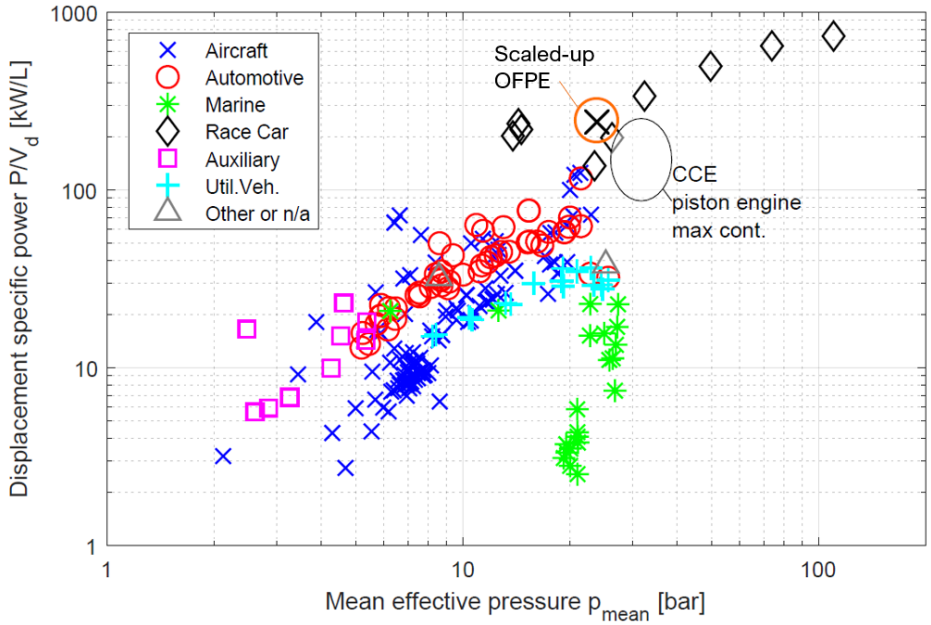

Figure 5.1: Displacement volume specific power over mean effective pressure categorised by engine application [21], also adding the scaled-up FPE from this study

the requirements. The results of the scaled-up piston showed that a feasible design piston made, the research question can be answered.

It is important to mention that the design of the scaled-up piston was made considering the requirements from the cruise conidition of the aicraft. In reality, the pistons would need to accommodate for off-design. For example, for the take-off condition, the mass flow requirement would be higher for the pistons therefore the design of the pistons would need to change accordingly. In a design that takes the whole LTO cycle into account, more complex ways of controlling the compression ratio is necessary. Optimizing the free piston operation for a single compression ratio is easier. If different compression ratios are needed in different operating conditions, then the use of alternators to control the operation would be crucial.

FP-CCE Performance and Emissions

- **RQ2**: Does the FP-CCE engine concept achieve higher thermal efficiency with the designed free piston?
- **RQ3**: Does the FP-CCE engine concept have better emission characteristics?

The results from the proposed FP-CCE concepts will be discussed. Compared to the previous studies done on the CCE concepts, this study is unique because it uses the free piston model and considers hydrogen as fuel. In the previous analysis done by Kaiser, the free piston characteristics were calculated by interpolating from a crankshaft model[21]. Furthermore, in that study, hydrogen combustion is not considered. In the study made by Nickl [52], hydrogen combustion is considered for the CCE concept but not a free piston engine. This study sheds light on the characteristics to one of the most promising concepts that could be used for realizing the CCE in the future. Firstly, the composite thermal efficiencies of the CCE concepts, considering the alternator power, are higher than be baseline LEAP-1A. Meanwhile, without considering the alternator power, the expected increase in the thermal efficiency, by definition, has not been observed with the FP-CCE concepts regarding the cycle efficiency in turning fuel energy into kinetic energy. This is because of the LHV of the fuel, in this case H2, being much higher than the LHV of jet-A1. Even though a lower fuel mass is used, the high fuel energy of the hydrogen is not as efficiently converted into kinetic energy as the baseline LEAP-1A. It is also important to note that the combustor equivalence ratios for the FP-CCE concepts were quite low, for example for the multi-fuel concept around $\phi_{comb} = 0.05$ and $\phi_{piston} = 0.32$. The combustion at these equivalence ratios, so the lean blow-out limit of the combustors have to also be considered in

the future designs. In the meantime, a bigger proportion of the combustion assigned to the combustor in the H2 FP-CCE concept with $\phi_{comb} = 0.175$ and $\phi_{piston} = 0.29$. With leaner mixtures in the piston, a higher compression ratio can be employed and therefore, the power generated by the alternator will also increase. The FP-CCE concepts were projected to enter service by the year 2050 so it is assumed that lean combustor technology advancements will allow lower equivalence ratio combustion. When looking at the composite thermal efficiency, where the power generated in the alternators are also taken into account, the thermal efficiencies depend much more on the piston performance. Connection of the alternator to power in-flight avionics or something could be useful given that a large amount of electricity could potentially be produced with this engine. This is quite an additional benefit of using the free piston engine for this operation. Usually, the free piston engines that use the linear alternators are mainly used to generate electricity with the alternator. Unless compounded with something else, the main effect of the usually designs are just to generate electricity. With the combined cycle, the piston works to heat up the flow and generate electricity at the same time.The compression ratio and stroke length has a large effect on the alternator power generated over the engine operation. Therefore, the H2 FP-CCE concept had the highest compound thermal efficiency with 66% compared to the 46% baseline thermal efficiency. One thing that could improve the alternator power generated would be to increase the compression ratios reached in the piston engines. One of the methods to do this would be to decrease the piston inlet temperature[21]. By decreasing the temperature of the inlet mass flow to the piston, the volume flow decreases,and the piston will be smaller Furthermore, the lower peak pressures also decrease the cooling requirements for the piston engine [52].Therefore, the use of intercoolers can also be beneficial in terms of using the piston engines more efficiently and making them lighter. Looking at the emissions, one of the main advantages for using this concept becomes apparent. Firstly, the concepts using H2 have no CO or CO2 emissions which is very desirable to meet the emission requirements of the future. Furthermore, it was also observed that using both the piston and the combustor together substantially decreased the NOx emissions compared to the case where only the pistons are used. This finding shed light on the after burning mechanism when the combsutor is used after the piston. Still, the NOx production for the concepts with both the combustor and piston are still around 3 times higher than the baseline LEAP-1A. As a result of this analysis, it was decided that the H2 FP-CCE concepts shows highest potential with the high thermal efficiency and low carbon emission properties.

The FP-CCE concept comparison conducted in this study only takes the cruise condition into account. When also taking the off-design conditions, the winner of the trade-off could be different. This is especially because firstly, the cascading effects of adding the piston mass on board is not taken into account. With more components added to the engine, the required thrust also increases. In the only-piston H2 FP-CCE concept, there total engine mass is projected to be lower as there is no combustor. On the other hand, just having the piston engine is not as desirable due to safety of operations. The pistons are much more difficult to cold start and adjust power levels depending on the design point. Therefore, the H2 FP-CCE concept still could be more valuable to analyze than only-piston FP-CCE concept. Furthermore, the aero engine model used to analyze the FP-CCE concept is a simplified cycle code that does not take into account the details of the components. In a further design, the flow path generation could be made and the performance of the other components could also be realized. In addition, the design space considered in this thesis to take into account both the aircraft engine and the piston engine was small in terms of the design space. Due to the scope and time constraints of the project, optimizations with more variables was not considered. In the future, a more complex optimization study could be conducted to better understand the synergy between the parameters and come up with a more efficiency design. Lastly, the connection of the instationary operation of the FP to the aircraft engine is not considered in detail in this thesis. This is one of the main technological drawbacks in realization of the FP-CCE concept. In addition to the variation of compression ratio in the FP-CCE concept during operation, the connection to aircraft operation becomes even more difficult. More studies should be done in realizing control strategies where varying compression ratio and instationary operation could be connected to the aircraft.

6

Conclusion and Future Work

Finding solutions to increase the thermal efficiency and decrease the fuel consumption of the net-gen aircraft engines is crucial to ensure the longevity of the industry. Aircraft needs to emit significantly less emissions to meet the sustainability requirements set for the future. The FP-CCE concept were one of the solutions explored by the industry. In this report, the performance and emissions characteristics of various FP-CCE concepts are explored. Firstly, the free opposed piston engine is simulated. Then, the engine is scaled-up to fit the performance and mass flow requirements of the cruise condition of LEAP-1A26 engine. The scaled-up engine design resulted in an engine with an indicated thermal efficiency around 30%, generating around 150 kW of electricity per piston module. The scaled-up piston engines were implemented into three FP-CCE concepts: Multi-fuel, only H2 and only piston H2. The results of the analysis show that the concept with using both the piston and the combustor to burn H2 was the most promising. The H2 FP-CCE concept emits no carbon emissions, has a higgh thermal efficiency, above 60% but had 3 times higher NOX emissions compared to the baseline LEAP-1A. Although, the thermal efficiencies were calculated to be lower for the FP-CCE multi-fuel and H2 concepts. This is attributed to the fact that the LHV of H2 is much higher than the LHV of jet-A1 therefore, there is a decrease in thermal efficiency. When adding the power generated by the alternators to the thermal efficiency, it was found that the H2 FP-CCE concept had the highest thermal efficiency. In conclusion, it can be said that the free pistons can accommodate the performance requirements of the state-of-the-art high bypass turbofan engines with scaled-up models. Although the variable compression ratio and instationary operation of the pistons are difficult to control, implementation of complex control technolgies in the FPE can be considered in the future. In addition, the H2 FP-CCE concept showed significant increase in performance and decrease in emissions compared to the state-of-the-art high bypass turbofan engines. In order to be certain about the performance of the FP-CCE concepts, further studies would be valuable. All in all, the FP-CCE concept is a promising concept that needs further analysis to realize it for the next gen aircraft.

Future Work

The study detailed in this report had certain limitations as discussed before. So, further work will be necessary to bring this engine to life. Firstly, the implementation of a more complex scavenging model would have a significant effect on the performance. The FPE works in two-stroke operation so the losses due to scavenging will have to be taken into account. Furthermore, as the details of the free piston gets more realized, the geometric parameterisation can also be more detailed. This would help increase the complexity of the sub-models such as the alternator model, friction model and the bounce chamber model. Lastly, the designs made in this study were made through simple optimization models created using Optuna. The optimization models did not take both the piston and aircraft design in an integrated way. Furthermore, in the future analysis using the FP-CCE concept, the cascading effects of adding the piston engine mass could be considered. With the more complex geometry, the sizing of the piston can be conducted with higher accuracy. Then, the cascading effects would be much more valuable to explore for the FP-CCE concepts. In future work, it could be very valuable to set up an optimization model where the variables the free piston engine model could be optimized in conjunction

with the aircraft engine cycle variables. The future work will be conducted by the Flight Performance group of the TU Delft Faculty of Aerospace Engineering using the aircraft engine code and the OFPE model code to improve the scavenging models and improve the designs of the FP-CCE concepts.

References

[1] Kharina, A. , Rutherford, D. “Fuel efficiency trends for new commercial jet aircraft: 1960 to 2014”. In: *White paper of the International Council on Clean Transportation* (2015).

[2] Cumpsty, N., Mavris, D., Kirby. M. “Aviation and the environment: outlook”. In: *ICAO 2019 Environmental Report, Destination Green – The Next Chapter* (2019). URL: https://www.icao.int/environmentalprotection/%20Documents/EnvironmentalReports/2019/ENVReport2019_pg24-%2038.pdf.

[3] Grewe, V., Rao, A. G. et al. “Evaluating the climate impact of aviation emission scenarios towards the Paris agreement including COVID-19 effects”. In: *Nature Communications* (2021). DOI: https://doi.org/10.1038/s41467-021-24091-y.

[4] ICAO. “Annex 16 to the Convention on International Civil Aviation”. In: *Vol. IV Carbon Offsetting Scheme for International Aviation (CORSIA)* First Edition (2018).

[5] European Commission. “Flightpath 2050”. In: *Europe’s vision for aviation, report of the high level group on aviation research*. Luxembourg: Publications Office of the European Union (2011). DOI: https://doi.org/10.2777/50266.

[6] Tomas Grönstedt et al. “Conceptual design of ultra- efficient cores for mid-century aircraft turbine engines”. In: (Nov. 2020).

[7] Storm, R., Skor, M., et.al. *Pushing the Envelope: A NASA Guide to Engines*. Glenn Research Center Office of Educational Programs in Cleveland, OH, and the NASA Aeronautics Research Mission Directorate., 2013.

[8] Koff, B.L. “Gas Turbine Technology Evolution: A Designer’s Perspective”. In: *Propulsion and Power Research* (2004).

[9] van Buijtenen Prof. em. Ir. Jos P. et al. *Aero Engine Technology, AE4238*. Faculty of Aerospace Engineering, TU Delft, 2021.

[10] Dr. Feijia Yin. *Aero Engine Technology, Lecture 4: Aero Engine Efficiencies and Classification*. URL: https://brightspace.tudelft.nl/d2l/le/content/397958/viewContent/2492954/View (visited on 05/10/2023).

[11] Dr. Feijia Yin. *Aero Engine Technology, Lecture 3: Gas Turbine Cycle Efficiency*. URL: https://brightspace.tudelft.nl/d2l/le/content/397958/viewContent/2492052/View (visited on 05/10/2023).

[12] Feijia Yin. “Modelling and Characteristics of a Novel Multi-fuel Hybrid Engine for Future Aircraft”. PhD thesis. Sept. 2016. DOI: 10.4233/uuid:344b7d9c-f54c-4836-87ca-28582231a3d3.

[13] Zinon Vlahostergios et al. “Efforts to improve aero engine performance through the optimal design of heat recuperation systems targeting fuel consumption and pollutant emissions reduction”. In: Jan. 2017. DOI: 10.29008/ETC2017-356.

[14] Sascha Kaiser et al. “Unified Thermodynamic Evaluation of Radical Aero Engine Cycles”. In: June 2016. DOI: 10.1115/GT2016-56313.

[15] Dr. Feijia Yin. *Aero Engine Technology, Lecture 5: Engine Design Trends*. URL: https://brightspace.tudelft.nl/d2l/le/content/397958/viewContent/2496220/View (visited on 04/10/2023).

[16] Wikipedia. *Turbojet*. URL: https://en.wikipedia.org/wiki/Pratt_%5C%26_Whitney_PW1000G#Ultra_high-bypass_version.

[17] GE Engines. *GE9X Engine*. URL: https://www.geaerospace.com/propulsion/commercial/ge9x.

[18] Avellan, R. “On The Design of Energy Efficient Aero Engines: Some Recent Innovations”. PhD Thesis. Chalmers University of Technology, 2011.

[19] *Trent 7000*. URL: https://www.rolls-royce.com/products-and-services/civil-aerospace/widebody/trent-7000.aspx#/.

[20] Razak, A. M. Y. *Modern Gas Turbine Systems*. Woodhead Publishing Series in Energy, 2013. Chap. 11 Gas turbine performance modelling, analysis and optimisation.

[21] Sascha Kaiser. "Multidisciplinary Design of Aeronautical Composite Cycle Engines". PhD thesis. Jan. 2020. DOI: 10.13140/RG.2.2.14056.21764.

[22] Dr. Arvind Gangoli Rao, Dr. Ivan Langella , Prof. Dirk Roekaerts. *Hydrogen in Aero Engines: Opportunities and Challenges*. URL: https://brightspace.tudelft.nl/d2l/le/content/397970/viewContent/2623616/View.

[23] Rao, A.G., Yin,F., and van Buijtenen, J.P. "A Hybrid Engine Concept for Multi-fuel Blended Wing Body". In: *Aircraft Engineering and Aerospace Technology* 86 (2014).

[24] Energy Education. *Cetane number*. URL: https://energyeducation.ca/encyclopedia/Cetane_number.

[25] Merker, G.P. , Schwarz, C., et.al. *Simulating Combustion*. Springer, 2021.

[26] Schmitigal, J. , Tebbe, J. *JP-8 AND OTHER MILITARY FUELS*. URL: https://apps.dtic.mil/sti/pdfs/ADA554221.pdf.

[27] Wikipedia. *Aviation fuel*. URL: https://en.wikipedia.org/wiki/Aviation_fuel.

[28] Nygren, E., Aleklett, K. , Mikael, H. "Aviation fuel and future oil production scenarios". In: *Energy Policy* 37 (2009).

[29] *Alternative aviation fuels*. URL: https://alternative-fuels-observatory.ec.europa.eu/transport-mode/aviation/alternative-fuels-for-aviation.

[30] Yilmaz, N., Atmanli, A. "Sustainable alternative fuels in aviation". In: *Energy* 140 (2017).

[31] Bauen, A. "Sustainable Aviation Fuels". In: *Johnson Matthey Technology Review* 64 (2020).

[32] Janic, M. "Greening commercial air transportation by using liquid hydrogen (LH2) as a fuel". In: *International Journal of Hydrogen Energy* 39 (2014).

[33] Verhelst, S., Wallner, T. "Hydrogen-fueled internal combustion engines". In: *Progress in Energy and Combustion Science* 35 (2009).

[34] Perry, D. *P&W sees 2035 service entry potential for revolutionary hydrogen powerplant*. URL: https://www.flightglobal.com/engines/pandw-sees-2035-service-entry-potential-for-revolutionary-hydrogen-powerplant/147743.article.

[35] Airbus. *ZEROe*. URL: https://www.airbus.com/en/innovation/low-carbon-aviation/hydrogen/zeroe.

[36] Schäfer, A.W., Barrett, S.R.H. et al. "Technological, economic and environmental prospects of all-electric aircraft". In: *Nature Energy* 4 (2018). DOI: https://doi.org/10.1038/s41560-018-0294-x.

[37] Barzkar, A., Ghassemi, M. "Electric Power Systems in More and All Electric Aircraft: A Review". In: *IEEE Access* 8 (2020). DOI: https://doi.org/10.1109/ACCESS.2020.3024168.

[38] Wheeler, P., Bozhko, S. "The more electric aircraft: Technology and challenges". In: *IEEE Electric. Mag.* 2 (2014). DOI: https://doi.org/10.1109/MELE.2014.2360720.

[39] *Lilium*. URL: https://lilium.com.

[40] *Hybrid and electric flight*. URL: https://www.airbus.com/en/innovation/zero-emission-journey/hybrid-and-electric-flight.

[41] Kousoulidou, M., Lonza, L. "Biofuels in aviation: Fuel demand and CO2 emissions evolution in Europe toward 2030". In: *Transportation Research Part D* 46 (2016).

[42] Hari, T.K., Yakoob, Z., Binitha, N.N. "Aviation biofuel from renewable resources: Routes, opportunities and challenges". In: *Energy* 42 (2015).

[43] Sandquist, J., Guell, B.M. "Overview of Biofuels for Aviation". In: *Chemical Engineering Transactions* 29 (2012). DOI: https://doi.org/10.3303/CET1229192.

[44] M. Guynn et al. *Performance and Environmental Assessment of an Advanced Aircraft with Open Rotor Propulsion*. Tech. rep. NASA, 2012.

[45] *Open rotor installation effects*. URL: https://whittle.eng.cam.ac.uk/research-areas/open-rotor-installation-effects/.

[46] *The Pratt and Whitney PW1100G Geared Turbofan Engine*. URL: https://theflyingengineer.com/2013/07/08/the-pratt-and-whitney-pw1100g-geared-turbofan-engine/.

[47] Tomas Grönstedt et al. “Ultra Low Emission Technology Innovations for Mid-Century Aircraft Turbine Engines”. In: June 2016. DOI: 10.1115/GT2016-56123.

[48] Sascha Kaiser et al. “A Composite Cycle Engine Concept with Hecto-Pressure Ratio”. In: July 2015. DOI: 10.2514/6.2015-4028.

[49] Sascha Kaiser, Oliver Schmitz, and Hermann Klingels. “Aero Engine Concepts Beyond 2030: Part 2 - The Free-Piston Composite Cycle Engine”. In: *Journal of Engineering for Gas Turbines and Power* 143 (Jan. 2021). DOI: 10.1115/1.4048993.

[50] Sascha Kaiser et al. “Investigations of Synergistic Combination of the Composite Cycle and Intercooled Recuperation”. In: Sept. 2017.

[51] Sascha Kaiser et al. “A Composite Cycle Engine Concept for Year 2050”. In: Sept. 2018.

[52] Nickl, M. et. al. “Piston Engine Modelling for Hydrogen Fueled Composite Cycle Engines”. In: *IOP Conference Series: Materials Science and Engineering* (2022). DOI: 10.1088/1757-899X/1226/1/012033.

[53] Brosnan, P., Tian, G et.al. “A Comprehensive Review of the Free Piston Engine Generator and Its Control”. In: *International Journal of Automotive Manufacturing and Materials* 2 (2023). DOI: https://doi.org/10.53941/ijamm0201006.

[54] Woo, Y., Lee, Y.J. “Free piston engine generator: Technology review and an experimental evaluation with hydrogen fuel”. In: *International Journal of Automotive Technology* 15 (2014). DOI: https://doi.org/10.1007/s12239-014-0024-8.

[55] Mikalsen, R., Roskilly, A.P. “A review of free-piston engine history and applications”. In: *Applied Thermal Engineering* 27 (2007). DOI: https://doi.org/10.1016/j.applthermaleng.2007.03.015.

[56] Yu, H., Xu, Z., et. al. “Two-Stroke Thermodynamic Cycle Optimization of a Single-Cylinder Free-Piston Engine Generator”. In: *Hindawi- Advances in Materials Science and Engineering* (2019). DOI: https://doi.org/10.1155/2019/9783246.

[57] Nsabwa Kigezi, T. “Stability, Control, and State Estimation of Free Piston Engine Generators”. Phd. University of Sussex, 2019.

[58] Achten, P.A.J. “A Review of Free Piston Engine Concepts”. In: *SAE Technical Paper Series* (1994). DOI: https://doi.org/10.4271/941776.

[59] Xuezhen Wang et al. “A Review of the Design and Control of Free-Piston Linear Generator”. In: *Energies* 11 (Aug. 2018), p. 2179. DOI: 10.3390/en11082179.

[60] Hasan, M.M., Rahman, M.M. “Homogeneous Charge Compression Ignition Combustion: Advantages over Compression Ignition Combustion, Challenges and Solutions”. In: *Renewable and Sustainable Energy Reviews* 57 (2016). DOI: http://dx.doi.org/10.1016/j.rser.2015.12.157.

[61] Verma, S.K., Gaur, S. “Performance characteristic of HCCI engine for different fuels”. In: *Materials Today: Proceedings* 47 (2021). DOI: https://doi.org/10.1016/j.matpr.2021.04.609.

[62] Nissan Motor Corporation. *HCCI (Homogeneous-Charge Compression Ignition)*. URL: https://www.nissan-global.com/EN/INNOVATION/TECHNOLOGY/ARCHIVE/HCCI/.

[63] Goldsborough, S.S., Van Blarigan, P. “A Numerical Study of a Free Piston IC Engine Operating on Homogeneous Charge Compression Ignition Combustion”. In: *SAE Technical Paper Series* (1999). DOI: https://doi.org/10.1016/j.matpr.2021.04.609.

[64] Michael T. Leick and Ronald W. Moses. “Experimental Evaluation of the Free Piston Engine - Linear Alternator (FPLA)”. In: (Mar. 2015). DOI: 10.2172/1177159. URL: https://www.osti.gov/biblio/1177159.

[65] S Goldsborough and Peter Blarigan. “2003-01-0001 Optimizing the Scavenging System for a Two-Stroke Cycle, Free Piston Engine for High Efficiency and Low Emissions: A Computational Approach”. In: 1 (Mar. 2003). DOI: 10.4271/2003-01-0001.

[66] Shuaiqing Xu et al. “Numerical analysis of two-stroke free piston engine operating on HCCI combustion”. In: *Applied Energy* 88.11 (2011), pp. 3712–3725. ISSN: 0306-2619. DOI: https://doi.org/10.1016/j.apenergy.2011.05.002. URL: https://www.sciencedirect.com/science/article/pii/S0306261911002935.

[67] Y Zhu, Z Tang, and H Feng. “Simulation of the in-cylinder working process of an Opposed-Piston Free-Piston Linear Generator”. In: *IOP Conference Series: Materials Science and Engineering* 592.1 (Aug. 2019), p. 012093. DOI: 10.1088/1757-899X/592/1/012093. URL: https://dx.doi.org/10.1088/1757-899X/592/1/012093.

[68] Mohammad Alrbai. “Modeling and Simulation of a Free-Piston Engine with Electrical Generator Using HCCI Combustion”. PhD thesis. West Virginia University, Jan. 2016.

[69] Soyhan, H.S.,Yasar, H. Walmsley, H. , et. al. “Evaluation of heat transfer correlations for HCCI engine modelling”. In: *Applied Thermal Engineering* 29 (2008). DOI: ff10.1016/j.applthermaleng.2008.03.014.

[70] David G. Goodwin et al. *Cantera: An Object-oriented Software Toolkit for Chemical Kinetics, Thermodynamics, and Transport Processes*. https://www.cantera.org. Version 3.0.0. 2023. DOI: 10.5281/zenodo.8137090.

[71] Matthew Robinson and Nigel Clark. “Effect of Combustion Timing and Heat Loss on Spring-Assisted Linear Engine Translator Motion”. In: *SAE International Journal of Engines* 9 (Apr. 2016), pp. 554–572. DOI: 10.4271/2016-01-0560.

[72] Chang-Ping Lee. “Turbine-Compound Free-Piston Linear Alternator Engine.” In: (Jan. 2014).

[73] Boru Jia et al. “A study and comparison of frictional losses in free-piston engine and crankshaft engines”. In: *Applied Thermal Engineering* 140 (May 2018). DOI: 10.1016/j.applthermaleng.2018.05.018.

[74] Matthew C. Robinson and Nigel N. Clark. “Effect of Combustion Timing and Heat Loss on Spring-Assisted Linear Engine Translator Motion”. In: *SAE International journal of engines* 9 (2016), pp. 546–564. URL: https://api.semanticscholar.org/CorpusID:111912993.

[75] Chiara Saggese et al. “A physics-based approach to modeling real-fuel combustion chemistry – V. NOx formation from a typical Jet A”. In: *Combustion and Flame* 212 (2020), pp. 270–278. ISSN: 0010-2180. DOI: https://doi.org/10.1016/j.combustflame.2019.10.038. URL: https://www.sciencedirect.com/science/article/pii/S001021801930495X.

[76] Günter F. Hohenberg. “Advanced Approaches for Heat Transfer Calculations”. In: *SAE Transactions* 88 (1979), pp. 2788–2806. ISSN: 0096736X, 25771531. URL: http://www.jstor.org/stable/44699090 (visited on 04/03/2024).

[77] Abdul Aziz Hairuddin, Andrew Wandel, and T.F. Yusaf. “Effect of Different Heat Transfer Models on a Diesel Homogeneous Charge Compression Ignition Engine”. In: *International Journal of Automotive and Mechanical Engineering* 8 (Dec. 2013), pp. 1292–1304. DOI: 10.15282/ijame.8.2013.18.0106.

[78] Gerhard Woschni. “A Universally Applicable Equation for the Instantaneous Heat Transfer Coefficient in the Internal Combustion Engine”. In: *SAE transactions* 76 (1967). URL: https://api.semanticscholar.org/CorpusID:93390707.

[79] Junseok Chang et al. “New Heat Transfer Correlation for an HCCI Engine Derived from Measurements of Instantaneous Surface Heat Flux”. In: *SAE Transactions* 113 (2004), pp. 1576–1593. ISSN: 0096736X, 25771531. URL: http://www.jstor.org/stable/44723615 (visited on 04/03/2024).

[80] Dennis N. Assanis and Edward Badillo. “Evaluation of Alternative Thermocouple Designs for Transient Heat Transfer Measurements in Metal and Ceramic Engines”. In: *SAE Transactions* 98 (1989), pp. 1036–1051. ISSN: 0096736X, 25771531. URL: http://www.jstor.org/stable/44581007 (visited on 04/03/2024).

[81] Hakan Soyhan et al. “Evaluation of heat transfer correlations for HCCI engine modeling”. In: *Applied Thermal Engineering - APPL THERM ENG* 29 (Feb. 2009), pp. 541–549. DOI: 10.1016/j.applthermaleng.2008.03.014.

[82] T.M. Cain. “Autoignition of hydrogen at high pressure”. In: *Combustion and Flame* 111.1 (1997), pp. 124–132. ISSN: 0010-2180. DOI: https://doi.org/10.1016/S0010-2180(97)00005-9. URL: https://www.sciencedirect.com/science/article/pii/S0010218097000059.

[83] *Gas Turbine Emissions*. Cambridge Aerospace Series. Cambridge University Press, 2013.

[84] MTU. *LEAP-1A/-1B*. URL: https://www.mtu.de/engines/commercial-aircraft-engines/narrowbody-and-regional-jets/leap-1a/-1b/.

[85] Eric Hendricks and Justin Gray. “pyCycle: A Tool for Efficient Optimization of Gas Turbine Engine Cycles”. In: *Aerospace* 6 (Aug. 2019), p. 87. DOI: 10.3390/aerospace6080087.

[86] URL: https://www.easa.europa.eu/en/domains/environment/icao-aircraft-engine-emissions-databank.

[87] Feijia Yin, Floris Tiemstra, and Arvind Gangoli Rao. “Development of a Flexible Turbine Cooling Prediction Tool for Preliminary Design of Gas Turbines”. In: *Journal of Engineering for Gas Turbines and Power* 140 (Mar. 2018). DOI: 10.1115/1.4039732.

[88] F. Bakhtiari and H.-P. Schiffer. “Numerical approach to the modelling of transient interaction of prospective combustor concepts and conventional high pressure turbines”. In: *Propulsion and Power Research* 8.1 (2019), pp. 1–12. ISSN: 2212-540X. DOI: https://doi.org/10.1016/j.jppr.2019.01.008. URL: https://www.sciencedirect.com/science/article/pii/S2212540X19300082.

[89] Victor Bicalho Civinelli de Almeida and Dieter Peitsch. “Aeroelastic assessment of a highly loaded high pressure compressor exposed to pressure gain combustion disturbances”. In: *Journal of the Global Power and Propulsion Society* 2 (2018), pp. 477–492. DOI: 10.22261/JGPPS.F72OUU. URL: https://doi.org/10.22261/JGPPS.F72OUU.

[90] Harjot Singh Saluja et al. “Effect of Engine Design Parameters on the Climate Impact of Aircraft: A Case Study Based on Short-Medium Range Mission”. In: *Aerospace* 10.12 (2023). ISSN: 2226-4310. DOI: 10.3390/aerospace10121004. URL: https://www.mdpi.com/2226-4310/10/12/1004.

A

Appendix A

A.1. Derivation of Total Length

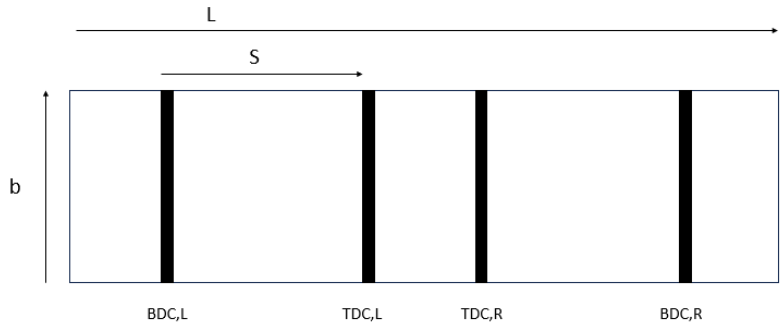

Figure A.1: Simple Parameterisation of the Free Opposed Piston Engine

$$CR = \frac{V_0}{V_f} \tag{A.1}$$

$$V_0 = A_{pistonhead} * (x_{BDC,R} - x_{BDC,L}) \tag{A.2}$$

$$V_f = A_{pistonhead} * (x_{TDC,R} - x_{TDC,L}) \tag{A.3}$$

$$x_{BDC,R} = R_{BDC} * L \tag{A.4}$$

$$x_{TDC,R} = x_{BDC,R} - S \tag{A.5}$$

$$x_{BDC,L} = (1 - R_{BDC}) * L \tag{A.6}$$

$$x_{TDC,L} = x_{BDC,R} + S \tag{A.7}$$

The derivation starts with the compression ratio definition. The piston areas on both sides get cancelled out

$$CR = \frac{V_0}{V_f} = \frac{x_{BDC,R} - x_{BDC,L}}{x_{TDC,R} - x_{TDC,L}} = \frac{x_{BDC,R} - x_{BDC,L}}{(x_{BDC,R} - S) - (x_{BDC,L} + S)}$$

$$= \frac{x_{BDC,R} - x_{BDC,L}}{(x_{BDC,R} - S) - (x_{BDC,L} + S)} = \frac{(1 - R_{BDC}) * L - R_{BDC} * L}{(1 - R_{BDC}) * L - S - (R_{BDC} * L + S)}$$

Dividing both sides by L:

$$CR = \frac{1 - 2 * R_{BDC}}{1 - 2 * R_{BDC} - 2 * S/L}$$

The, the expression can be re-written as:

$$CR * (1 - 2 * R_{BDC} - 2 * S/L) = 1 - 2 * R_{BDC}$$

$$CR * (-2 * S/L) = 1 - 2 * R_{BDC} - CR * (1 - 2 * R_{BDC}) = (1 - CR) * (1 - 2 * R_{BDC})$$

The, taking the compreesion ratios to one side,

$$2 * S/L = \frac{CR - 1}{CR} * (1 - 2 * R_{BDC})$$

Finally, plugging in the bore-to-stroke ratio b/s,the total length of the module can be expressed as:

$$L = \frac{1}{(b/s)} * b * 2 * \frac{CR}{(CR - 1) * (1 - 2 * R_{bdc})} \tag{A.8}$$

A.2. T-S diagrams with Different Heat Transfer Modes

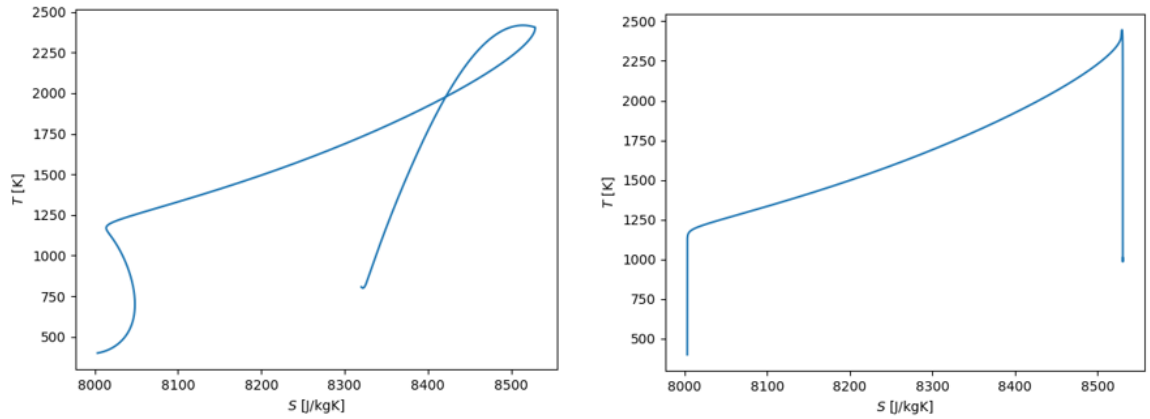

(a) T-S diagram of the baseline engine with heat loss

(b) T-S diagram of the baseline engine with NO heat loss

Figure A.2: Cycle results